Impact of *BCL11B* Loss-of-Heterozygosity on Mutation Frequency

Hedyeh Rahimian

Department of Biochemistry

McGill University, Montreal

July 2021

A thesis submitted to McGill University in partial fulfillment

of the requirement for the degree of Master of Science

ABSTRACT

Previously, our lab showed that CUX1 and other CUT domain proteins function as auxiliary factors in BER, stimulating the enzymatic activity of the OGG1 DNA glycosylase, which is responsible for the repair of oxidized purines. As CUT domain proteins do not stimulate other DNA glycosylases, we aimed to identify auxiliary factors of NTHL1, the DNA glycosylase that removes oxidized pyrimidines. Bio-ID approach results using NTHL1 fused with BirA* showed that BCL11B was biotinylated. BCL11B is a zinc finger transcription factor involved in the development of various tissues. While *BCL11B* is overexpressed in some cancers and is associated with resistance to radiomimetic drugs, it has been characterized genetically as a haploinsufficient tumor suppressor gene. DNA repair assays in cells and with purified proteins provided convincing evidence that BCL11B functions as a DNA repair auxiliary factor that stimulates the enzymatic activities of the NTHL1 DNA glycosylase and the Pol β DNA polymerase. Therefore, we hypothesized that the inactivation of one *BCL11B* allele in non-transformed cells could increase the frequency of spontaneous mutations as well as the mutation frequency following exposure to ionizing radiation. To test our hypothesis, we inactivated one allele of the *BCL11B* using the CRISPR-Cas9 approach in the TK6 lymphoblastoid cell line and obtained three independent clones. To compare the mutation rate in the parental *BCL11B*$^{+/+}$ and heterozygous *BCL11B*$^{+/-}$ TK6 cells, we performed a fluctuation assay to measure the number of *HPRT* mutants that arise spontaneously over a period of eleven to twelve days. In parallel, we measured the number of HPRT mutants that arise following treatment with ionizing radiation. We also analyzed the type of mutation (missense, nonsense, frameshift, or

larger deletions) in a large number of mutants. While the fluctuation assay indicated that the mutation rate was increased approximately two-fold in heterozygous *BCL11B*$^{+/-}$ TK6 cells, the experiments with ionizing radiation produced variable results. I discuss a number of issues that may explain the variations in the latter experiments. One important variable is the moment at which a mutation occurs during the so-called "mutation expression time", the period of time required for a genetic mutation to produce a new phenotype. Mutants arising early will divide and produce a higher apparent number of mutants once selection is applied. Historically, this problem led to the development of the fluctuation assay by Luria and Delbruck in 1943. Another is that *BCL11B* knockdown in some cells causes an increase in the expression of BCL11A, which also functions as an accessory factor in BER. In light of these caveats, the results of our *HPRT* assays do not confirm or infirm the hypothesis that the function of BCL11B in DNA repair explains its role as a haploinsufficient tumour suppressor gene in cells that have been submitted to radiation.

RÉSUMÉ

Il a été montré que la protéine CUX1 et d'autres protéines qui possèdent le domaine CUT fonctionnent comme facteurs auxiliaires dans la voie de réparation des bases. Ces protéines stimulent l'activité enzymatique de la glycosylase OGG1, qui répare les purines oxydées. Étant donné que les domaines CUT ne stimulent pas d'autres glycosylases, nous avons entrepris d'identifier des facteurs auxiliaires pour NTHL1, une autre glycosylase de la voie de réparation des bases, qui répare les pyrimidines oxydées. La méthode du BioID, utilisant la protéine NTHL1 fusionnée à un tag BirA a permis l'identification de la protéine BCL11B. BCL11B est un facteur de transcription, possédant des doigts de zinc en extrémité C-terminale, qui est impliqué dans le développement de divers tissus. La protéine BCL11B est surexprimée dans certains cancers et elle est associée à la résistance de ces cancers à des drogues radiomimétiques. Cependant, BCL11B a également été décrit comme un gène suppresseur de tumeur haploinsuffisant. Des expériences *in vitro* avec la protéine purifiée de BCL11B ont permis de montrer que BCL11B stimule l'activité de la glycosylase NTHL1 mais aussi de la polymérase β, confirmant ainsi son rôle comme facteur auxiliaire de la réparation de l'ADN. Nous avons donc émis l'hypothèse que l'hétérozygocité de BCL11B, l'inactivation d'un seul allèle de *BCL11B*, dans des cellules immortalisées mais non transformées entrainerait une hausse du nombre de mutations spontanées et du nombre de mutations après radiation ionisante. Afin de tester cette hypothèse, nous avons inactivé un allèle de *BCL11B* à l'aide de la méthode de CRISPR-Cas9 dans la lignée lymphoblastique TK6. Nous avons ainsi obtenu trois clones indépendants. Pour comparer la fréquence de mutations spontanées entre la lignée parentale TK6 *BCL11B*$^{+/+}$ et la lignée hétérozygote TK6 *BCL11B*$^{+/-}$, nous avons effectué un test de fluctuation et mesuré le nombre de

mutants générés spontanément dans le gène HPRT pendant une période de 12 jours. Nous avons également mesuré le nombre de mutants générés après radiation ionisante. Parmi les clones possédant des mutations, nous avons analysé plus spécifiquement le type de mutation (nonsense, mutations décalant le cadre de lecture ou délétions). Le test de fluctuation a montré que la fréquence de mutations spontanées est multipliée par deux dans les deux lignées hétérozygotes *BCL11B*$^{+/-}$ testées. Cependant, les résultats après exposition à des radiations ionisantes sont très variables. Nous avons émis plusieurs hypothèses qui pourraient expliquer la variation dans les résultats. Un paramètre important à prendre en considération est le moment auquel une mutation se produit durant la « période d'expression de la mutation », qui correspond à la période de temps nécessaire pour qu'une mutation génétique produise un phénotype. Des clones exprimant une mutation précoce auront plus de temps pour se diviser et produiront *in fine* un plus grand nombre de mutants bien que provenant d'un clone unique. Historiquement, ce biais avait conduit Luria et Delbrück à développer le test de fluctuation en 1943. Nous avons également observé dans certaines lignées de cellules que l'inhibition de BCL11B peut entrainer la surexpression de BCL11A, une protéine analogue qui fonctionne également comme facteur auxiliaire de la voie de réparation des bases, ce qui pourraient contrer les effets de l'inactivation d'un allèle de *BCL11B*. Considérant ces différents biais et hypothèses, les résultats des expériences de mutations dans le gène *HPRT* après radiation ionisante ne permettent pas de conclure si la fonction de BCL11B comme facteur auxiliaire explique son rôle de gène suppresseur de tumeur haploinsuffisant suite à l'exposition à des radiations ionisantes.

ACKNOWLEGMENTS

I would first like to thank my supervisor, Dr. Alain Nepveu, for his valuable comments, remarks and engagement through my learning process. He has taught me the methodology to carry out the research and to present the research work as clearly as possible. I am very thankful for the time he invested in my training, assisting me with studentship applications, RAC meeting presentation, and the revision of this thesis.

I would like to thank my Research Advisory Committee members, Dr. Selena Sagan and Dr. Maria Vera Ugalde, for giving me valuable suggestions on my project during my RAC meeting.

I would like to thank members of the Nepveu laboratory who all helped me in numerous ways during various stages of this journey: Lam Leduy, Zubaidah Ramdzan, Shusen Zhu, Camila Faraco, Elise Vickridge, and Shahrzad Tavakolfar. I would like to say a special thank you to Lam and Zubaidah who trained me and gave me technical and intellectual support whenever needed. I was truly inspired by their remarkable work ethic and dedication. I would also like to thank Elise for translating the abstract.

I would like to thank my parents for their continuous and unparalleled love and support, and I am grateful to my brother, Ehsan, for always being there for me as a friend.

Finally, I would like to thank my caring, loving, and supportive husband, Behrad. This journey would not have been possible if not for him, and I dedicate this milestone to him.

ACKNOWLEGMENTS OF WORK

Zi Yang Liu

Established *BCL11B* mutants (B101, B201, B203), performed T7EI mismatch detection assay and *in vitro* Cas9 nuclease digestion assay.

Shusen Zhu

Designed primers for *HPRT* RT-PCRs and genomic DNA PCRs, performed the Fluctuation assay and the mutation assay following irradiation on 2021/01/24, collected all *HPRT* mutants in the fluctuation assay and some *HPRT* mutants following irradiation.

Elise Vickridge and Lam Leduy

Helped with BCL11B immunoblotting.

Camila Faraco

Helped pelleting samples for RNA extraction.

Dr. Daniela Quail laboratory

Provided instrumentation: Countess® II FL Automated Cell Counter and Amersham Imager 680 (Blot & Gel Imager).

TABLE OF CONTENTS

INTRODUCTION

Oncogenes

Oncogenes are active forms of proto-oncogenes that have undergone a gain of function by one mechanism or another (1). Historically, oncogenes were discovered in a class of retroviruses that could produce a neoplastic phenotype and later were found to be associated with different types of cancers (2). Various mechanisms can activate oncogenes: one mechanism can be a point mutation, leading to a codon change, such as in *KRAS* mutants. Single base substitution in *KRAS* oncogenes affects codons 12 and 13 more frequently, changing glycine to aspartate or valine in codon 12 and glycine to aspartate in codon 13 (3), making the KRAS protein bound to GTP. Chromosomal rearrangement is another event associated with oncogene activation. For example, following a t(8:14) translocation in Burkitt lymphoma (BL), (4), MYC expression is regulated by the promoter or enhancer of the immunoglobin heavy chain gene which leads to MYC overexpression. Sometimes, the translocation forms a fused gene, producing a chimeric protein with new characteristics. For example, the *BCR-ABL* fused gene in chronic myelogenous leukemia (CML) patients leads to dysregulated activity of ABL tyrosine kinase, mediating CML pathogenicity (5). In addition, genome amplification could increase gene dosage, which can be seen as extrachromosomal copies of the oncogene (double minutes) or Intra chromosomal copies (tandem arrays or distributed)(6). Finally, some studies showed that epigenetic modification such as promoter hypomethylation could activate oncogenes (7-9)

Tumour Suppressor Genes

Tumour suppressors genes (TSG) are a class of genes that function to suppress cancer. Any alteration in tumour suppressor genes can increase the risk of cancer. It has shown that most of

cancer driver mutations occur within tumor suppressor genes rather than in oncogenes (10-12). Furthermore, a comparative study on the data from the Pan-Cancer project showed that tumor suppressors ranked one in mutation frequency rate, while oncogenes were positioned second (13). Tumour suppressors are classified into different groups based on their function: 1) intracellular proteins regulating cell cycle progression, 2) receptors or signal transducers that suppress cell proliferation, 3) inhibitors of cell cycle checkpoints which cause cell cycle arrest in case of DNA damage, 4) apoptosis mediators and 5) proteins associated with DNA repair mechanism (reviewed in (14)).

In 1997, Knudson introduced the "two-hit" model stating that two alleles of a tumour suppressor gene must be inactivated to cause a cancer phenotype. According to the "two-hit model", retinoblastoma gene (*RB1*) would be inactivated in two steps in familial retinoblastoma patients: while individuals have inherited one mutated allele (germinal mutation), the other allele will undergo a mutational event later on (sporadic mutation), leading to a complete loss-of-function of *RB1* (15). However, not all tumour suppressors follow the "two-hit" model. There is another class of tumour suppressor genes in which the inactivation of just one allele is enough to cause a phenotype that increases the risk of tumorigenesis (16). This class of TSG is known as haploinsufficient tumor suppressor genes. The cyclin-dependent kinase inhibitor $p27^{kip1}$, reported by Fero et al. in 1997, was the first haploinsufficient tumor suppressor gene (17). Recent studies showed that collaboration of some haploinsufficient tumour suppressors, referred to as "compound haploinsufficiency", can lead to cancer phenotypes, such as the 5q deletion (5q-) and 7q deletion (7q-) syndromes (16).

Oncogene Addiction

Oncogene addiction was first introduced by Weinstein 2000, which is defined as the dependency of cancer cells to certain oncogenes to maintain their malignant phenotype (18). One of the clinical examples of oncogene addiction is *BCR-ABL* in chronic myeloid leukemia. Chronic myeloid leukemia patients show an abnormal chromosome named Philadelphia, which was discovered first in 1960 (19). The Philadelphia chromosome results from a translocation between human chromosomes 9 and 22, producing the BCR-ABL fusion gene and chimeric protein, which is associated with CML pathogenesis (reviewed in (20)). Treatment of CML patients with Imatinib, a small-molecule tyrosine kinase inhibitor, showed promising results in pre-clinical and later clinical studies, leading to the FDA approval of this drug in 2001 (reviewed in (20)). Therefore, CML cancer cells being addicted to BCR-*ABL* oncogene is an example of oncogene addiction and explains how BCR-ABL inhibition is "synthetically lethal" for CML cancer cells.

Non-oncogene Addiction

Although oncogenes can be valuable targets to target cancers in the case of oncogene addiction, only a few are druggable (21). Therefore, it was proposed to target not only direct oncogenes but non-mutated targets to which cancer cells are dependent (22). Non-oncogene addiction refers to the dependency of cancer cells on proteins and pathways which are not classical oncogenes (23). During tumorigenesis, cells undergo different types of changes to acquire their transformed phenotype, leading cancer cells to experience various stresses such as DNA damage, oxidative, replicate, and metabolic stresses (reviewed in (24)). Cellular stresses could easily affect the viability of cancer cells unless they find a way to alleviate associated

adverse effects, leading to non-oncogene addiction. For example, cancer cells could adapt to proteotoxic stress by overexpressing the heat-shock factor 1 (HSF1), which explains why the non-oncogene addiction to *HSF1* could be a potential therapeutic target to treat cancer (23).

Base Excision Repair

Base excision repair is the DNA repair pathway that repairs damaged bases, including uracil, oxidized, deaminated, and alkylated bases, as well as single-strand breaks. It was estimated that 30,000 base damage occur in a daily basis in normal human cells(25). This pathway starts with the function of either monofunctional or bifunctional DNA-glycosylases by cleaving the N-glycosyl bond and making an abasic site (26). When monofunctional DNA glycosylases remove the damaged base, the apurinic endonuclease I (APE1) introduce a single-strand break (SSB) 5' to the abasic site. However, in case of oxidized damages, bi-functional DNA glycosylases can produce a SSB by cutting the DNA 3' to the abasic site through beta (OGG1, NTHL1) or beta-delta (NEIL1, NEIL2) eliminations (27). The next step would be end processing, which is mediated by enzymes such as DNA polymerase beta (pol β), APE1, and polynucleotide kinase-phosphatase enzymes (PNKP), all of which ultimately produce 3' hydroxyl and 5' phosphate ends (28). Then repair synthesis step can proceed in two ways: short patch (SP) or long-patch repair (LP). In SP, the nucleotide gap is filled by the action of pol β enzyme assisted by X-ray repair cross-complementing 1 enzyme (XRCC1), and the ligation will be mediated by DNA ligase 3 α (LIG3α) (29). However, in LP, a polymerase (β, δ, ε) synthesizes 2-13 nucleotides creating a 5' DNA flap. The flap is removed by flap endonuclease 1 (FEN1) prior to the ligation with LIG1 (30).

Accessory Factors in Base Excision Repair

It has been shown that enzymes in the BER pathway do not work in isolation and can be stimulated by the activity of auxiliary factors. Studies by our lab showed that cut-like homeobox 1 (CUX1), cut-like homeobox 2 (CUX2), and special AT-rich sequence-binding protein 1 (SATB1) can stimulate the DNA glycosylase and AP lyase activities of OGG1 (31-34). Moreover, CUX1 was also shown to stimulate the endonuclease activity of APE1 and polymerase and deoxyribose phosphate (dRP)-lyase activities of Pol β enzyme (35,36). However, apart from CUT domains, other types of protein can function as accessory factors in BER. For example, YB-1 can stimulate the enzymatic function of NTH1 and NEIL2, whereas HMGB1 is an auxiliary factor for APE1 and FEN1 endonucleases (reviewed in (37)). In addition, pol β was shown to be stimulated by P53 (reviewed in (37)).

CUX1 Role in DNA Repair

CUT-like homeobox 1 or *CUX1* gene has been implicated both in cancer progression and suppression. Although *CUX1* loss-of-heterozygosity (LOH) has been reported in different cancers (38-40), no mutation was found in the remaining allele (41,42). These studies identified CUX1 as a haploinsufficient tumour suppressor. Paradoxically, CUX1 is upregulated in many cancers, and its overexpression is associated with worse survival (43,44). Moreover, a fraction of tumours and tumou cell lines with *CUX1* loss of heterozygosity show amplification of the remaining allele (reviewed in (45)). Overall, these studies are consistent with a dual role of *CUX1* in cancer. While many transcriptional targets of CUX1 could explain why CUX1 overexpression can promote cancer (reviewed in(45)), there is so far no explanation how CUX1

could act as a haploinsufficient tumour suppressor. Recent discoveries by our laboratory raised the possibility that the tumour suppressor function of CUX1 is due to its role in DNA repair (31). It has been shown that cancer cells with activated RAS produce more reactive oxygen species (ROS), leading to oxidative damage lesion and cellular senescence (46,47). One of the solutions for cancer cells to deal with the deleterious effect of ROS is to increase their BER capacity through CUX1 overexpression to remove oxidative damage lesions (31,48). As mentioned before, CUX1 can stimulate different enzymes in the BER pathway, such as OGG1, which is the DNA glycosylase responsible to remove oxidized purine in genomic DNA (27). Our lab aimed to find any potential auxiliary factor to stimulate NTH1, the DNA glycosylase responsible for removing oxidized pyrimidines(27). Using a BioID approach, our lab discovered that BCL11A and BCL11B interact with NTH1.

BCL11B **Gene**

B cell leukemia/lymphoma-11b (BCL*11B*) is a C2H2 zinc finger transcription factor that was shown to have transcriptional regulatory activity (49). *BCL11B* was independently identified as chicken ovalbumin upstream promoter transcription factor interacting protein 2 (*CTIP2*) (50), and radiation-induced tumor suppressor gene 1 (*Rit1*) (51). BCL11B plays a critical role in the development of various tissues such as neural tissues (52,53), skin (54), craniofacial (55), and T-cells (56,57) during embryogenesis. In 2003, Wakabayashi et al. discovered a tumour suppressor which went through homozygous deletion and point mutation in y-ray induced mouse thymic lymphomas and named it radiation-induced tumor suppressor gene 1 (*Rit1*) (51). Wakabayashi et al. discovered that Rit1 protein corresponds to the *BCL11B* and *CTIP2* in human (51), which was the first evidence of BCL11B acting as a tumour suppressor. Further mutational

analysis on human T-cell acute lymphoblastic leukemia (T-ALL) revealed *BCL11B* monoallelic inactivation and point mutation (58,59). In addition, *BCL11B* $^{+/-}$ mice were more susceptible to develop lymphoma upon radiation or crossing with *P53*$^{+/-}$ mice; however, the remaining allele exhibited wild-type BCL11B expression (60). These studies suggest that *BCL11B* could function as a haploinsufficient tumour suppressor gene.

On the other hand, BCL11B overexpression has been reported in many cancers such as Ewing sarcoma (61), T-cell lymphoma (62,63), head and neck squamous cell carcinoma(64), and glioblastoma (65). In addition, it was shown that BCL11B overexpression is associated with resistance to radiomimetic treatments (66,67). These results are in contrast with the role of *BCL11B* as a tumour suppressor. Moreover, some studies showed that *BCL11B* could act as a regulator of apoptosis in cells. For example, when BCL11B was inhibited in glioblastoma and T-cell lymphoma, cells underwent apoptosis (68,69). However, there is no data showing that BCL11B could have a transcriptional regulatory effect on genes associated with apoptosis. Like CUX1, *BCL11B* appears to play a dual role in cancer. Yet, the molecular basis for the role of BCL11B as a haploinsufficient tumour suppressor has not been elucidated.

Rationale and Objectives of the Study

Our lab aimed to find any potential auxiliary factor stimulating NTHL1, the main DNA glycosylases responsible for removing oxidized pyrimidines (27). Bio-ID approach results using NTHL1 fused with BirA* showed that BCL11B protein was biotinylated. Using bacterially expressed and purified protein in DNA repair assays with fluorophore-based probes and radioactively labeled oligonucleotides, BCL11B was shown to stimulate the enzymatic activities of NTHL1. Moreover, BCL11B was also found to stimulate the enzymatic activities of Pol β, the

DNA polymerase of the base excision repair pathway. Using single-cell gel electrophoresis (comet assays), we observed that *BCL11B* knockdown increases DNA damage in cancer cells that exhibit high levels of reactive oxygen species (ROS) and causes a delay in the repair of oxidative DNA damage following treatment with hydrogen peroxide (Vickridge et al., manuscript in preparation).

These results suggest that BCL11B functions as an auxiliary factor in BER. Therefore, we hypothesized that the DNA repair function of BCL11B may explain why the inactivation of one *BCL11B* allele promotes tumour development. Based on this hypothesis, we aimed to test whether the inactivation of one *BCL11B* allele in non-transformed cells could increase the rate of spontaneous mutations as well as the mutation frequency following exposure to ionizing radiation.

To test this hypothesis, we pursued the following objectives:

1. Generating *BCL11B*$^{+/-}$ heterozygous TK6 cells using CRISPR-Cas9 technology
2. Studying the mutation frequency of *BCL11B* haploid cells following treatment with ionizing radiation
3. Studying the spontaneous mutation rate of *BCL11B* haploid cells through the fluctuation assay
4. Analyzing of *HPRT* mutants arising from *BCL11B*$^{+/-}$ heterozygous cells

HPRT Mutation Assay

HPRT mutation assay is the first and most common mutation assays to study induced specific-locus mutation in cultured mammalian cells (70). *HPRT* mutation assay was established based on conferring resistance to a toxic chemical in mutants. The hypoxanthine phosphoribosyl

transferase (*HPRT)* gene is located on the mammalian X chromosome. *HPRT* gene span approximately 40 kb containing nine exons, which makes it a large target for mutational events (71). *HPRT* gene encodes HGPRT enzyme, which can restore purines from degraded DNA and reintroduced them through the salvage pathway in cells (72). In addition, HGPRT can mediate incorporation of 6-thioguanineinto DNA (73), which destroys cells, whereas cells with mutated *HPRT* gene will survive (73). There are three advantages of using *HPRT* mutation assay over other mutation assays: 1) once *HPRT* gene is mutated, mutation phenotype would be expressed in cells derived from the male gender due to the presence of one active allele, 2) it is possible to select against *HPRT* mutants using the CHAT medium and to select for *HPRT* mutants using toxic purine analogs such as 6-thioguanine. This enables one to start an experiment with a population that is devoid of any pre-existing *HPRT* mutants 3) mutation from the same gene can be compared between different cell lines, animal models and humans (74). In addition, it is relatively easy to expand and analyze mutants to study the spectrum of the mutations (75-77). Interestingly, Maiti et al. in 2008 studied mutation frequency and spectrum in both Chinese hamster V79 and human bronchial A549 cell lines following 70-80% NEIL1 downregulation, showing an increase in spontaneous mutations as well as following treatment can causes oxidative damage (76).

Fluctuation Assay

Fluctuation assay was first described by Salvador Luria and Max Delbruck in 1943 (78) when they studied spontaneous mutation rate in bacteria, making them resistant against viruses. Lea and Coulson in 1949 extended the fluctuation assay presented by Luria and Delbruck and introduced improved equation to calculate the mutation rate (79). The fluctuation assay is

based on the premise that the number of mutants in a culture depends on the time at which the mutation event took place. Mutants occurring early in a culture with have time to divide several times, thereby increasing the number of mutants that are counted once the selection is applied. Therefore, mutation rate refers to the number of mutational events within a population during a certain period of time, whereas mutation frequency displays the proportion of mutants in a population (80). It is believed that mutation rate is a better indicator of spontaneous mutation than mutation frequency (80). To perform a fluctuation assay, we need several parallel cultures expanding simultaneously and during the same period to look at the number of spontaneous mutations that occur during the expansion time (79).

There are some assumptions based on which the fluctuation assay is established: 1) parallel cultures started from a single cell, or at least a small number of cells compared to the final population, 2) growth-rate of mutants and non-mutants are the same, 3) there is no post-plating mutations, 4) all mutants are being detected by the selective media, 5) The final number of cells in parallel cultures are the same, 6) there would not be any reverse mutation (81). These assumptions are likely to be violated (81); however, it is better not to dismiss those under our control such as number 1 and 5.

MATERIALS AND METHODS

Cell Culture

Human lymphoblastoid cells TK6 were maintained in Roswell Park Memorial Institute (RPMI) medium (Wisent), supplemented with 10 % fetal bovine serum (FBS) (Gibco) and 1 %

penicillin/streptomycin (Wisent). During the study, TK6 cells were maintained at 37°C between 0.2-1 x 10^6 cells/ml in a humidified incubator with 5 % CO_2.

Designing CRISPR RNAs for *BCL11B*

Because all *BCL11B* mRNA variants share exon 2, we aimed to design CRISPR RNAs (crRNA) on exon 2. The crRNAs were designed by inputting the target genomic sequence into two online crRNA designers: CRISPOR and IDT's CRISPR-Cas9 guide RNA design checker. Considering selection criteria for optimal targeting and no off-target effects, three crRNA were selected and used in our study (sequences are provided in table 1). Selection criteria included their specificity score, predicted cleavage efficiency score, and the nature of off-targets.

Annealing of crRNA and tracrRNA to Form Guide RNA

crRNA and tracrRNA-ATTO550 (fluorophore-labeled) were diluted in the nuclease-free duplex buffer to a final concentration of 1 µM. The complex was heated to 95°C for 5 minutes and slowly cooled down to room temperature to form gRNA

Nucleoporation

To increase the probability of inactivating one allele only, we opted to transfer the Cas9 protein instead of a vector expressing Cas9. For each sample, 1.2 µL of gRNA (100 µM) and 1.7 µL of Cas9 (61 µM) in 2.1 µL PBS were combined and added to 100 µL of supplemented nucleofector solution from the Lonza nucleofection kit: Type SF (82 µL of nucleofector solution and 18 µL of supplement). 1 x 10^6 TK6 cells were resuspended in the supplemented nucleofector solution and transferred to a nucleocuvvet. The nucleocuvvet was then placed in the Lonza 5D nucleofector, and cells were nucleofector with the program: Cell Type: RPMI 8826, Pulse Code: DN-100.

Fluorescence-Activated Cell Sorting (FACS)

Following the nucleoporation, cells were resuspended carefully and transferred into a 15 mL conical tube. Individual fluorescent cells were sorted into two 96-well plates and collected in the McGill FACS facility. The rest of the cells were maintained in bulk.

Wells were tagged with a three-digit identification number where the first digit signifies which gRNA was used to target the gene, and the second and third digit indicates the clonal ID

DNA Extraction

1 x 10^6 cells underwent DNA extraction using the Qiagen's DNeasy Blood and Tissue kit.

Amplification of the *BCL11B* Genomic DNA with a Potential Indel

Primers were designed to flank the cleavage site. Attention was paid to have the two cleavage fragments large enough to be visible and distinct on the gel (preferably over 250 bp) and at least 100 bp apart from each other. PCR reaction was prepared in a total volume of 50 µL using GoTaq® G2 DNA Polymerase kit (Promega) and dNTPs mixture (Bio Basic Canada) as per the manufacturer protocol. PCR amplification products were tested in the T7EI mismatch detection assay and the *in vitro* Cas9 nuclease digestion assay.

T7EI Mismatch Detection Assay

This assay was performed for two reasons:

1- To calculate indel frequency in the nucleoporated bulk population.
2- To confirm the presence of an indel in individual fluorescent sorted cells.

10 µL of PCR amplification product, 2 µL of 10X T7EI reaction buffer, and 6 µL of nuclease-free water were combined. The PCR amplification products were denatured and renatured to form the heteroduplex using the following program:

1. 95°C for 10 min;

2. 95°C –85°C at 2°C/sec

3. 85°C –25°C at 0.3°C/sec.

The heteroduplex was then incubated with 2 µL of T7EI at 37°C for one hour. The cleaved fragments were separated by DNA electrophoresis using a 7% agarose gel.

In Vitro Cas9 Nuclease Digestion of PCR Amplification Products

In vitro Cas9 nuclease digestion was performed using the guide-it sgRNA screening Kit (Takara). Purified Cas9 nuclease and gRNA were incubated together in the thermal cycler at 37°C for 5 min for annealing. Following that, 2 µL of *BCL11B* genomic DNA PCR amplification product, 1 µL of 15X Cas9 reaction buffer (Takara), 1 µL of 15X BSA, 6.5 µL of RNase-free water, and 1.5 µL of Cas9/sgRNA mix were combined and incubated for one hour at 37°C and heated to 80°C. DNA fragments were separated by DNA electrophoresis using a 7% agarose gel.

Nuclear Extraction

Approximately 10 x 10^6 cells were collected at the concentration of 0.8 -10 x 10^6 followed by washing with PBS. Next, the cell pellet was resuspended in 400 µl of buffer A containing 10 mM HEPES, pH 7.9, 10 mM KCl, 1.5 mM $MgCl_2$, 0.5 mM DTT, and protease inhibitor (Sigma). In order to lyse cells, cell suspensions went through three cycles of freezing-thawing using liquid nitrogen and a 37°C water bath followed by a short centrifugation at maximum speed. After removing the supernatant containing cytoplasmic proteins, the pellet containing nuclear proteins was resuspended in 100 µl of buffer C consists of 20 mM HEPES pH 7.9, 25 % glycerol, 1.5 mM $MgCl_2$, 420 mM $NaCl_2$, 0.2 mM EDTA, 0.5 mM DTT, and protease inhibitor (Sigma). Following 30 minutes of incubation on ice, samples were centrifuged at 13000 rpm for 20

minutes, and the supernatant containing the nuclear extract was transferred to another tube. Protein concentration was quantified using a spectrophotometer before samples being frozen in a -80°C freezer for long-term preservation.

Immunoblotting

Before performing the *HPRT* mutation assay, Immunoblotting was performed to analyze the BCL11B protein expression in *BCL11B* heterozygous (B101, B201, and B203) and wild-type cells. Following nuclear extraction and quantification, SDS loading buffer was added to 20 µg of protein before boiling samples for approximately 5 minutes. Proteins were separated through sodium dodecyl sulfate-polyacrylamide gel electrophoresis (SDS-PAGE) using 8% polyacrylamide gel. Following electrophoresis, proteins were transferred onto polyvinylidene difluoride (PVDF) membrane for an overnight period. The next day, the membrane was blocked using 5 % powdered milk and 2 % bovine serum albumin (BSA) in TBS-T (10 mM Tris pH 8, 150 mM NaCl, 0.1 % Tween X-100) for two hours at room temperature, followed by a quick rinse using TBS-T. The upper half of the membrane was incubated with a rabbit antibody against BCL11B (Bethyl/ A300-383A) at the dilution of 1:1000. In addition, the lower half was probed with a mouse antibody against tubulin (Sigma) at the dilution of 1:10000. Upon two hours of incubation with primary antibodies, membranes were washed with TBS-T solution three times with 15 minutes intervals, during which membranes were shaking on a rocking platform in rinsing solution. Next, membranes were incubated using their respective secondary antibody, anti-rabbit or anti-mouse, for one hour, followed by the same rinsing steps as was mentioned above. Finally, membranes were exposed using Amersham Imager 680 (Blot & Gel Imager) in Dr. Daniela Quail's laboratory.

Counter Selection with CHAT Treatment to Eliminate Pre-Existing *HPRT* Mutants

To reduce the number of pre-existing *HPRT*$^-$ mutants, cells were treated with CHAT supplement (including deoxycytidine, hypoxanthine, aminopterin, and thymidine) for three days (82). The final concentration of the CHAT supplement was 0.1 mM of hypoxanthine, 0.4 µM of aminopterin, and 16 µM of thymidine using 50X HAT (Gibco) in addition to 20 µM of deoxycytidine. Following three days of incubation, cells were spined down and washed three times with PBS to remove any aminopterin residue. Next, cells were plated at 0.4 x 10^6 cells/ml in CHT medium containing 50 µM of hypoxanthine in addition to 8 µM of thymidine using 100X HT (Thermofisher Scientific) and 10 µM of deoxycytidine for two to three days until the cell viability percentage reached above the 90%.

Plating for Clonogenic Efficiency Following Ionizing Radiation

After the cleansing of pre-existing *HPRT*$^-$ mutants, cells were divided into two falcon tubes (1 x 10^7 each, at 1 x 10^6 cells/ml) and were subjected or not to radiation, from 0.5 to 2 Gy. After changing the medium, multiple serial dilutions were prepared to plate cells at low density (2 cells/well) in two 96-well plates using a multipipetter. Following two weeks of incubation at 37°C in a humidified incubator, wells with viable cells were identified over a microscope. The rest of the cells were maintained in T-75 flasks seven days following radiation to allow the expression of *HPRT*$^-$ phenotype (82). Because of the massive cell death due to radiation, we plated cells at a high density (1.5 x 10^6 cells/ ml) following radiation, whereas 0 Gy populations were plated at 0.2 x 10^6. Within the seven days post-irradiation, cells were monitored and counted every day and split if necessary to maintain cell density between 0.2- 1 x 10^6 cells/ml.

Plating for Mutation Frequency Following Ionizing Radiation

Seven days post-irradiation, cells were plated in two 96-well plates at a density of 4 x 10^4 cells per well, supplemented with the purine analog 6-thioguanine (6-tg) at 15 µM to select for *HPRT*$^-$ cells. Three weeks after incubation with 6-tg, wells with viable cells were counted over a microscope, and mutation frequency was calculated using the poisson distribution statistical method.

Calculation of Clonogenic Efficiency and Mutation Frequency Following Ionizing Radiation

We calculated clonogenic efficiency and mutation frequency based on the poisson distribution statistical analysis described by Furth et al., who developed a quantitative mutation assay using the microtiter plating technique (83). Based on the Poisson distribution statistical analysis used by Furth, mutation frequency rate depends on the ability of low-density plated cells to grow in non-selective media, known as the clonogenic efficiency (83). Clonogenic efficiency percentage was calculated using the following formula where X_0 is the number of wells without colonies, N_0 is the total number of plated wells, and D_0 is the number of initial cells plated/well.

$$Clonogenic\ effieicny\ \% = \frac{-\ln\ (X_0/N_{0)}}{D_0}$$

Mutation frequency was calculated using the following formula where X_s is the number of wells without colonies in the selective media, N_s is the total number of plated wells with selective media, and D_0 is the number of initial cells plated/well in the selective media.

$$Mutation\frac{frequency}{million} = \frac{-\ln\ (X_s/N_{s)}}{-\ln\ (X_0/N_{0)}} \times \frac{D_0}{D_s}$$

Starting Parallel Cell Culture for Fluctuation Assay.

To start the fluctuation assay, pre-existing *HPRT*$^{-}$

cells were removed using CHAT treatment as discussed before. Following CHAT and CHT treatment, at least 24 parallel cultures/samples were started at the density of 100 cells/well and expanded during a period of eleven days for the parental cells and twelve days for the *BCL11B*$^{+/-}$ heterozygous cells until they reach approximately 8 x 10^6 cells, ensuring that cell concentrations remained below 1 x 10^6 cells/ml

Plating for Clonogenic Efficiency in the Fluctuation Assay

When a population reached 8 x 10^6 , cells were plated at low density (2 cells/ well) in non-selective media in 2 x 96-well plates to determine clonogenic efficiency. Number of positive wells was quantified two weeks post-plating.

Plating for Spontaneous Mutation Rate in the Fluctuation Assay

Cells were plated with 6-tg in parallel with the plating for the clonogenic efficiency plating to determine spontaneous mutation rate. In two 96-well plates, 4 x 10^4 cells were plated per well and incubated with 15 µM of 6-tg. Following three weeks of incubation, number of positive wells were quantified under the microscope.

Figure 1: *HPRT* Mutation Assay

HPRT mutation assay was performed in two different ways to calculate mutation frequency following radiation and spontaneous mutation rate in the fluctuation assay. Both ways started with CHAT treatment to remove pre-existing *HPRT* mutants in the population. After radiation, cells were plated at low density in two 96-well plates to calculate the clonogenic efficiency. The rest of the cells were maintained in culture for one week to let the *HPRT* mutation phenotype be expressed following radiation. Cells were plated at 40000/well supplemented with 6-thioguanine to select *HPRT* mutants following seven days of incubation. However, to calculate the spontaneous mutation rate, 24 wells were inoculated with 100 cells and expanded until they reach 8×10^6 cells. Cells were plated for clonogenic efficiency and mutation rate in non-selective and selective media, respectively. The number of positive wells was quantified two weeks and three weeks following plating in non-selective media (clonogenic efficiency) and selective media (mutation rate).

Figure 1: *HPRT* Mutation Assay

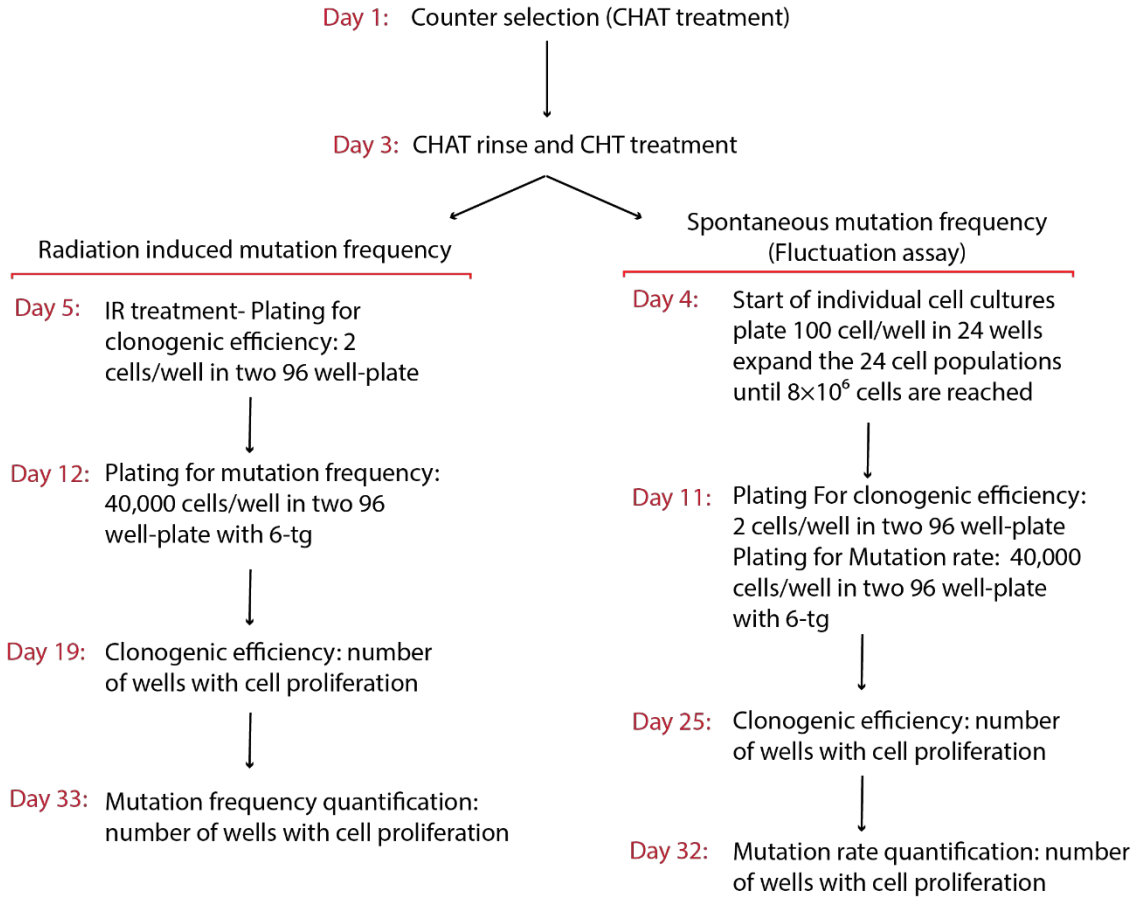

Calculation of Clonogenic Efficiency and Mutation Frequency Following Ionizing Radiation

Clonogenic efficiency was calculated for each independent culture, as it is mentioned before. The average of clonogenic efficiencies for each independent culture was calculated by summing up all clonogenic efficiencies divided by the total number of parallel cultures. The average was applied to calculate spontaneous mutation rate using the P_0 method (84), where P_0 is the number of cultures without positive wells, P is the total number of parallel cultures, N_0 is the total number of cells plated in mutation rate plates, and CE is the average of clonogenic efficiencies

$$Spontaneous\ mutation\ \frac{rate}{million} = \frac{-\ln\left(P_0/P\right)}{N_0 \times CE}$$

Clonal Expansion of *HPRT*$^-$ Mutants

Following HPRT mutation assays, several mutants were collected and expanded, including 79, 134, and 81 mutants originated from the TK6 parental, B101, and B203 populations, respectively. Cells were transferred to bigger plates as they were expanded until they reach 15 x 10^6 cells. Four cell pellets of approximately 1-2 x 10^6 were collected and washed with PBS buffer. Next, cell pellets were preserved in a -80°C freezer for RNA and genomic DNA extractions. Moreover, two vials per mutant were frozen using DMSO at -80°C and liquid nitrogen for further analysis.

RNA Isolation and cDNA Synthesis

Using RNeasy Plus Mini Kit (Qiagen), RNA was isolated from each HPRT $^{-}$ clone as per the manufacturer protocol. Extreme care was taken to prevent RNA degradation and avoid contamination. Once RNAs were extracted, the protocol from GoScript™ Reverse Transcriptase kit (Promega) was applied to synthesize cDNA, using oligo(dT) and 1 µg of RNA. Moreover, to increase the specificity and sensitivity of the RT-PCR reaction, we used 0.1 µM of the HPRT specific primer, HPRT-rt (table 1). cDNAs were stored at 4°C for immediate usage or -20°C for long-term storage.

HPRT RT-PCR Amplification

Following cDNA synthesis, cDNAs were subjected to the reverse transcription-polymerase chain reaction (RT-PCR) using the GoTaq® G2 DNA Polymerase kit (Promega) and dNTPs (Bio Basic Canada) as per the manufacturer protocol. In order to increase specificity and the yield of products, we performed a nested PCR amplification strategy. Using F1 and P1 outer primers in the first PCR reaction, samples underwent 20 cycles of amplification and were diluted five times to use as template for the second PCR. The second PCR reaction was set up at 20 µl using the previously diluted samples, and F2 and R3 inner primers, amplifying for 40 cycles. All primer sequences designed by the Primer-BLAST tool and manufactured by Integrated DNA Technologies (IDT) are described in table 1. Following the second PCR reaction, DNA was separated using gel electrophoresis in 1% agarose gel. Each gel electrophoresis contained a positive control displaying the expected full-length PCR amplification product at 756bp and a negative control including the same PCR reaction without the template.

RT-PCR Analysis of *HPRT*$^-$ Clones

Following gel electrophoresis of the second RT-PCR reaction, mutants exhibiting a full-length or a shorter PCR amplification product underwent Sanger Sequencing by Genome Quebec, using F2 and R3 primers from the second RT-PCR. Mutants displaying multiple PCR amplification products were subjected to gel purification, and each band was sequenced individually using F2 and R3 primers. Finally, *GAPDH* RT-PCR amplification was performed on those mutants yielding no PCR amplification product as a control to ensure that the cDNA was of good quality.

GAPDH RT-PCR

Several mutants did not show any PCR amplification product upon two-step *HPRT* RT-PCR. To ensure these negative results were not due to the poor quality or low amount of RNA, *GAPDH* RT-PCR was performed using GoTaq® G2 DNA Polymerase kit (Promega), dNTPs (Bio Basic Canada), and GAPDH-RT primers (table 1). The reaction underwent 25 cycles of amplification, and PCR amplification products were separated using DNA electrophoresis in 1% agarose gel.

Genomic DNA Isolation

Those HPRT mutants yielding no *HPRT* RT-PCR amplification product but displayed the full-length *GAPDH* RT-PCR amplification products were submitted to genomic DNA isolation to check the presence of *HPRT* genomic DNA. Genomic DNA was extracted from approximately 1-2 x 10^6 cells, using DNeasy Blood & Tissue Kits (Qiagen) as per the manufacturer protocol. In order to purify and de-salt the extracted DNA, samples were precipitated using ethanol and 0.3M sodium acetate.

Amplification of *HPRT* Gene 3'- and 5'- Ends Using Genomic DNA

Following genomic DNA extraction, the 5' region of the *HPRT* gene, including the promoter sequences, the first exon, and a portion of intron 1, was amplified using HPRT-5gF and HPRT-5gR primers. In parallel, HPRT-6F and HPRT-6R primers were used to amplify the 3'- end of the *HPRT* gene covering the polyadenylation site. Both PCRs were performed using GoTaq® G2 DNA Polymerase (Promega), dNTPs (Bio Basic Canada). In addition, 10% DMSO was added to the 5'-end PCR reaction to facilitate amplifying the GC reach area of the promoter region. Finally, PCR amplification products were separated by electrophoresis in 1% agarose gel. Finally, mutants were categorized accordingly in three groups: 1- mutants yielding both 5'- and 3'- end PCR amplification products, 2- mutants amplifying either 5'- or 3'- end, 3- mutants with no 5'- and 3'- ends PCR amplification products. While mutants from the first group were sent for Sanger Sequencing, others were further analyzed by *GAPDH* PCR amplification to control for the genomic DNA quality.

Sequencing Analysis of *HPRT* Gene 5'- and 3'- Ends

While several mutants demonstrated no *HPRT* RT-PCR amplification product, they showed positive results for both 5'- and 3'- ends of HPRT genomic DNA PCR. Any potential mutation in the promoter region or polyadenylation site could interfere with transcription or reduce the stability of RNA. Therefore, HPRT gene 5'- and 3'- ends amplification products were subjected to Sanger Sequencing using HPRT-5gF and HPRT-5gR primer and HPRT-6F and HPRT-6F primers, respectively.

GAPDH PCR Using Genomic DNA

Some mutants did not show any band upon *HPRT* genomic DNA PCRs. To ensure that negative results were not due to the poor quality or low concentration of the extracted genomic DNAs, *GAPDH* PCR amplification was performed using GoTaq® G2 DNA Polymerase (Promega), dNTPs from (Bio Basic Canada) and GAPDH-gDNA primers (table 1).

Figure 2: Steps for Analysis of Mutants

After preserving cell pellets and cryopreservation of *HPRT* mutants with DMSO, one of the cell pellets was subjected to RNA extraction, followed by cDNA synthesis. *HPRT* RT-PCR amplification was performed by a nested PCR strategy, using F1 and P1 primers in the first round and F2 and R3 primers in the second round to amplify the coding part of the *HPRT* gene. Positive RT-PCR amplification products were sent for sequencing, whereas mutants without RT-PCR amplification products were subjected to *GAPDH* PCR to ensure the quality of RNAs and cDNAs. When the *GAPDH* RT-PCR results were positive, the 3'- and 5'-ends of the *HPRT* gene were PCR-amplified. PCR amplification products of mutants with both 3'-end and 5'-end *HPRT* genomic DNA were subjected to sequencing to find any potential mutation in the promoter sequences, or polyadenylation site. However, in the case of mutants producing no *HPRT* gene 3'-end and 5'-end amplification products, *GAPDH* PCR amplification was performed to verify the quality of genomic DNA.

Figure 2: Steps for Analysis of Mutants

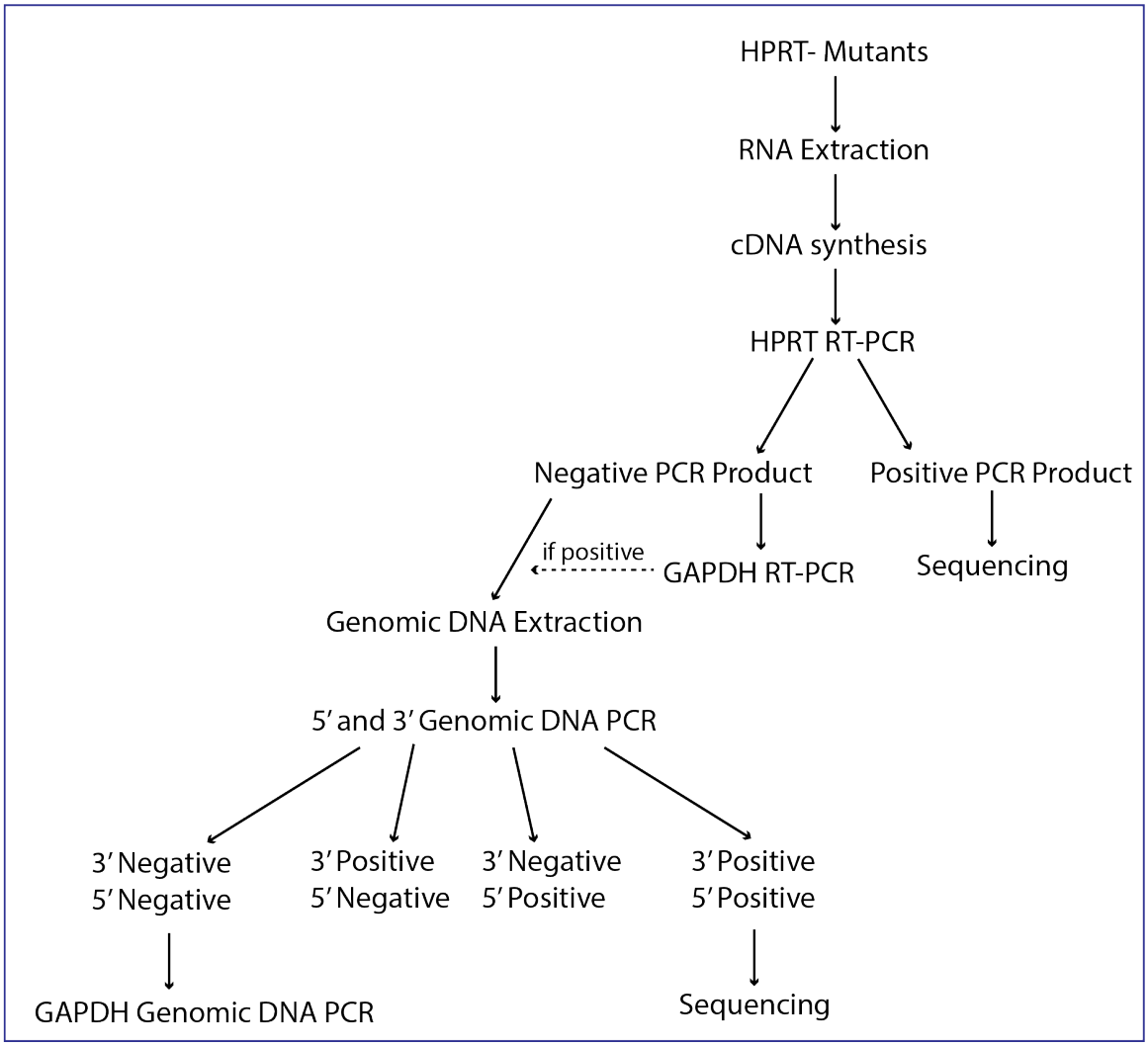

Table 1: Primers and DNA Fragments Used in the Study

The following table shows the list of primers and fragments, their application, and their corresponding PCR amplification product size

Name of primer	Sequence (from 5' to 3')	Application
BCL11B crRNA 1	CAGGUGGUCA UCUUCGUCGG	*BCL11B* CRISPR Cas9 targeting
BCL11B crRNA 2	GAUCCCGAUC UCCACCGGCU	*BCL11B* CRISPR Cas9 targeting
BCL11B crRNA 3	ACUUGGAUCC CGAUCUCCAC	*BCL11B* CRISPR Cas9 targeting
BCL11B long F1	ACCGCCTAAGCCCATCTCTA	Amplifying *BCL11B* genomic DNA for T7 endonuclease I mismatch assay and *in vitro* Cas9 nuclease digestion on PCR amplification products (target size: 880)
BCL11B long R	CGTCCTCACAGCAACCCTAA	
HPRT-rt	TTT AGG AAT GCA GCA ACT G	cDNA synthesizing
F1-RT-PCR	CTGCTCCGCCACCGGCTTCC	First round of *HPRT* RT-PCR amplification (target size: 811)
P1-RT-PCR	CTAAGCAGATGGCCACAGAA	
F2-RT-PCR	CTTCCTCCTCCTGAGCAGTC	Second round of *HPRT* RT-PCR amplification (Target size: 756bp)/ *HPRT*$^{-}$ RT PCR sequencing
R3-RT-PCR	CTGGCGATGTCAATAGGACTCC	
HPRT-5gF	ACAGAGCAGTTAAGTGTCCTCTCA	*HPRT* gene 5'-end DNA amplification (target size: 756bp) / *HPRT* gene 5'-end DNA sequencing
HPRT-5gR	GCGTGACGTAAAGCCGAAC	
HPRT-6F	ACCACAGCACTATTGAGTGAAAC	*HPRT* gene 3'-end DNA amplification (target size: 526 bp)/ *HPRT* gene 3'-end DNA sequencing
HPRT-6R	CCGCCAACCCATTCTACCAC	
GAPDH-RT-F	ACCACAGTCCATGCCATCAC	*GAPDH* RT-PCR/ (target size: 450 bp)
GAPDH-RT-R	CCCCAAAGCACATTTCTTCCATT	
GAPDH-gDNA-F	CCTCAACTACATGGTGAGTGCT	*GAPDH* genomic DNA PCR/ (target size: 248 bp)
GAPDH-gDNA-R	CCCCAAAGCACATTTCTTCCATT	

RESULTS

CRISPR Cas9 Efficiency

We verified the CRISPR Cas9 efficiency using T7 endonuclease I mismatch assay, in which T7 endonuclease can cut mispaired DNA. In this experiment, we nucleoporated cells directly with a ribonucleoprotein (RNP) complex consists of Cas9 protein and single-guide RNAs (positions indicated in figure 3). We chose to introduce the Cas9 protein instead of an expression vector to reduce the time during which Cas9 would be active within cells and therefore increase the chance of monoallelic mutation. Following DNA extraction of each nucleoporated population, DNA surrounding the potential indel was amplified and went through denaturing and reannealing steps to form heteroduplexes of DNA. In the case of a $BCL11B^{+/-}$ heterozygous mutant clone, denaturation/renaturation of the amplified DNA will produce three types of double-stranded DNAs: $BCL11B^{+}/BCL11B^{+}$ (not cleaved by the T7 endonuclease), $BCL11B^{-}/BCL11B^{-}$ (not cleaved by the T7 endonuclease), and $BCL11B^{+}/BCL11B^{-}$ (cleaved by the T7 endonuclease to produce two smaller fragments). The PCR amplification product was then incubated with T7 endonuclease I and the products were separated by gel electrophoresis (Figure 4). Three bands were displayed in figure 4 in all three populations nucleoporated with guide RNAs 1, 2, and 3, meaning that designed sgRNAs are able to guide Cas9 enzyme toward the target sites, making an indel in some cells. After quantifying band intensities in figure 4, indel frequencies were calculated (Table 2), ranging from 11.5% to 19.1 %

Nucleoporation of Cas 9 and *BCL11B* Guide RNAs Generated Stable *BCL11B* Mutants

We used different approaches to confirm *BCL11B* inactivation mutations in our study. First, we performed the T7 endonuclease I mismatch assay on individual cells sorted through FACS (Figure 5). Among individual clones sorted by FACS, clones 101, 202, 203, 201, 211,212, and 213 showed cleaved fragments after electrophoresis, confirming an Indel in mentioned clones. To confirm the monoallelic mutation in *BCL11B* mutants, we used *in vitro* Cas9 nuclease digestion of *BCL11B* PCR amplification products (Figure 6). Clones B101, B306, B201, and B203, showed three bands, confirming monoallelic mutations. In the case of monoallelic mutations, Cas9 enzyme was able to cleave one wild-type allele, producing two small fragments, whereas the previously mutated allele could not be cleaved again (showing as full-length PCR). Clone 102 in figure 6 displays only the full-length PCR amplification product, meaning that both alleles had been previously mutated and were not cleaved again. Results from *in vitro* Cas9 nuclease digestion showed that our strategy to nucleoporate Cas9 protein instead of Cas9 expressing plasmid was successful because 4 out of 5 clones exhibited monoallelic mutation. We selected three clones, B101, B201, and B203, for sequencing analysis, all of which showed deletions leading to frameshifts (Figure 7). Protein analysis using immunoblotting confirmed lower expression of BCL11B protein in B101, B201, and B203 clones (Figure 8). Tubulin antibody was used as a control to confirm that equal amount of proteins was loaded in each lane (Figure 8)

Clonogenic Efficiency Following Ionizing Radiation

Following different radiation levels from 0.5Gy to 2 Gy, clonogenic efficiencies of *BCL11B* $^{+/+}$ and *BCL11B*$^{+/-}$ populations were calculated as explained before. Results are shown in table 3 as well as in figure 9A. In addition, for a better comparison, clonogenic efficiency results of each

BCL11B heterozygous population were illustrated individually compared to that of wild-type in figures 9B, 9C, and 9D. In non-IR cells, clonogenic efficiency was decreased 5 out of 6 times and 4 out of 6 times in B101 and B203 populations compared to TK6 parental (Figure 9B and 9D). However, in the non-IR B201 population, clonogenic efficiency just decreased 2 times out of 4 times (Figure 9C). Previous results in our lab showed that *CUX1* knockdown decreased the clonogenic efficiency of cancer cells that display high ROS levels due to the critical role of CUX1 in alleviating oxidative damages in the cell. (48). For the same reason, *CUX1* knockdown decreased the clonogenic efficiency of all cancer cell lines following radiation. Radiation of TK6 cells following CUX1 down-regulation reproduced the same results (unpublished data). However, clonogenic efficiency following radiation of *BCL11B* mutants showed variable results. In B101 heterozygous irradiated population, clonogenic efficiency decreased 5 out of 8 times (Figure 9B), which is almost similar to B203 clonogenic efficiency results (Figure 9D), 4 times reduction out of 8 times. However, the clonogenic efficiency of B201 was not decreased following radiation. Finally, statistical analysis was performed using the non-parametric Kruskal-Wallis test followed by Dunn's test, which enables us to compare the mean of multiple groups (B101, B201, and B203) with the mean of a control group (TK6 parental). Analysis was performed on non-irradiated and 1Gy, and 2Gy irradiated *BCL11B* heterozygous cells individually because there were multiple replicates for non-IR, 1Gy, and 2 Gy radiation. According to statistical analysis, there is no significant difference between the clonogenic efficiency of $BCL11B^{+/+}$ and $BCL11B^{+/-}$ populations in 0 Gy (Figure 10A), 1Gy (Figure 10B), and 2 Gy (Figure 10C) groups.

BCL11B Loss-of-Heterozygosity Caused variable Mutation Frequency Results Following Ionizing Radiation

Mutation frequency following radiation was quantified using the poisson distribution formula as discussed before (83). Results are shown in table 3 as well as in figure 11A. Furthermore, mutation frequency of each *BCL11B* heterozygous population is shown in individual graphs compared to that of the corresponding TK6 parental cells (Figures 11B, 11C, and 11D). Following radiation, mutation frequency was increased 6 out of 8, 4 out of 5, and 7 out of 8 times in B101, B201, and B203 populations, respectively (Figures 11B, 11C, and 11D). Statistical analysis was performed on mutation frequency of non-irradiated cells as well as 1, and 2 Gy irradiated populations. Due to variation in mutation frequency at various dates, we corrected the numbers of mutants in *BCL11B*$^{+/-}$heterozygous cells as if there were 100 mutants/million in TK6 parental cells. Next, we used the one-sample T-test to perform statistical analysis comparing actual means of *BCL11B*$^{+/-}$ with the theoretical mean of 100. Although there was an increase in mutation frequency of B101, B201, and B203 cells compared with parental in 0 Gy, 1 Gy, and 2 Gy bar charts (Figures 12A, 12B, and 12C), statistical analysis showed the increase is not significant.

Reverse Transcriptase PCR Results of Collected HPRT Mutants Following Ionizing Radiation

After quantifying mutation frequency following radiation, some *HPRT* mutants were collected to analyze the spectrum of mutations. Populations from which *HPRT* mutants were collected are shown with black arrows in figure 11A. Following RNA extraction and cDNA synthesis, samples went through a nested PCR amplification with F1-P1 primers at the first round and F2-

R3 primers at the second round. Images of PCR amplification products are arranged according to the dates on which the experiment was performed. *HPRT* RT-PCR amplification results from experiments 2020/05/05, 2020/10/01, and 2021/04/06 are shown in figures 13, 14, and 15, respectively. Based on the nature of mutations, samples showed full-length PCR amplification products, shorter-length PCR amplification products, multiple PCR amplification products, or no PCR amplification products. Full-length PCR amplification products probably contain point mutations, whereas shorter-length PCR amplification products show either deletion or splicing mutations. Mutants from these two groups were sequenced with F2 and R3 primers to find the exact types of mutations and their location. In addition, bands from multiple PCR amplification products were purified from the gel and were sequenced individually. Finally, samples with no PCR amplification products went through *GAPDH* RT-PCR amplification to ensure the negative results are not due to the bad quality of RNA.

Sequencing Analysis of *HPRT* RT-PCR Amplification Products Following Ionizing Radiation

Full-length and shorter *HPRT* RT-PCR amplification products were sequenced using F2 and R3 primers (primer sequenced are indicated in table 1). In addition, each band from mutants with multiple *HPRT* RT-PCR amplification products was sequenced separately with the same primers. Table 4, showing type of mutation and its effect at the nucleotide level, is inspired by the article from Nicklas et al. in 2015, who did a comprehensive study on the *HPRT* mutation spectrum of American veterans exposed to depleted uranium during the 1991 Gulf war (77). Some mutants originating from the same experiment showed the same mutational pattern. These mutations are probably replicates of a mutation occurring early the in culture. As these early mutants

divided during the seven days incubation required for the *HPRT*$^-$ phenotype expression, the same mutations were identified repeatedly. Name of replicated mutants are shown in the same cells. Figure 21 shows positions of mutations on *HPRT* mRNA and protein in the case of mutants that generated a positive result in *HPRT* RT-PCR amplification. Types of mutation are indicated as complex (C), one nucleotide deletion (F-1), splicing (S), nonsense (N), missense (M), out-of-frame deletion (OFD), and in-frame deletion (IFD). There were some silent mutations (indicated by Si in red color) in sequencing analysis; however, those mutants were selected due to other mutational events indicated in the same cell in table 4 (such as P-IR-14 and P-IR-23).

GAPDH Reverse Transcriptase PCR Amplification Confirmed High Quality of Synthesized cDNAs

GAPDH PCR was performed to ensure that negative *HPRT* RT-PCR amplification results of mutants following radiation are not due to the cDNA or RNA being of bad quality or not being abundant enough. *GAPDH* PCR amplification using GAPDH-gDNA-F and GAPDH-gDNA-R confirmed the high quality of synthesized cDNAs (Figure 16).

Genomic PCR Results Amplifying *HPRT* 5'- and 3'- Ends in *HPRT* Mutants Following Ionizing Radiation

Several *HPRT* mutants did not show any band following *HPRT* RT-PCR amplification (Figures 13, 14, and 15). The absence of *HPRT* mRNA could be due to a large genomic deletion or a mutation in promoter sequences, or polyadenylation site. Therefore, we investigated the integrity of the HPRT gene by performing PCR amplifications to analyze the 5' and 3' portions of the gene, using HPRT-5gF and HPRT-5gR primers and HPRT-6F and HPRT-6R primers, respectively. Figures 17, 18 and 19 show the results of *HPRT* genomic PCR amplifications of mutants from TK6 parental,

B101 and B203 populations, respectively. Mutants showing neither extremities or one of the extremities must have suffered a large deletion, whereas mutants with both ends of the gene may have a mutation in promoter sequences, the polyadenylation site or other more distant regulatory sequences. Therefore, PCR amplification products from the latter category were sequenced, but no mutation was detected in neither *HPRT* gene 3'- nor 5'- ends. *GAPDH* genomic DNA PCR was carried out on mutants with no *HPRT* genomic DNA PCR amplification products to ensure that negative results are not due to the bad quality of extracted genomic DNAs.

GAPDH Gene PCR Amplification Confirmed High Quality of Extracted Genomic DNAs Following Ionizing Radiation

GAPDH genomic DNA PCR amplification was performed on mutants that did not show any *HPRT* genomic DNA PCR amplification products, to ensure that negative results are not due to the poor quality of genomic DNAs. The presence of the expected *GAPDH* genomic DNA fragment in each case confirmed the good quality of the genomic DNA (Figure 20).

Analysis of Mutations Following Ionizing Radiation

We categorized mutants following irradiation based on sequencing analysis of *HPRT* RT-PCR amplification products and results from *HPRT* gene PCR amplification (Table 5A). Mutants with point mutations are those with full-length PCR amplification products showing complex, one base pair deletion, out-of-frame deletion, out-of-frame insertion, missense, or nonsense mutations (Table 5B). The mutational event in shorter-length PCR amplification products that missed one or two exon(s) is considered to be a point mutation in a splice donor or acceptor site, leading to an alternative splicing event (85). However, mutants B203-IR-11 and B101-IR 4

showed a shorter-length PCR amplification product which was due to a large genomic deletion and not a splicing mutation. In addition, we interpret that a large genomic deletion occurred in mutants that lack the *HPRT* gene 5'-end or 3'-end of both. However, we could not define the type of mutation in mutants whose intact *HPRT* gene 5'- and 3'- ends were analyzed by DNA sequencing and did not include any mutation. These mutants could be the result of a mutation in distant regulatory sequences that our *HPRT* genomic DNA analysis did not cover (86,87). Although we sequenced individual bands from some mutants with multiple PCR amplification products, we cannot specify the exact type of mutation in this category, which could be due to a point mutation (88-90) or multiple *HPRT* mutants growing in the same well. Finally, poor sequencing results were obtained for a small number of mutants.

BCL11B Loss-of-Heterozygosity does not Affect Clonogenic Efficiency in the Fluctuation Assay

In the fluctuation assay, clonogenic efficiencies were calculated in TK6 parental, B101, and B203 parallel cultures (Figure 22 and Table 6). Each point in figure 22 represents the clonogenic efficiency of an independent population, and the mean is indicated with black lines. According to the clonogenic efficiency graph, we cannot conclude that *BCL11B* loss-of-heterozygosity increase or decrease the clonogenic efficiency in TK6 cells in the fluctuation assay because the clonogenic efficiency of B101 cells was decreased, whereas that of B203 cells was increased.

BCL11B Loss-of-Heterozygosity Increased the Mutation Rate in the Fluctuation Assay

Mutation rate was calculated according to the method developed by Luria and Delbruck (78,81) in $BCL11B^{+/+}$ TK6 parental cells and heterozygous $BCL11B^{+/-}$ B101 and B203 cells (Figure 23 and

Table 7). Mutation rate in the fluctuation assay was increased approximately two-fold in both *BCL11B* $^{+/-}$ cell clones compared to wild-type population.

Reverse Transcriptase PCR Amplification of Collected *HPRT* Mutants in the Fluctuation Assay

After quantifying mutation rate in the fluctuation assay, we collected one to three spontaneous *HPRT* mutants from different mutation rate plates. Following RNA extraction and cDNA synthesis, samples went through a nested PCR amplification with F1-P1 primers at the first round and F2-R3 primers at the second round (Figure 24). Based on the nature of mutations, samples showed full-length PCR amplification products, shorter-length PCR amplification products, multiple PCR amplification products, or no PCR amplification products. Full-length PCR amplification products probably contain point mutations, whereas shorter-length PCR amplification products show either deletion or splicing mutations. Mutants from these two groups were sequenced with F2 and R3 primers to find the exact types of mutations and their location. In addition, bands from multiple PCR amplification products were purified from the gel and were sequenced individually. Finally, samples with no PCR amplification products went through *GAPDH* RT-PCR amplification to ensure the negative results are not due to the bad quality of RNA

Sequencing Analysis of *HPRT* RT-PCR Amplification Products in the Fluctuation Assay

As it was explained in the analysis of *HPRT* RT-PCR amplification products following radiation, we analyzed sequencing results of mutants with positive *HPRT* RT-PCR amplification products in the fluctuation assay. Type of mutations and the corresponding effect on the protein are shown in table 8, while positions of mutants are indicated in figure 28. No silent mutation was found

in mutants originating from the fluctuation assay. Multiple mutants were collected from the same individual cultures such as B203-7-1, B203-7-2, and B203-7-3, which are three mutants collected from the B203 population number 7. We interpret that these mutants showed the same mutation because they originated from one mutational event that occurred early in culture. However, some mutants from the same individual culture, such as B203-26-1 and B203-26-2, harboured different mutations, meaning that they originated from two mutational events. Having said that, these sequencing results do not affect the mutation rate calculation since we only consider the number of populations without mutants in the mutation rate formula (Figure 23).

GAPDH Reverse Transcriptase PCR Confirmed High Quality of Synthesized cDNAs of Mutants in the Fluctuation Assay

We performed *GAPDH* RT-PCR amplification for the *HPRT* mutants with no *HPRT* RT-PCR amplification product. The results confirmed the good quality of RNAs and cDNAs (Figure 25).

Genomic PCR Amplification of the *HPRT* gene 5'- and 3'- Ends in the Fluctuation Assay

No HPRT RT-PCR amplification products were obtained for some *HPRT* mutants. We therefore purified the genomic DNA and performed PCR amplification to investigate the integrity of the *HPRT* gene at its 5'- and 3'- ends (Figure 26). As mentioned before, mutants with no *HPRT* genomic PCR amplification products or either 5'- or 3'- extremities were considered to have a large genomic deletion. However, there was just one mutant, B203-1-1, which showed both *HPRT* 5'- and 3'- genomic ends. Both PCR amplification products were subjected to sequencing and did not show any mutation. Mutants with neither *HPRT* 5'- nor 3'- genomic ends underwent *GAPDH* genomic PCR to check the DNA quality.

GAPDH Gene PCR Amplification Confirmed High Quality of Extracted Genomic DNAs in the Fluctuation Assay

GAPDH gene PCR amplification confirmed the high quality of genomic DNAs (Figure 27), indicating that negative results in amplifying *HPRT* 5'- and 3'- genomic ends were not due to the poor quality of DNA.

Analysis of Mutations in the Fluctuation Assay

Based on sequencing analysis of *HPRT* cDNAs and genomic sequences at the 5'- and 3'- ends of the gene, we categorized mutants in the fluctuation assay after removing replicates (Table 9A). All mutants with full-length or shorter-length *HPRT* RT-PCR amplification products were considered to have point mutations, either one base pair deletion, out-of-frame deletion, missense, and splicing (Table 9B). As discussed before, we were not able to define the type of mutation in mutants with multiple PCR amplification products and mutant with both *HPRT* 5'- and 3'- genomic DNA PCR amplification products (B203-1-1). However, mutants with negative results for one or both sides of the *HPRT* genomic DNA were interpreted as large genomic deletions.

FIGURES

Figure 3: Schematic Representation of *BCL11B* Genomic DNA and Guide RNA Positions in CRISPR-Cas9 Experiments

The *BCL11B* gene located on the human chromosome 14 has four exons. There are four transcript variants. Variant 1 encodes the longest isoform. Variant 3 uses an alternative in-frame splicing junction at the 5'-end of an exon, making it one amino acid shorter than variant

1. Variant 2 lacks an alternative in-frame exon (exon 3) compared to variant 1. Variant 4 has an alternative in-frame splicing junction at the 5'-end of an exon, removing one amino acid as compared to variant 2. All variants have the same N- and C-termini and contain the second exon. Guide RNAs were designed to target the second exon using *CRISPOR* and IDT's *CRISPR-Cas9 guide RNA design* checker.

* Number 1 corresponds to the first base of the first *BCL11B* exon.

Figure 3: Schematic Representation of *BCL11B* Genomic DNA and Guide RNA Positions in CRISPR-Cas9 Experiments

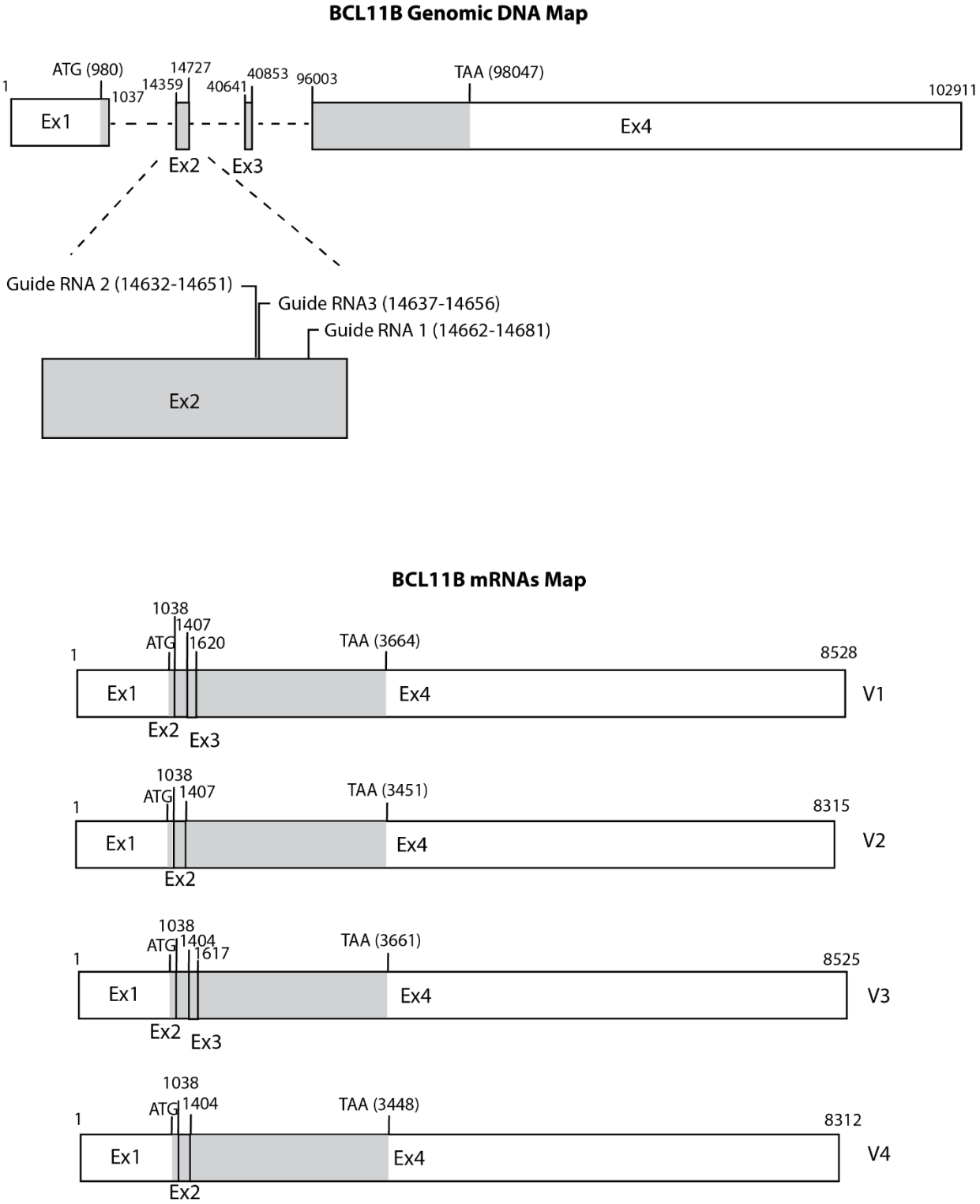

Figure 4: T7 Endonuclease I Mismatch Assay on Cas9-Treated TK6 Bulk Populations

Indel frequency was calculated using the T7 endonuclease I mismatch assay. Following nucleoporation, genomic DNA was purified from the cell population and a fragment of the *BCL11B* gene encompassing the targeted sequence was amplified using BCL11B long F1 and BCL11B long R primers (indicated in table 1). Next, PCR amplification products underwent denaturing and reannealing steps before incubation with the T7 endonuclease I enzyme. Cleaved fragments were visualized after DNA electrophoresis on 7% agarose gel, which confirms the presence of an indel in all three populations. Band intensities were estimated using ImageJ software to calculate the indel frequency in table 2.

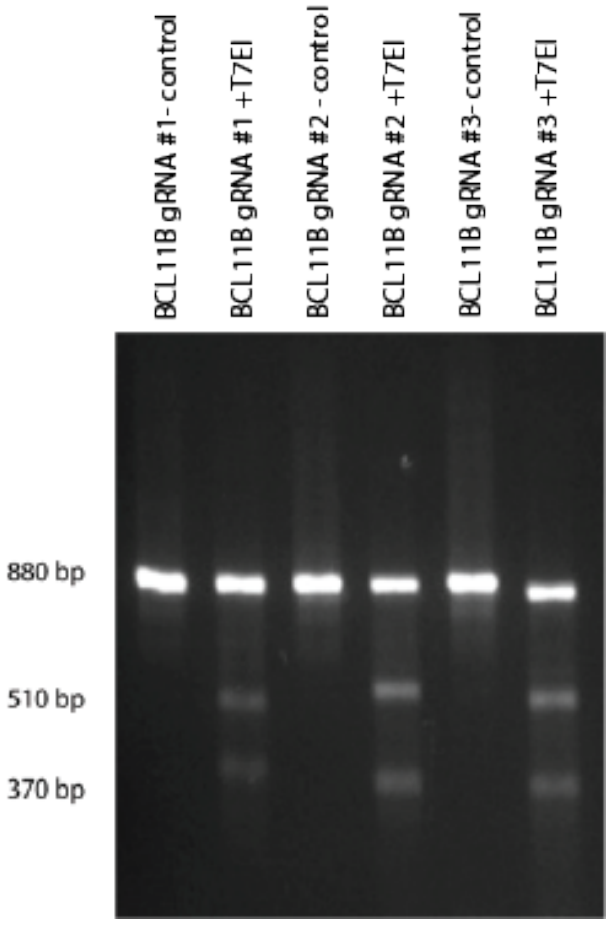

Figure 5: T7 Endonuclease I Mismatch Assay on Individual *BCL11B* Mutant Clones

Following fluorescence-activated cell sorting (FACS), genomic DNA was purified from individual clones and the T7 endonuclease I mismatch assay was performed to confirm the presence of indels in cells from each clone. A fragment of the *BCL11B* gene encompassing the targeted sequence was amplified using BCL11B long F1 and BCL11B long R primers (indicated in table 1). The DNA was denatured and renatured and then subjected to T7 endonuclease I following denaturing and reannealing steps. Cleaved fragments were identified in clones 101, 202, 203, 201, 211,212 and 213 on 7% agarose gel following DNA electrophoresis.

Figure 5: T7 Endonuclease I Mismatch Assay on Individual *BCL11B* Mutant Clones

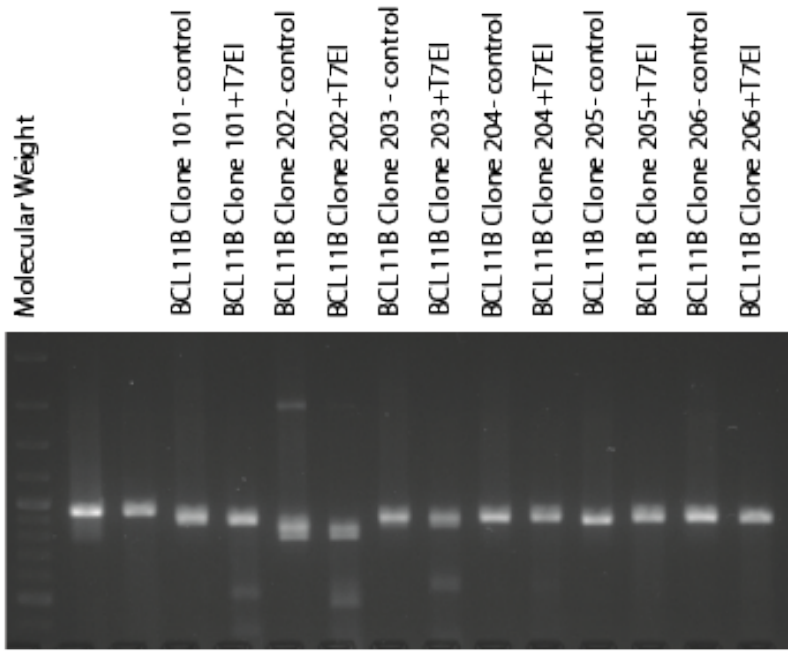

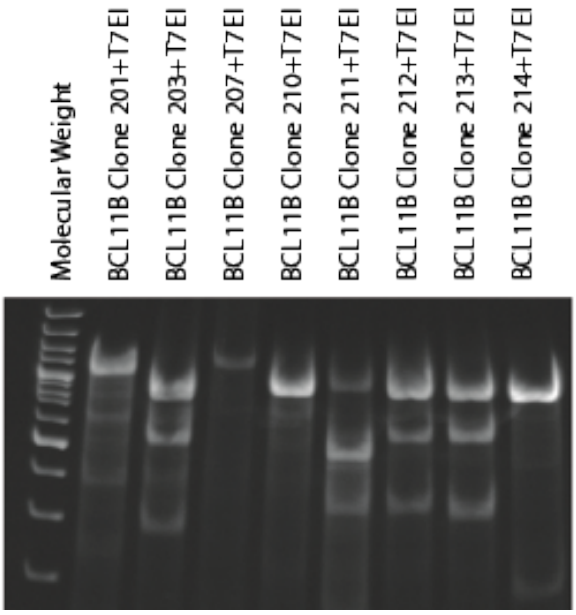

Figure 6: *In Vitro* Cas9 Nuclease Digestion of *BCL11B* PCR Amplification Products

Following fluorescence-activated cell sorting (FACS), *in vitro* Cas9 Nuclease Digestion on *BCL11B* PCR amplification products was performed to distinguish monoallelic and bi-allelic *BCL11B* inactivation. A fragment of the *BCL11B* gene encompassing the targeted sequence was amplified using *BCL11B* long F1 and *BCL11B* long R primers. Purified Cas9 nuclease and gRNA were annealed *in vitro* by incubating them at 37°C for 5 min. Next, Cas9/sgRNA mix was incubated with *BCL11 B* PCR amplification product for one hour at 37°C followed by heating up to 80°C. The reaction products were separated by DNA electrophoresis using a 7% agarose gel. Clones with monoallelic *BCL11B* inactivation would show three bands, whereas those with biallelic inactivation would demonstrate only the full-length PCR amplification product. Finally, clones with two cleaved fragments represent wild-type cells.

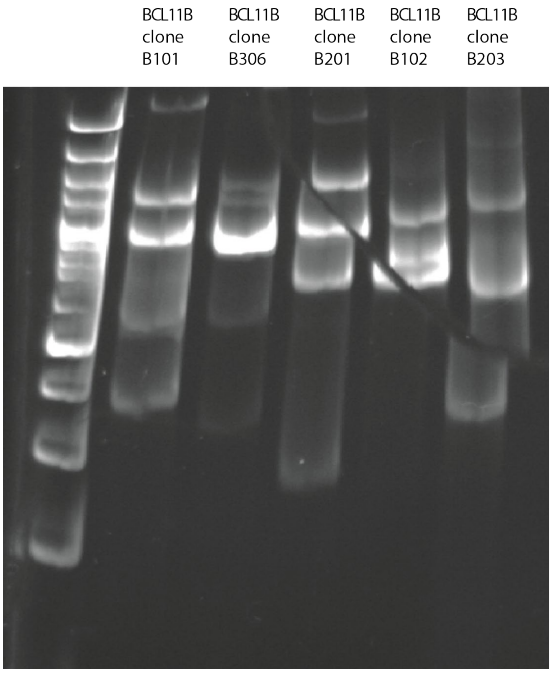

Figure 7: Sequencing Analysis of *BCL11B* Altered Alleles

After amplification of *BCL11B* genomic DNA using BCL11B long F1 and BCL11B long R (indicated in table 1), PCR amplification products of clones B101, B201, and B203 were sequenced to identify the length and position of the indel site. Deletions of 16, 1, and 88 base pairs were found in clones B101, B201, and B203, all of which leading to a frameshift mutation followed by a new stop codon somewhere downstream in the new frame. Deleted nucleotides are shown in red.

Figure 8: Immunoblotting of BCL11B Proteins in *BCL11B*$^{+/-}$ Heterozygous Clones

Following nuclear protein extraction of TK6 parental, B101, B201, and B203 clones, samples were submitted to immunoblotting analysis using the indicated antibodies. TK6 parental cell shows a stronger expression of BCL11B protein at 117kDa than B101, B201 and B203. Immunoblotting result confirmed the successful *BCL11B* single allele inactivation using CRISPR-Cas9 approach

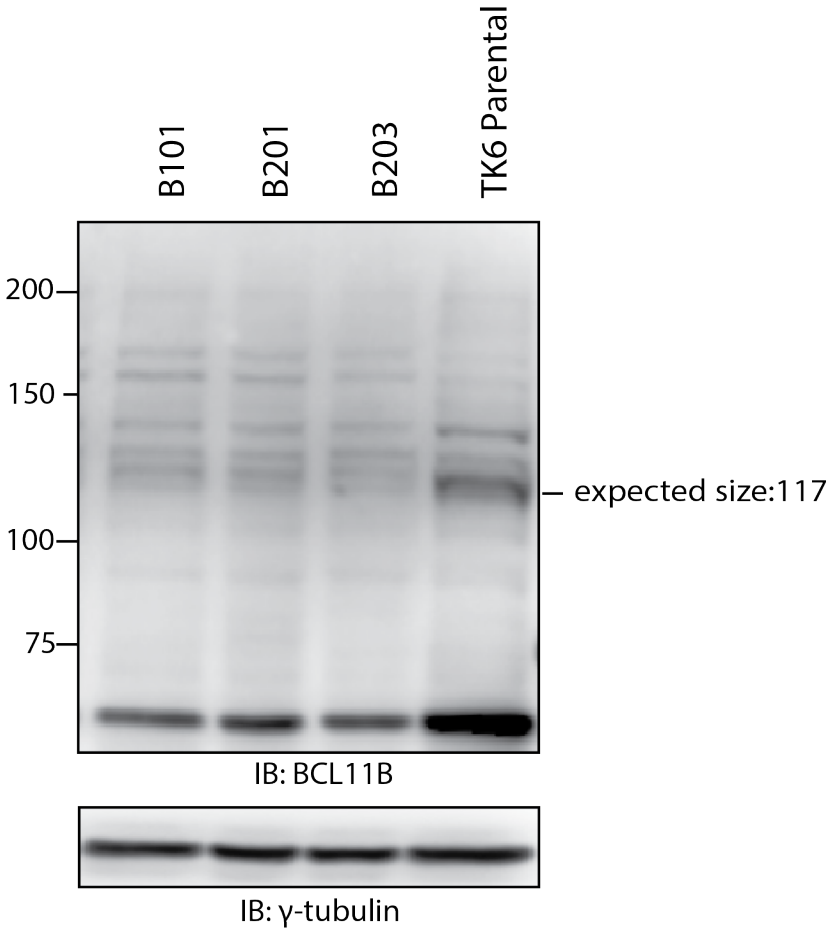

Figure 9: Clonogenic Efficiency Following Ionizing Radiation

Immediately after radiation, cells were plated for clonogenic efficacy at low density, 2 cells/well in two 96-well plates (total = 192 wells). Following two weeks of incubation, the number of wells with proliferating cells was counted to determine the clonogenic efficiency. Clonogenic efficiency percentages were calculated using the equation:

$CE = 1/D_0 \times -\ln(X_0/N_0) \times 100$, where D_0 is the number of cells plated per well (2), X_0 is the number of wells without colonies and N_0 is the number of wells plated in total (192). Y-axis indicated the clonogenic efficiency percentage, whereas radiation level and names of clones were specified on the X-axis. White, light gray, dark gray, and black bars represent TK6 parental, B101, B201, and B203 cells.

Figure A displays the clonogenic efficiency results of TK6 parental cells and three *BCL11B* heterozygous clones following exposure to different radiation levels at different times.

Figures B, C, and D illustrate the clonogenic efficiency results of individual *BCL11B* heterozygous clones (B101, B201, and B203) compared to parental cells.

Figure 9: Clonogenic Efficiency Following Ionizing Radiation

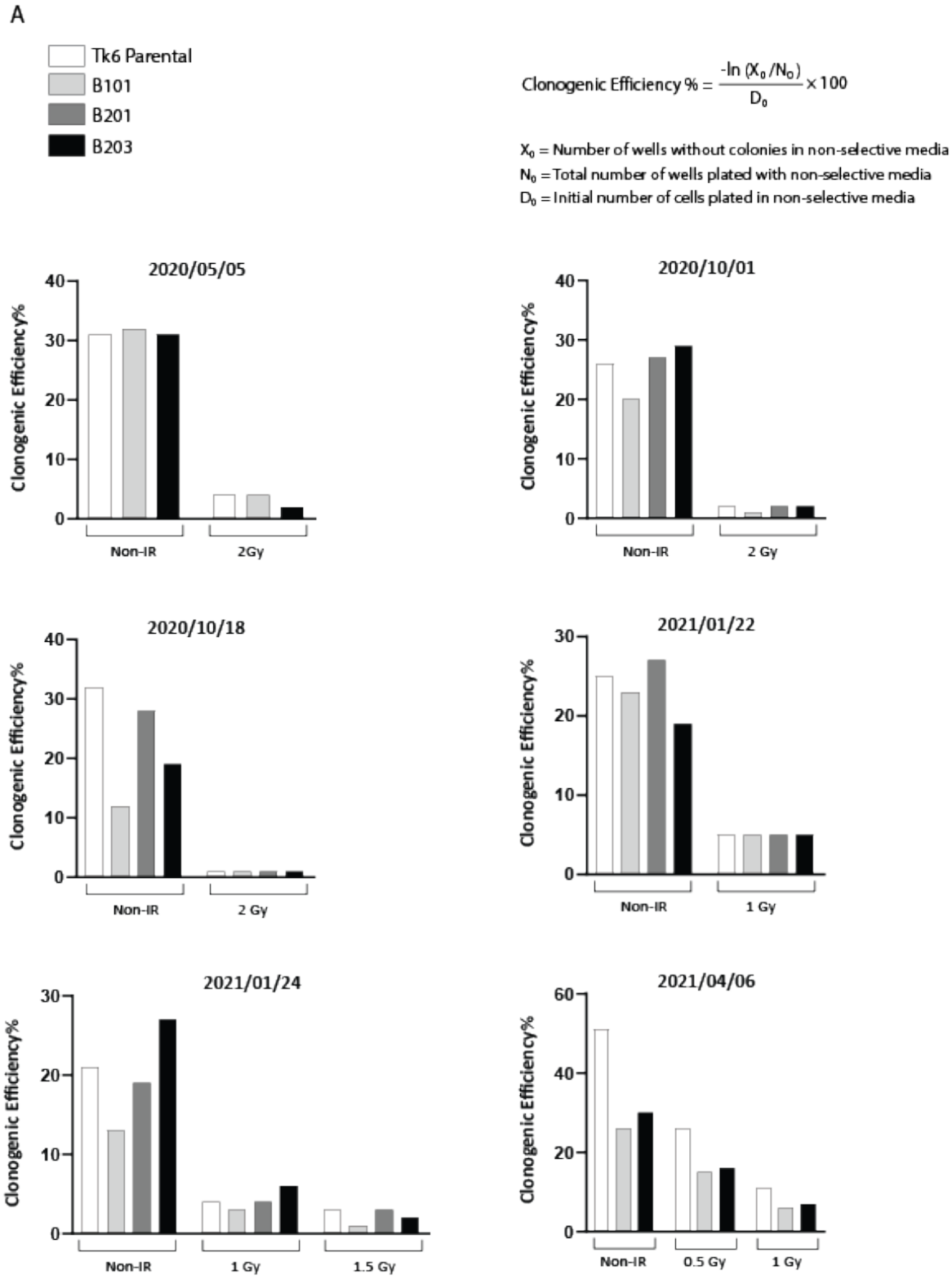

Figure 9: Clonogenic Efficiency Following Ionizing Radiation

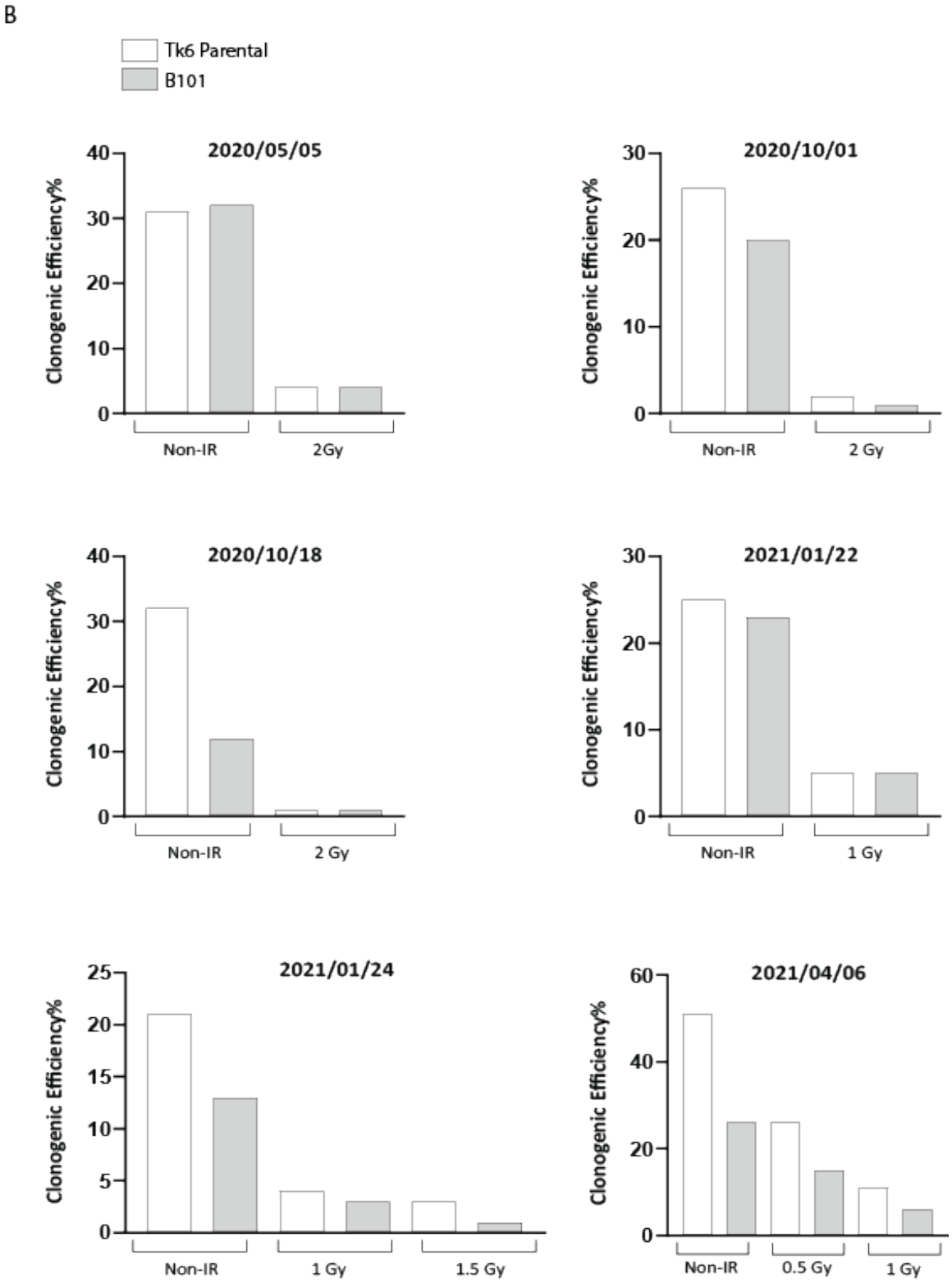

Figure 9: Clonogenic Efficiency Following Ionizing Radiation

C

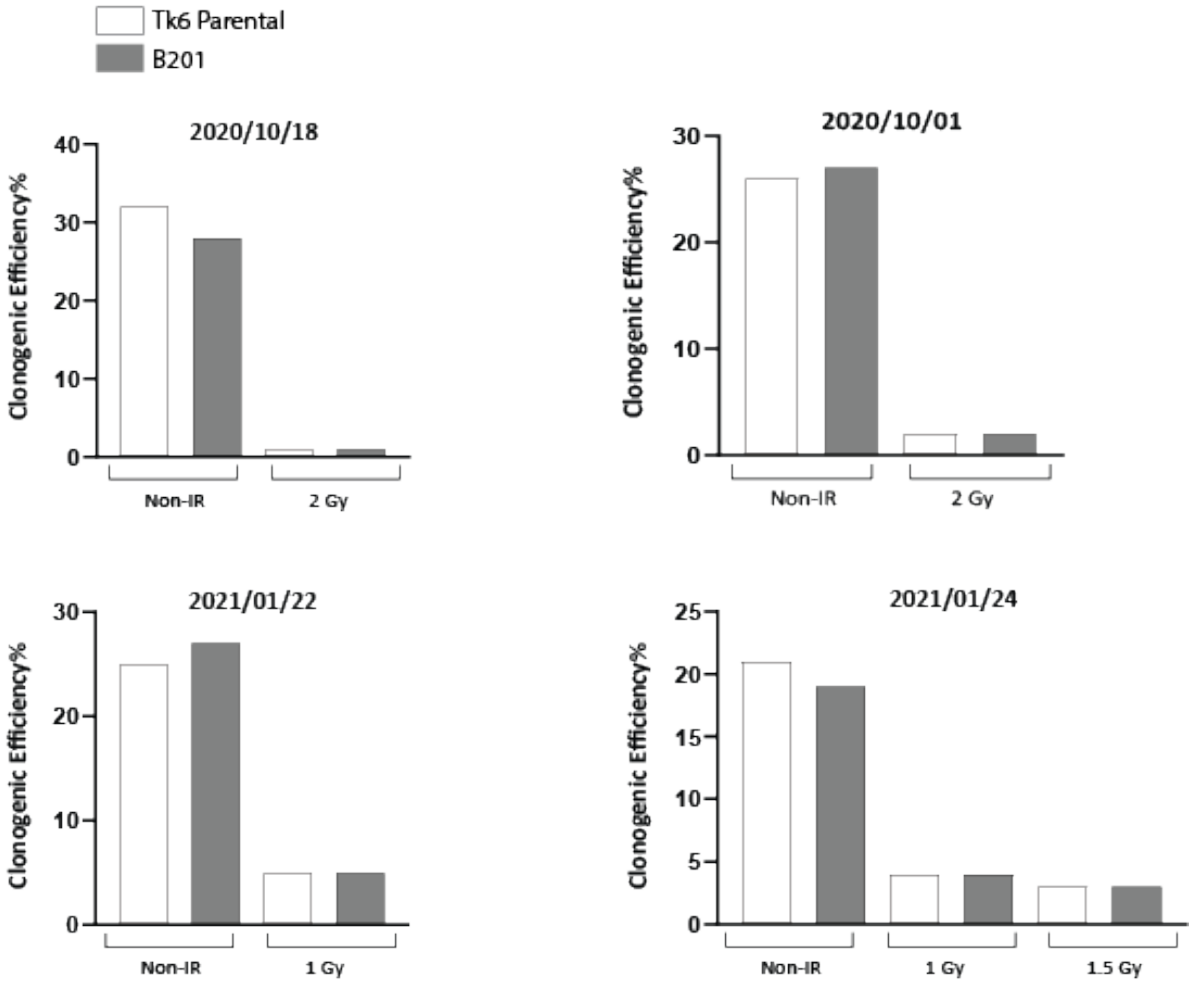

Figure 9: Clonogenic Efficiency Following Ionizing Radiation

D

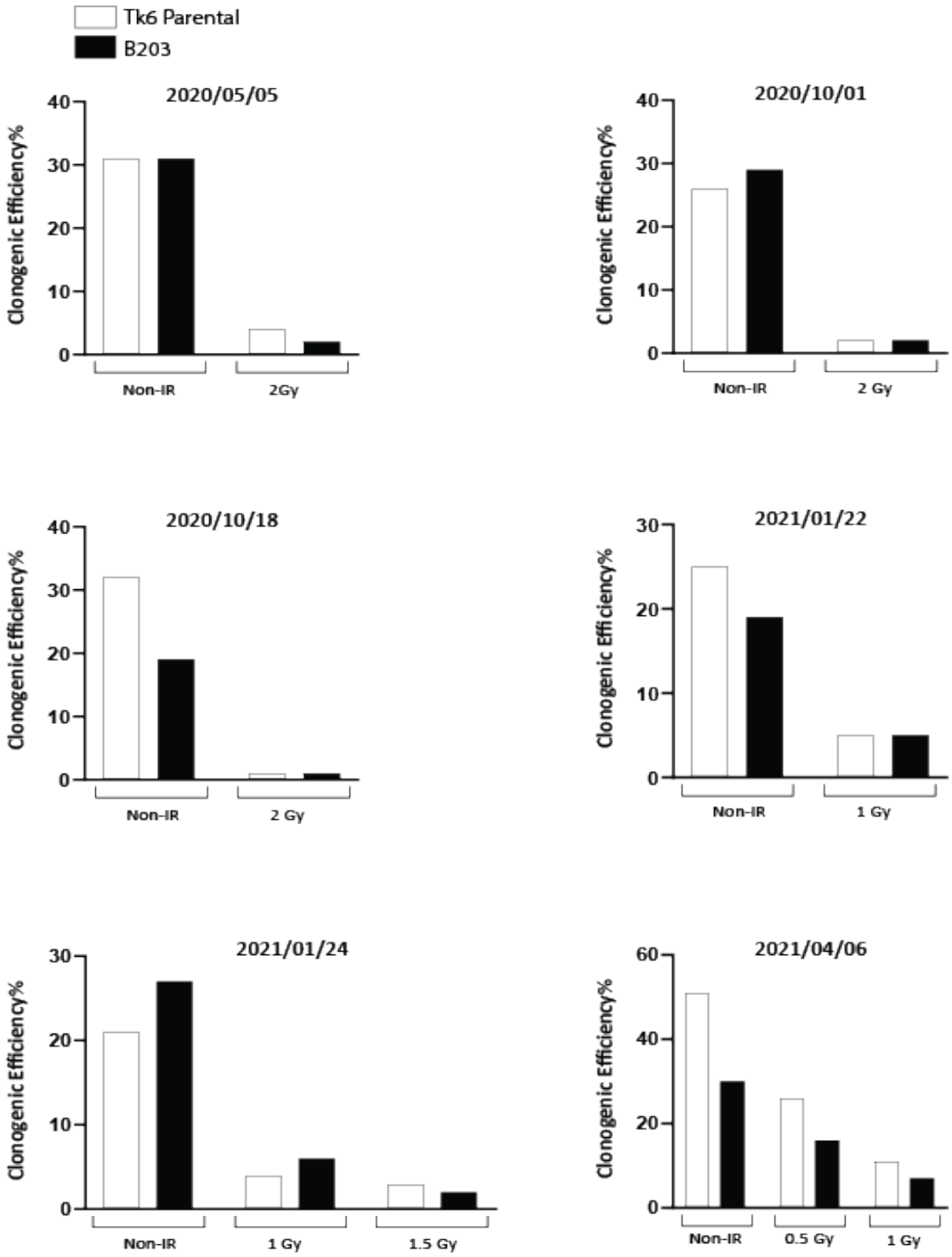

Figure 10: Statistical Analysis of Clonogenic Efficiency in 0, 1, and 2Gy Populations

The following image shows clonogenic efficiency results of all non-IR samples and clonogenic efficiency results following 1Gy (from experiments on 2021/01/22, 2021/01/24, and 2021/04/06) and 2 Gy (from experiments on 2020/05/05, 2020/10/01, and 2020/10/18) radiation and corresponding statistical tests. We used the non-parametric Kruskal-Wallis test followed by Dunn's test to compare clonogenic efficiency of *BCL11B* heterozygous cells with that of TK6 parental. According to the statistical test result, there is no significant difference between the clonogenic efficiency of B101, B201, and B203 compared to parental without radiation and following 1 and 2 Gy radiation.

Figure 10: Statistical Analysis of Clonogenic Efficiency in 0, 1, and 2Gy Populations

Gy

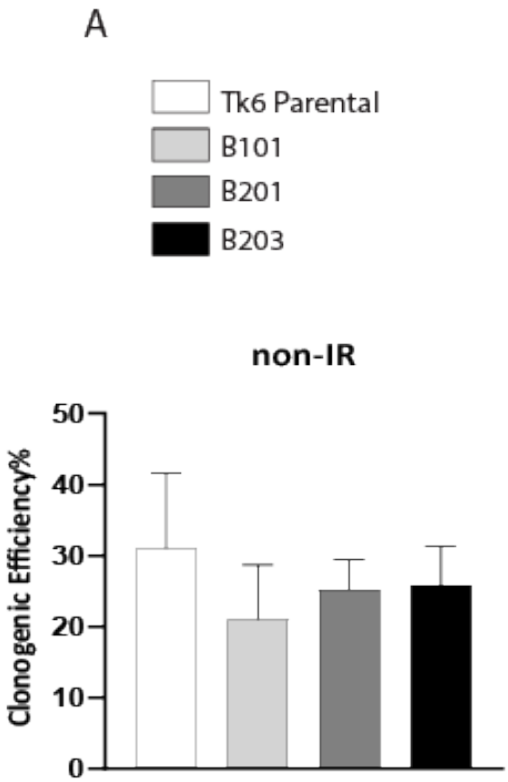

Kruskal-Wallis test	
P value	0.3662
Exact or approximate P value?	Exact
P value summary	ns
Do the medians vary signif. (P < 0.05)?	No
Number of groups	4
Kruskal-Wallis statistic	3.17

Dunn's multiple comparisons test	Mean rank diff.	Significant?	Summary	Adjusted P Value
Parental vs. B101	6.583	No	ns	0.2345
Parental vs. B201	3.333	No	ns	>0.9999
Parental vs. B203	2.5	No	ns	>0.9999

Figure 10: Statistical Analysis of Clonogenic Efficiency in 0, 1, and 2Gy Populations

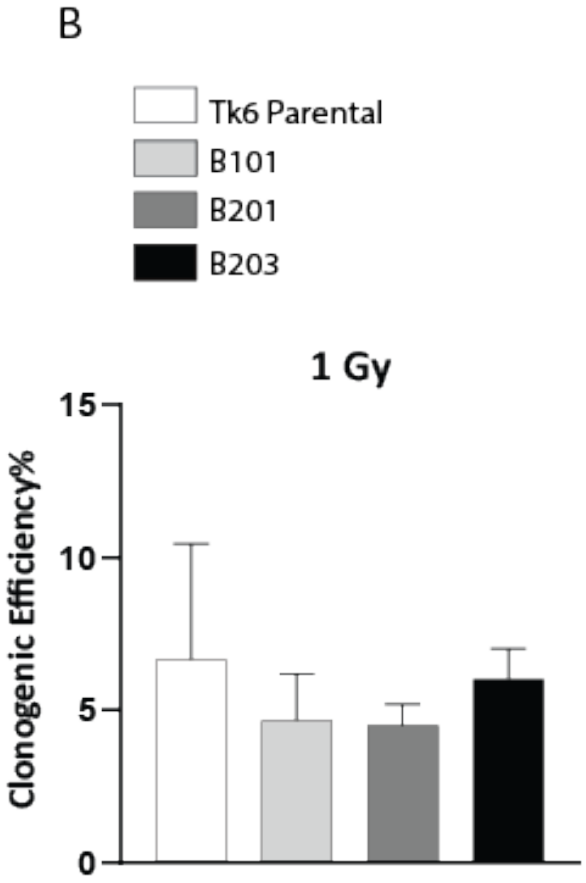

Kruskal-Wallis test	
P value	0.5875
Exact or approximate P value?	Exact
P value summary	ns
Do the medians vary signif. (P < 0.05)?	No
Number of groups	4
Kruskal-Wallis statistic	2.244

Dunn's multiple comparisons test	Mean rank diff.	Significant?	Summary	Adjusted P Value
Parental vs. B101	1.333	No	ns	>0.9999
Parental vs. B201	2.333	No	ns	>0.9999
Parental vs. B203	-1.667	No	ns	>0.9999

Figure 10: Statistical Analysis of Clonogenic Efficiency in 0, 1, and 2Gy Populations

C

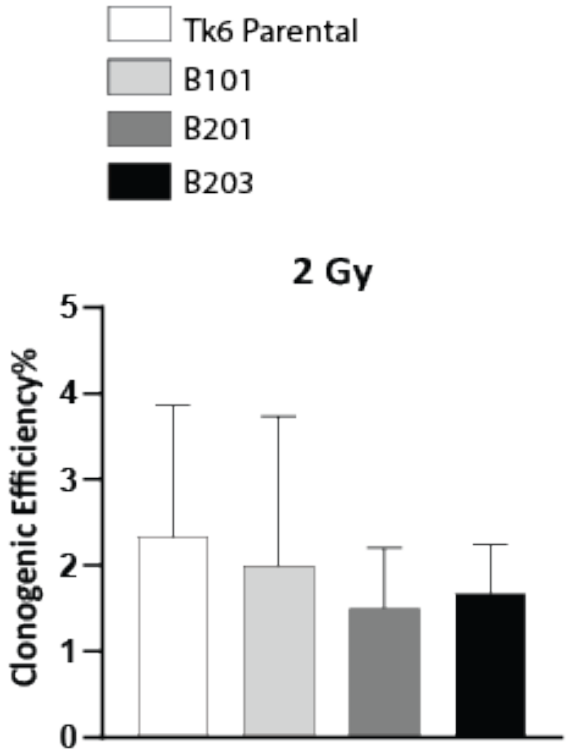

Kruskal-Wallis test	
P value	0.9766
Exact or approximate P value?	Exact
P value summary	ns
Do the medians vary signif. (P < 0.05)?	No
Number of groups	4
Kruskal-Wallis statistic	0.5159

Dunn's multiple comparisons test	Mean rank diff.	Significant?	Summary	Adjusted P Value
Parental vs. B101	1.5	No	ns	>0.9999
Parental vs. B201	1.75	No	ns	>0.9999
Parental vs. B203	1	No	ns	>0.9999

Figure 11: Mutation Frequency Following Ionizing Radiation

To calculate mutation frequency, cells were maintained in culture for seven days post-radiation to allow the phenotype expression of *HPRT* mutations. Following seven days of incubation, 40000 cells/well were plated with 6-thioguanine in two 96-well plates and maintained in culture for approximately 21 days. After determining positive wells in selective medium, the mutation rate was calculated using the equation:

$MF = -\frac{\ln(X_S/N_S)}{CE \times D_S}$, where X_S is the number of negative wells, N_S is the total number of wells (192) and D_S is the initial number of cells (40000) plated in the selective medium. While the Y-axis displays the number of mutants per one million cells, the X-axis indicates the name of samples with the corresponding radiation level.

Figure A displays the mutation frequency results of TK6 parental cells and three *BCL11B* heterozygous clones following different radiation levels at different times. Several mutants were collected to study the spectrum of mutations. Arrows indicate groups from which mutant were collected: 10, 21, and 23 mutants from TK6 Parental, B101 and B203 samples of experiment on 2020/05/05, 29 and 62 mutants from TK6 Parental and B101 samples of experiment on 2020/10/01 and 22, 20, and 21 mutants from TK6 Parental, B101 and B203 samples of experiment on 2021/04/06.

Figures B, C, and D show the mutation frequency results of individual *BCL11B* heterozygous clones compared to parental.

Figure 11: Mutation Frequency Following Ionizing Radiation

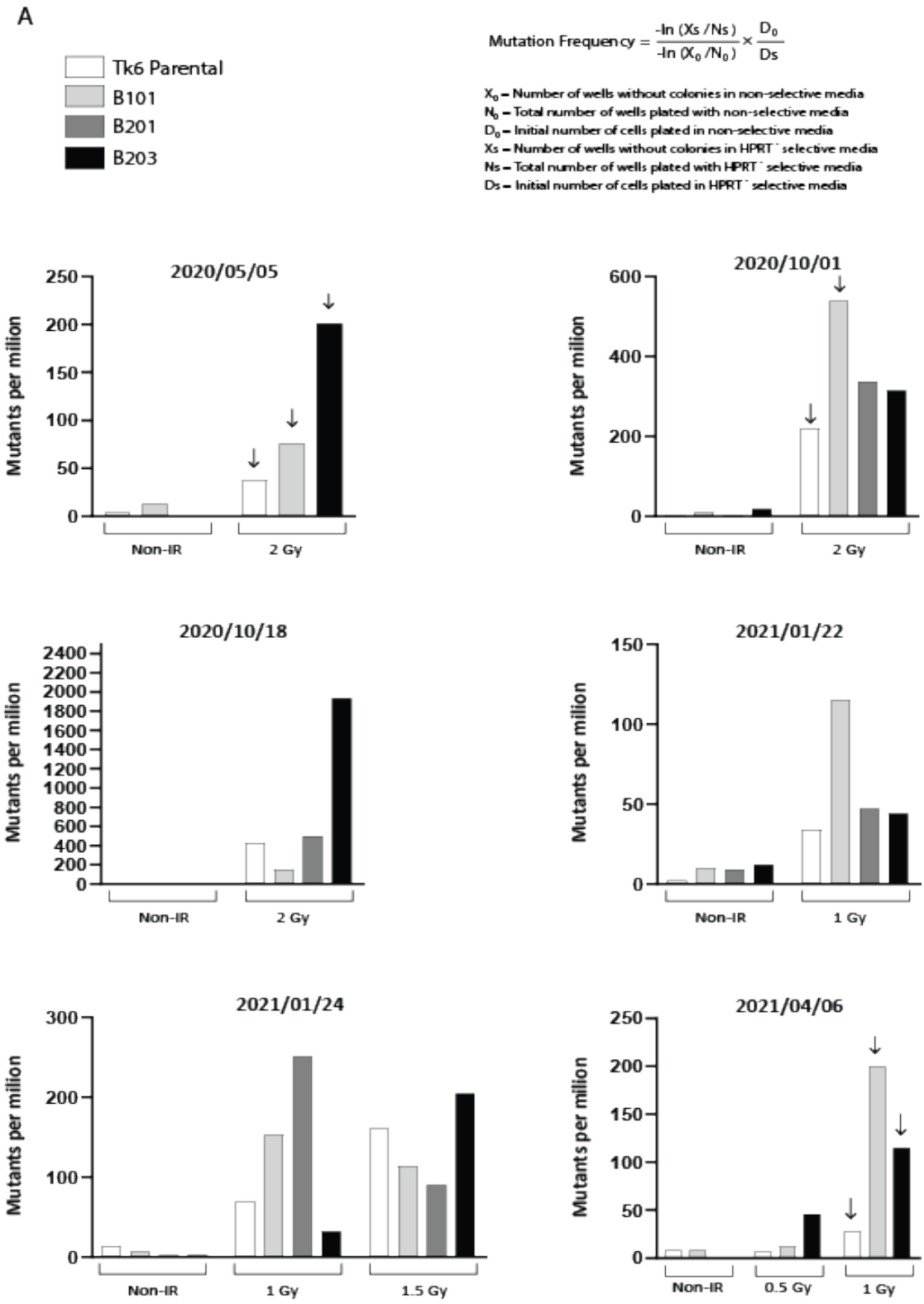

Figure 11: Mutation Frequency Following Ionizing Radiation

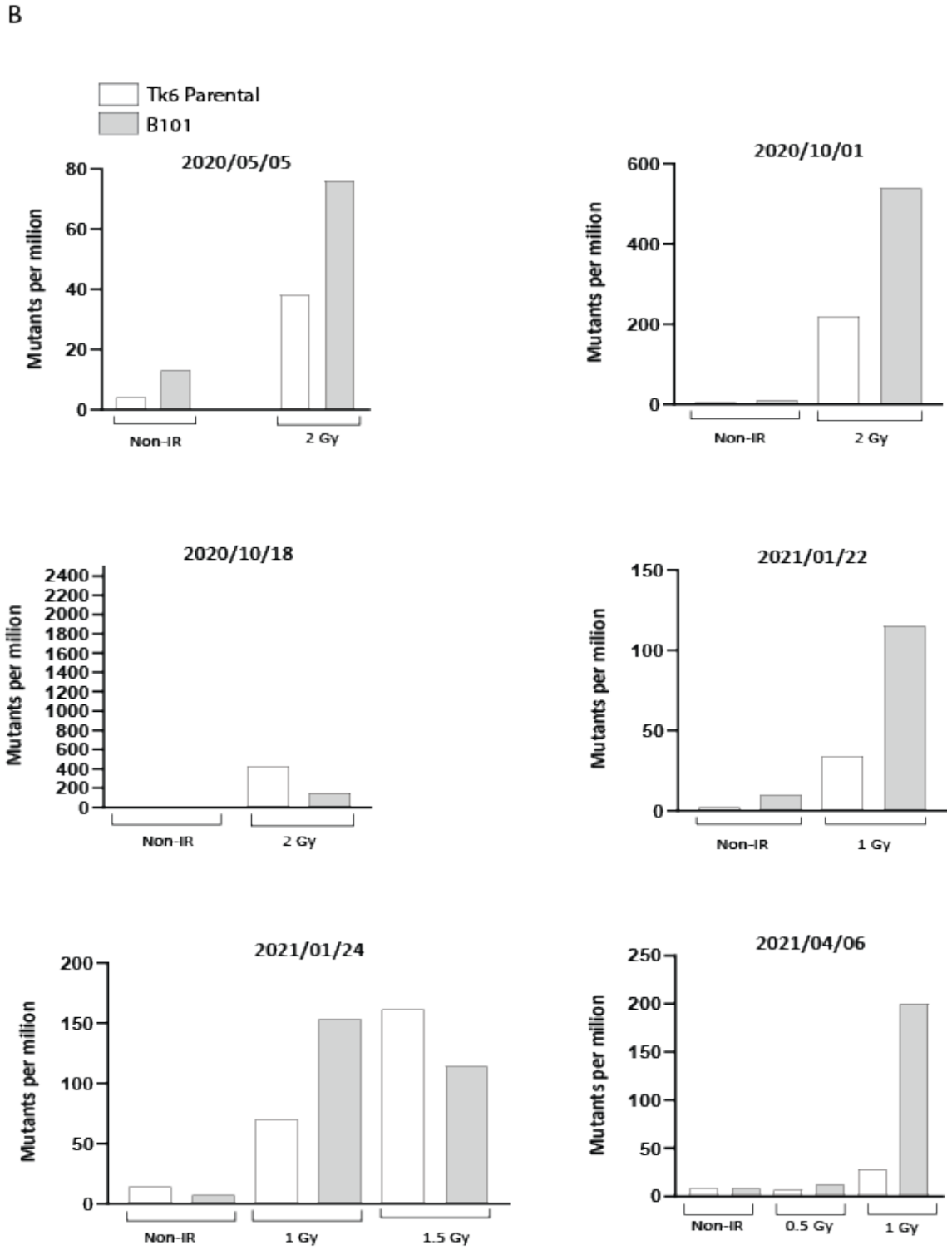

Figure 11: Mutation Frequency Following Ionizing Radiation

C

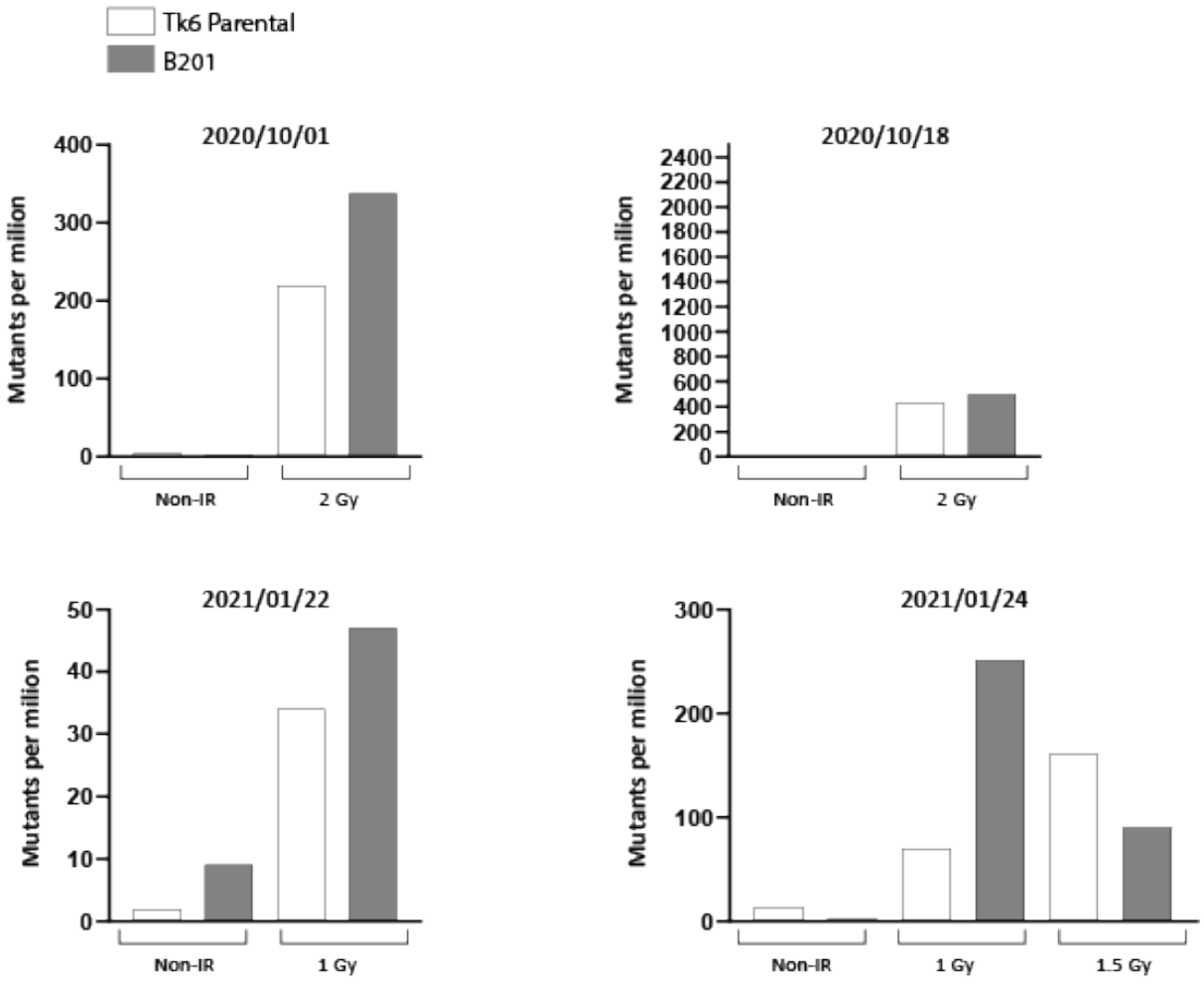

Figure 11: Mutation Frequency Following Ionizing Radiation

D

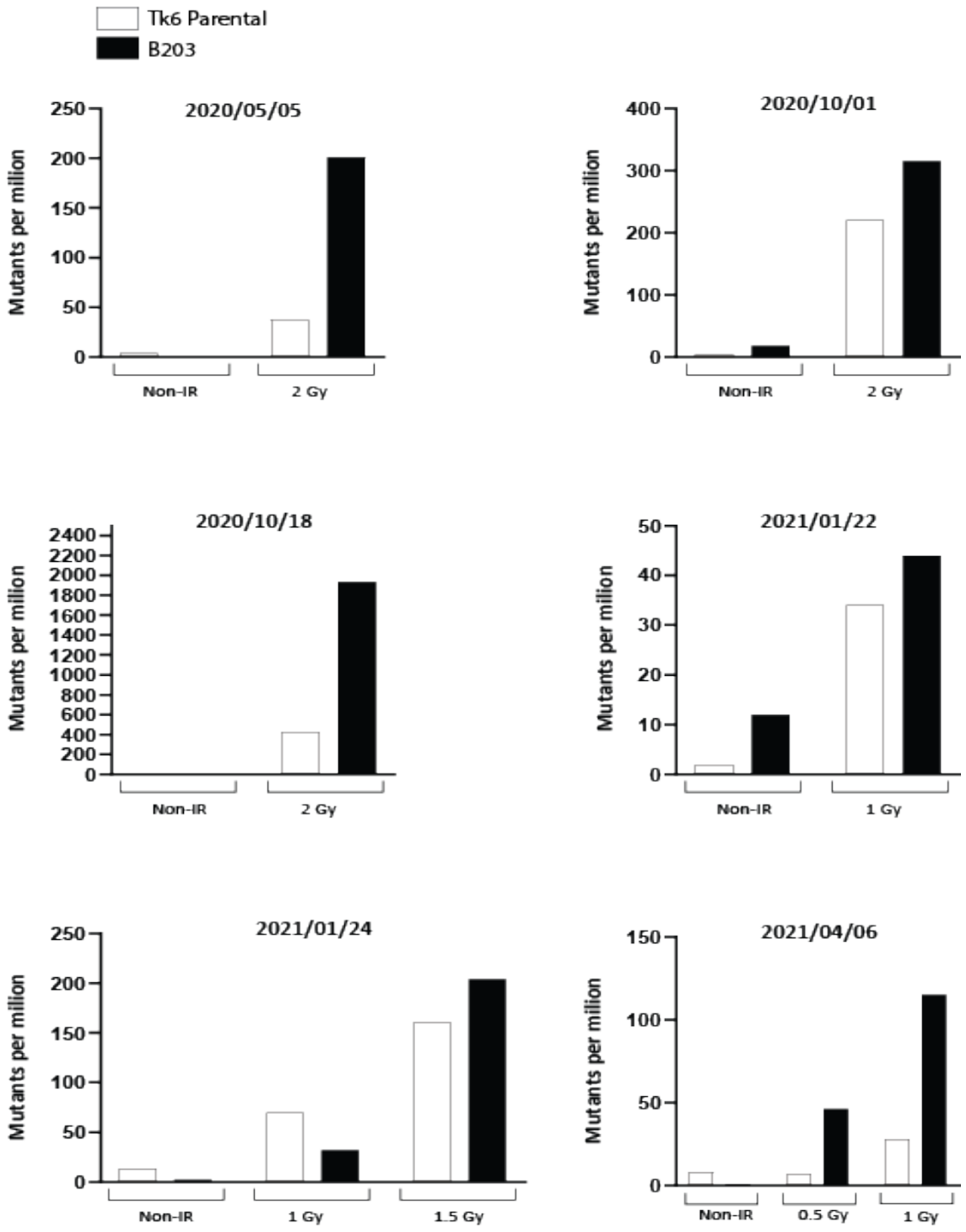

Figure 12: Statistical Analysis of Mutation Frequency in 0, 1, and 2Gy Populations

The following image shows mutation frequency results of non-irradiated cells, and following 1Gy (from experiments on 2021/01/22, 2021/01/24, and 2021/04/06) and 2 Gy (from experiments on 2020/05/05, 2020/10/01, and 2020/10/18) radiation and corresponding statistical tests. Due to variation in mutation frequency at various dates, we corrected the numbers of mutants in *BCL11B*$^{+/-}$heterozygous cells as if there were 100 mutants/million in TK6 parental cells. Next, we used the one-sample T-test to perform statistical analysis comparing actual means of *BCL11B*$^{+/-}$ heterozygous cells with the theoretical mean of 100. According to the statistical test result, there is no significant difference between the mutation frequency of neither B101 nor B203 compared to parental following in 0, 1 and 2Gy populations.

Figure 12: Statistical Analysis of Mutation Frequency in 0, 1, and 2Gy Populations

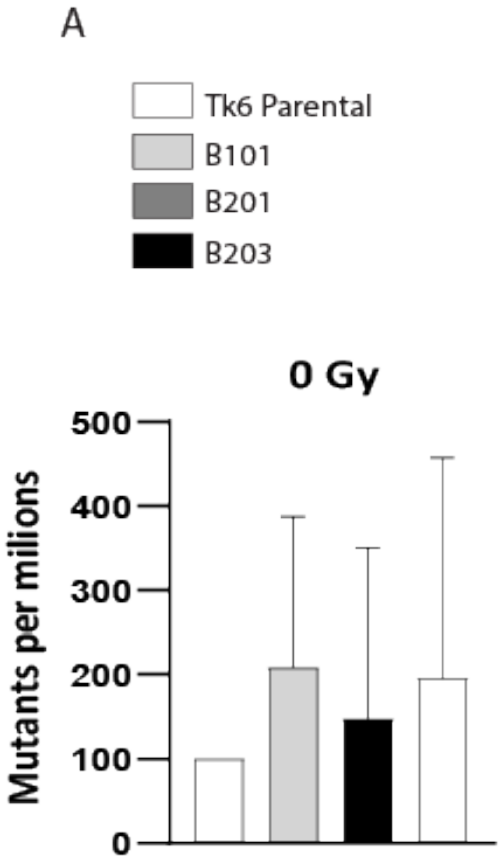

One Sample T Test	B101-0Gy	B201-0Gy	B203-0Gy
Theoretical mean	100	100	100
Actual mean	208.3	147.3	196.1
Number of values	6	4	6
One sample t test			
t, df	t=1.480, df=5	t=0.4652, df=3	t=0.9003, df=5
P value (two tailed)	0.1991	0.6735	0.4092
P value summary	ns	ns	ns
Significant (alpha=0.05)?	No	No	No
How big is the discrepancy?			
Discrepancy	108.3	47.3	96.13
SD of discrepancy	179.4	203.3	261.6
SEM of discrepancy	73.22	101.7	106.8
95% confidence interval	-79.88 to 296.6	-276.3 to 370.9	-178.4 to 370.6
R squared (partial eta squared)	0.3045	0.06729	0.1395

Figure 12: Statistical Analysis of Mutation Frequency in 0, 1, and 2Gy Populations

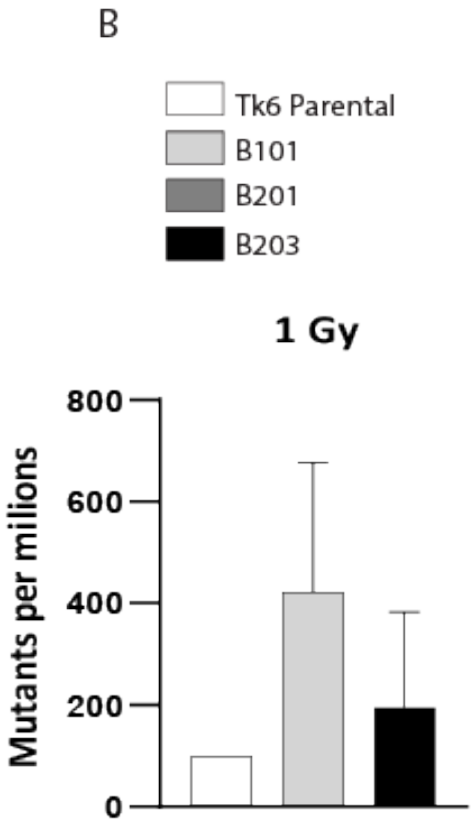

One Sample T Test	B101-1Gy	B203-1Gy
Theoretical mean	100	100
Actual mean	422.9	194.2
Number of values	3	3
One sample t test		
t, df	t=2.206, df=2	t=0.8676, df=2
P value (two tailed)	0.1581	0.4771
P value summary	ns	ns
Significant (alpha=0.05)?	No	No
How big is the discrepancy?		
Discrepancy	322.9	94.25
SD of discrepancy	253.5	188.2
SEM of discrepancy	146.4	108.6
95% confidence interval	-306.9 to 952.8	-373.2 to 561.7
R squared (partial eta squared)	0.7088	0.2734

Figure 12: Statistical Analysis of Mutation Frequency in 0, 1, and 2Gy Populations

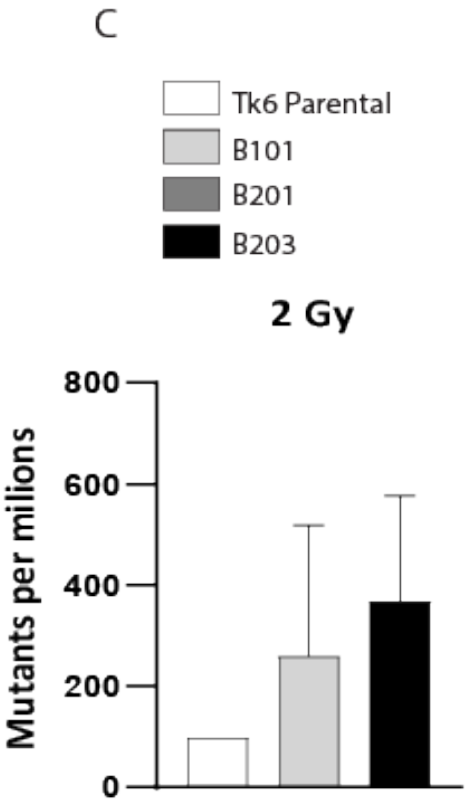

One Sample T Test	B101-2Gy	B203-2Gy
Theoretical mean	100	100
Actual mean	259.7	368.9
Number of values	3	3
One sample t test		
t, df	t=1.068, df=2	t=2.235, df=2
P value (two tailed)	0.3974	0.155
P value summary	ns	ns
Significant (alpha=0.05)?	No	No
How big is the discrepancy?		
Discrepancy	159.7	268.9
SD of discrepancy	258.9	208.4
SEM of discrepancy	149.5	120.3
95% confidence interval	-483.6 to 802.9	-248.8 to 786.5
R squared (partial eta squared)	0.3632	0.714

Figure 13: *HPRT* Reverse Transcriptase PCR Amplification Following Ionizing Radiation on 2020/05/05

The following images show electrophoresis results of *HPRT* RT-PCR amplification in *HPRT* mutants following radiation.

Following RNA extraction of collected mutants and cDNA synthesis, *HPRT* RT-PCR amplification was performed through a nested PCR strategy, using F1 and P1 primers in the first round and F2 and R3 primers in the second round to amplify the coding part of the *HPRT* gene (all primers are indicated in the table 1). PCR amplification products were separated using 1% agarose gel by DNA electrophoresis.

Positive PCR amplification products, including those with full-length and shorter-length PCR amplification products, were sequenced. In addition, bands from multiple PCR amplification products were cut and sequenced individually.

Figures 13A shows *HPRT* RT-PCR amplification results of TK6-parental IR-1 to 10 from experiment 2020/05/05

Figures 13B shows *HPRT* RT-PCR amplification results of B101-IR-1 to 21 from experiment 2020/05/05

Figures 13C shows *HPRT* RT-PCR amplification results of B203-IR-1 to 23 from experiment 2020/05/05

Figure 13: *HPRT* Reverse Transcriptase PCR Amplification Following Ionizing Radiation on 2020/05/05

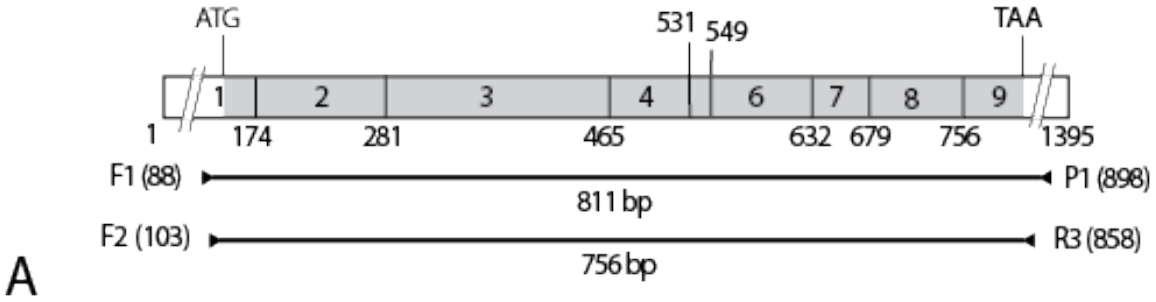

A

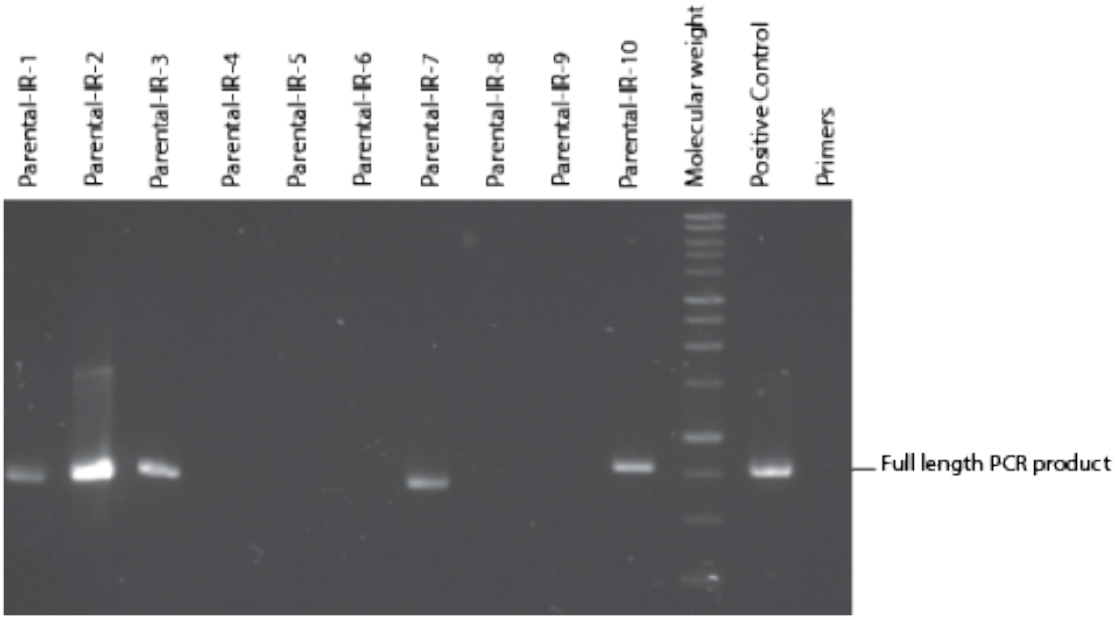

Figure 13: *HPRT* Reverse Transcriptase PCR Amplification Following Ionizing Radiation on 2020/05/05

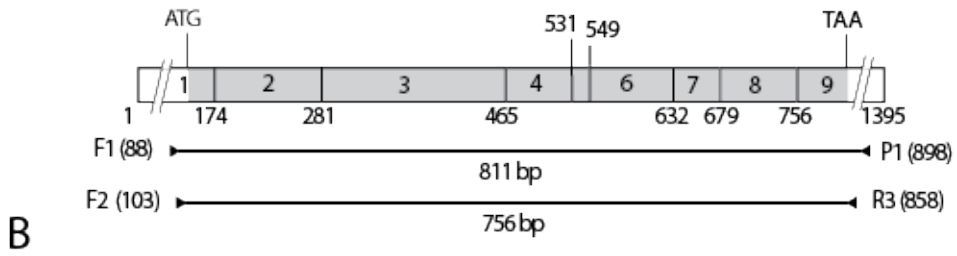

B

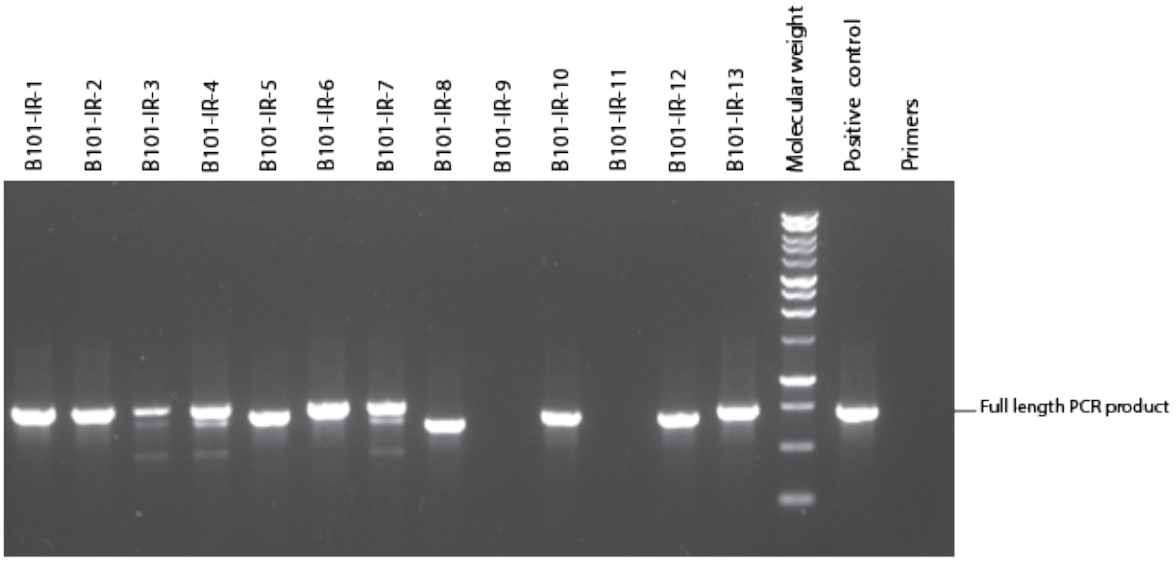

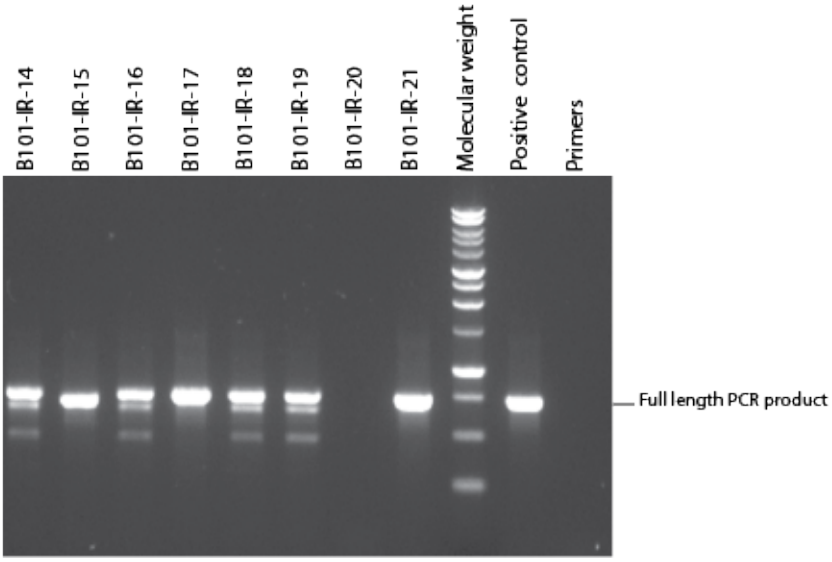

Figure 13: *HPRT* Reverse Transcriptase PCR Amplification Following Ionizing Radiation on 2020/05/05

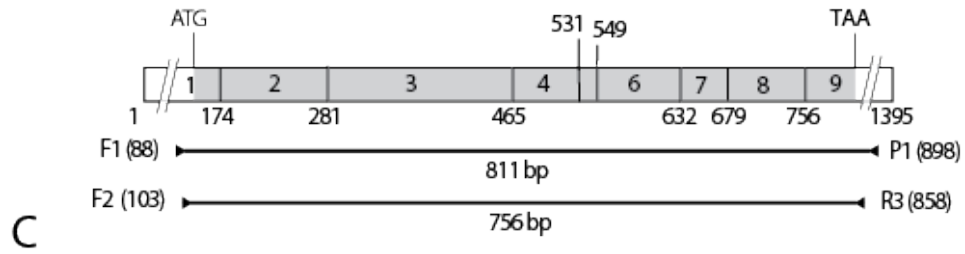

C

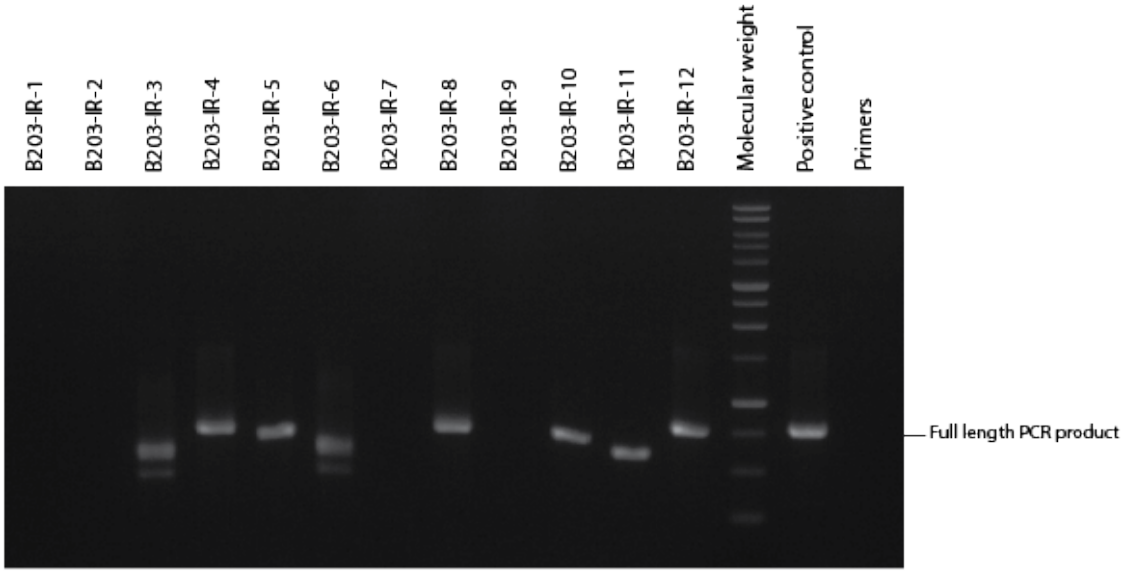

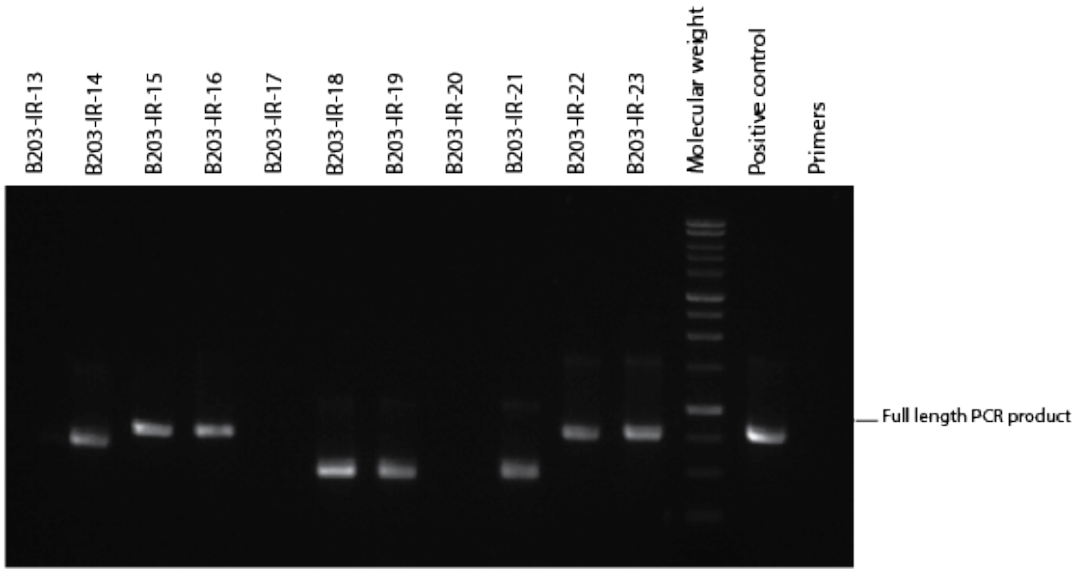

Figure 14: *HPRT* Reverse Transcriptase PCR Amplification Following Ionizing Radiation on 2020/10/01

The following images show electrophoresis results of *HPRT* RT-PCR amplification in *HPRT* mutants following radiation

Following RNA extraction of collected mutants and cDNA synthesis, *HPRT* RT-PCR amplification was performed through a nested PCR strategy, using F1 and P1 primers in the first round and F2 and R3 primers in the second round to amplify the coding part of the *HPRT* gene (all primers are indicated in the table 1). PCR amplification products were separated using 1% agarose gel by DNA electrophoresis.

Positive PCR amplification products, including those with full-length and shorter-length PCR amplification products, were sequenced. In addition, bands from multiple PCR amplification products were cut and sequenced individually.

Figures 14A and B show *HPRT* RT-PCR amplification results of TK6-parental-IR-11 to 40 from experiment 2020/10/01

Figures 14B, C and D shows *HPRT* RT-PCR amplification results of B101-IR-22 to 83 from experiment 2020/10/01

Figure 14: *HPRT* Reverse Transcriptase PCR Amplification Following Ionizing Radiation on 2020/10/01

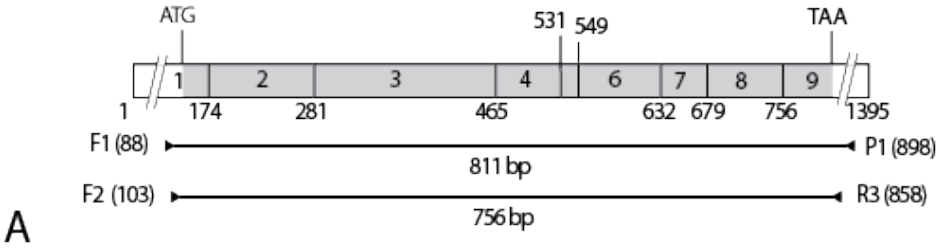

A

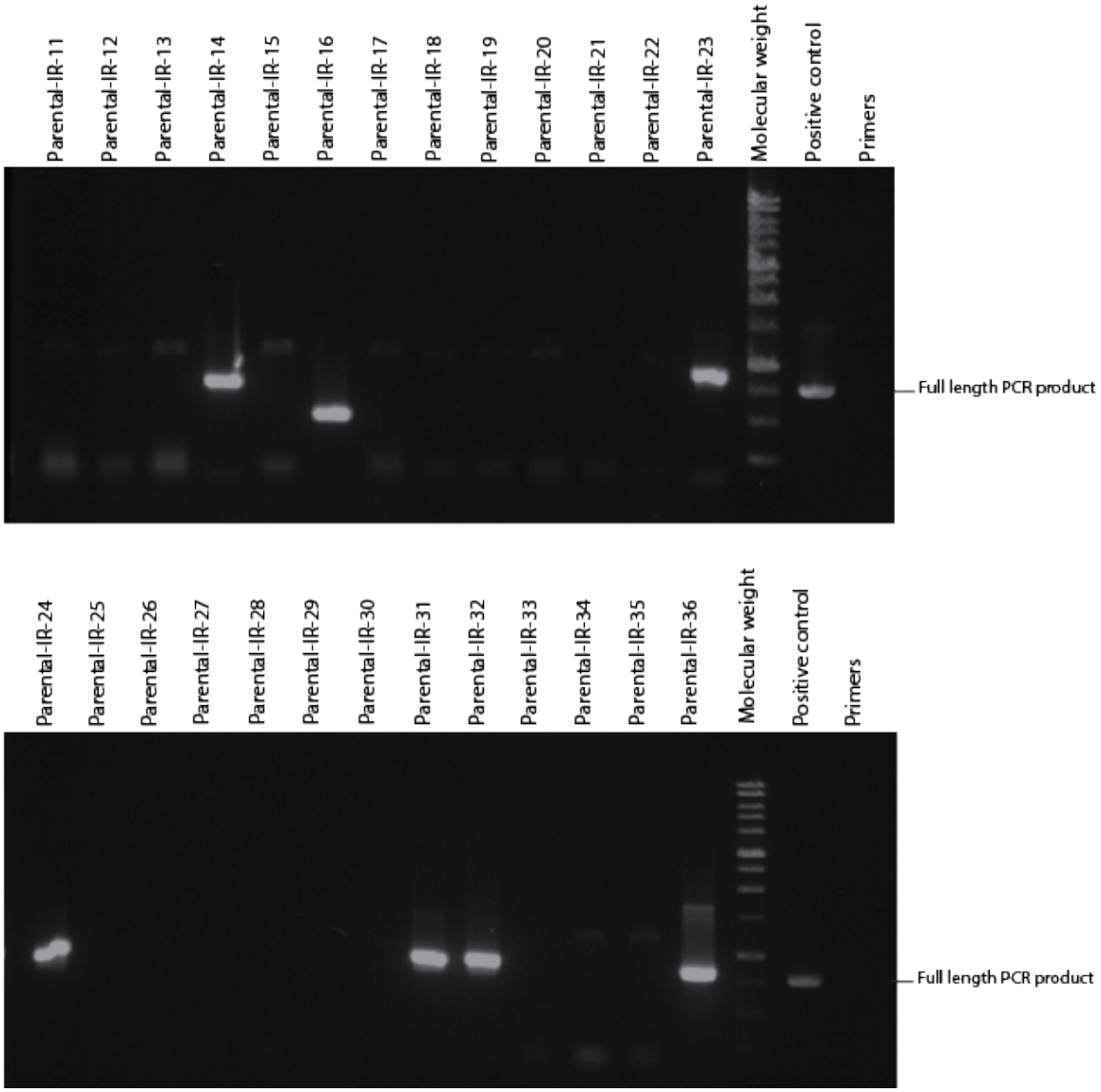

Figure 14: *HPRT* Reverse Transcriptase PCR Amplification Following Ionizing Radiation on 2020/10/01

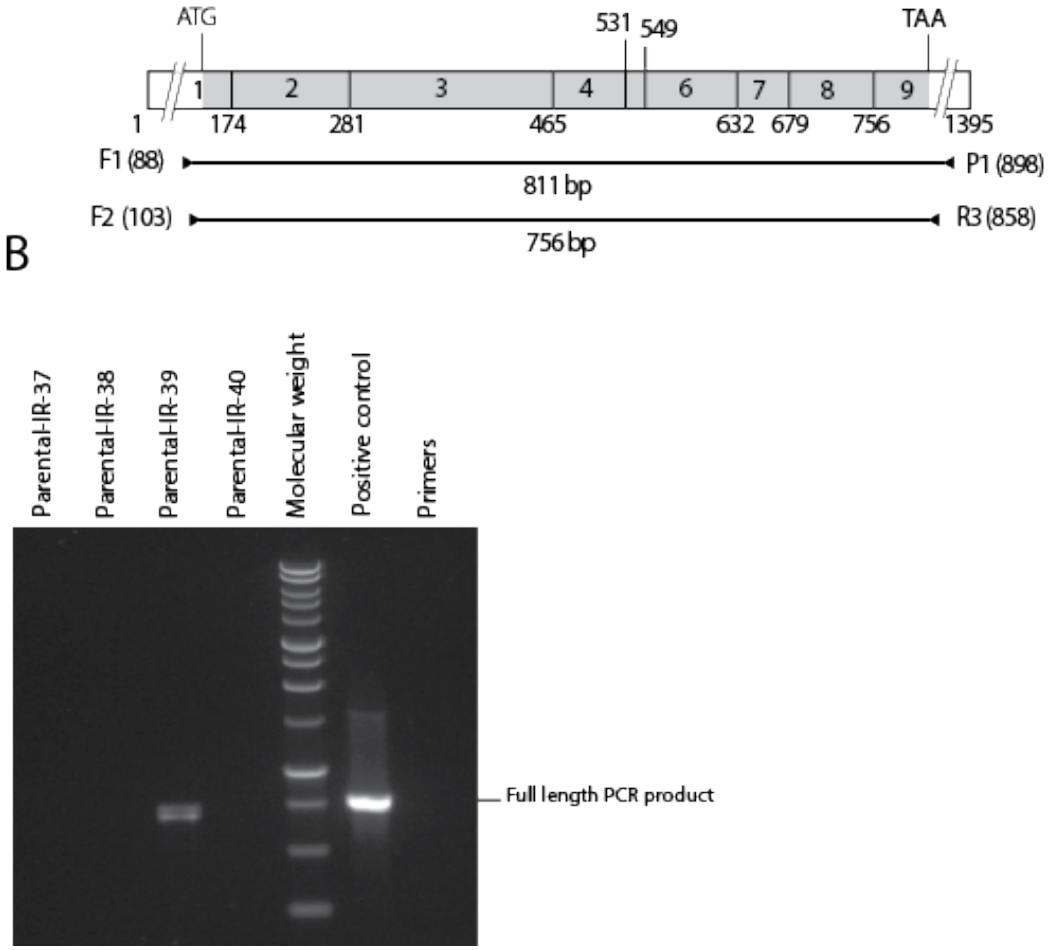

Figure 14: *HPRT* Reverse Transcriptase PCR Amplification Following Ionizing Radiation on 2020/10/01

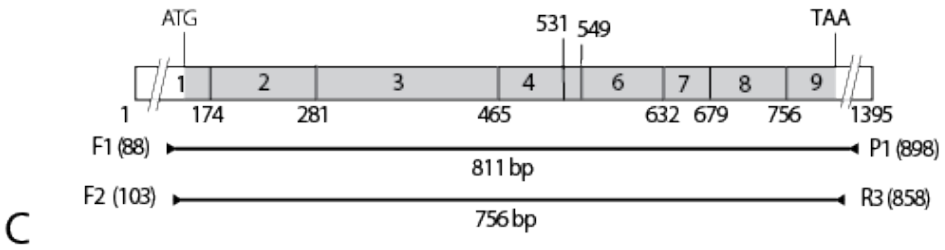

C

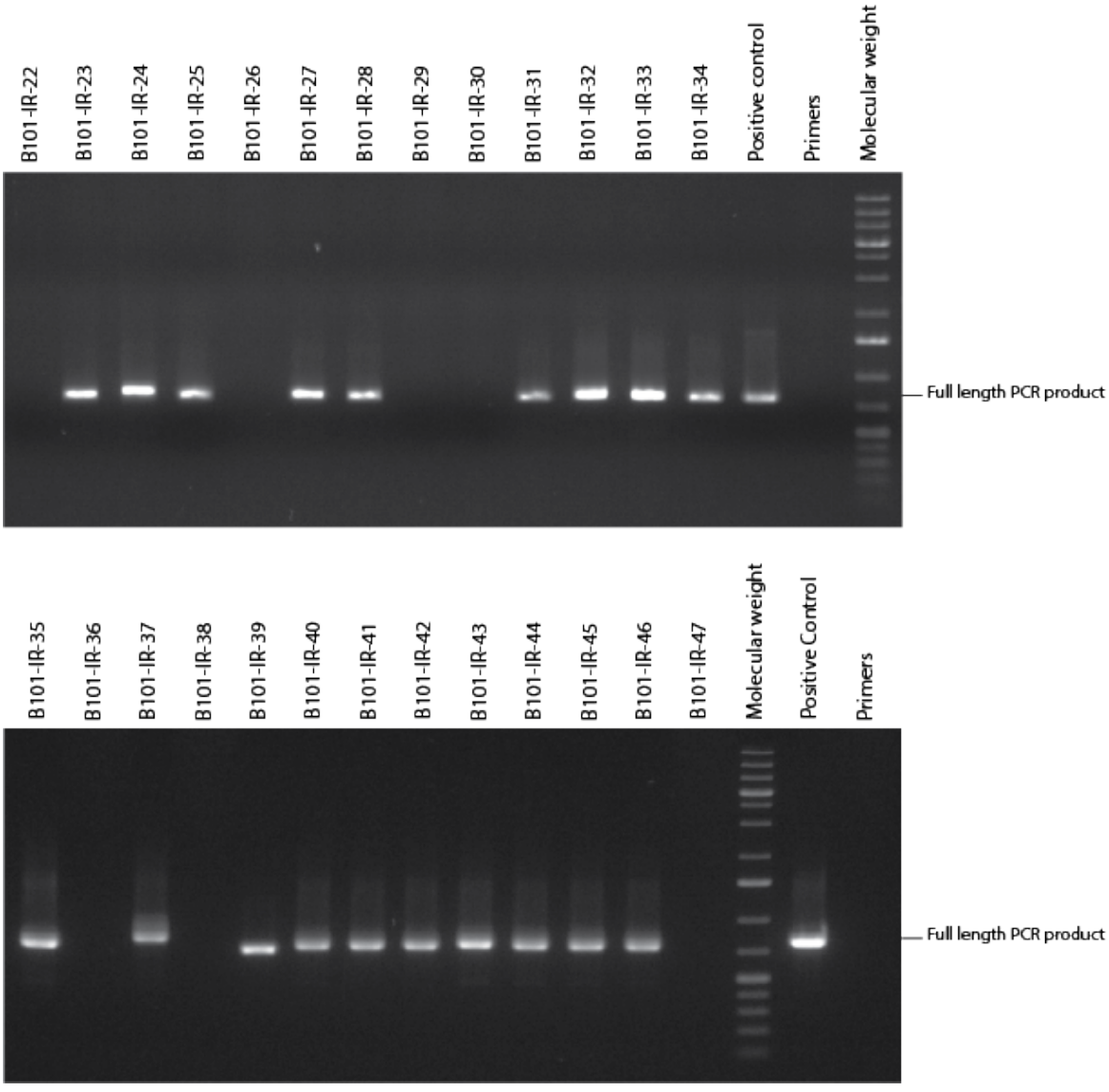

Figure 14: *HPRT* Reverse Transcriptase PCR Amplification Following Ionizing Radiation on 2020/10/01

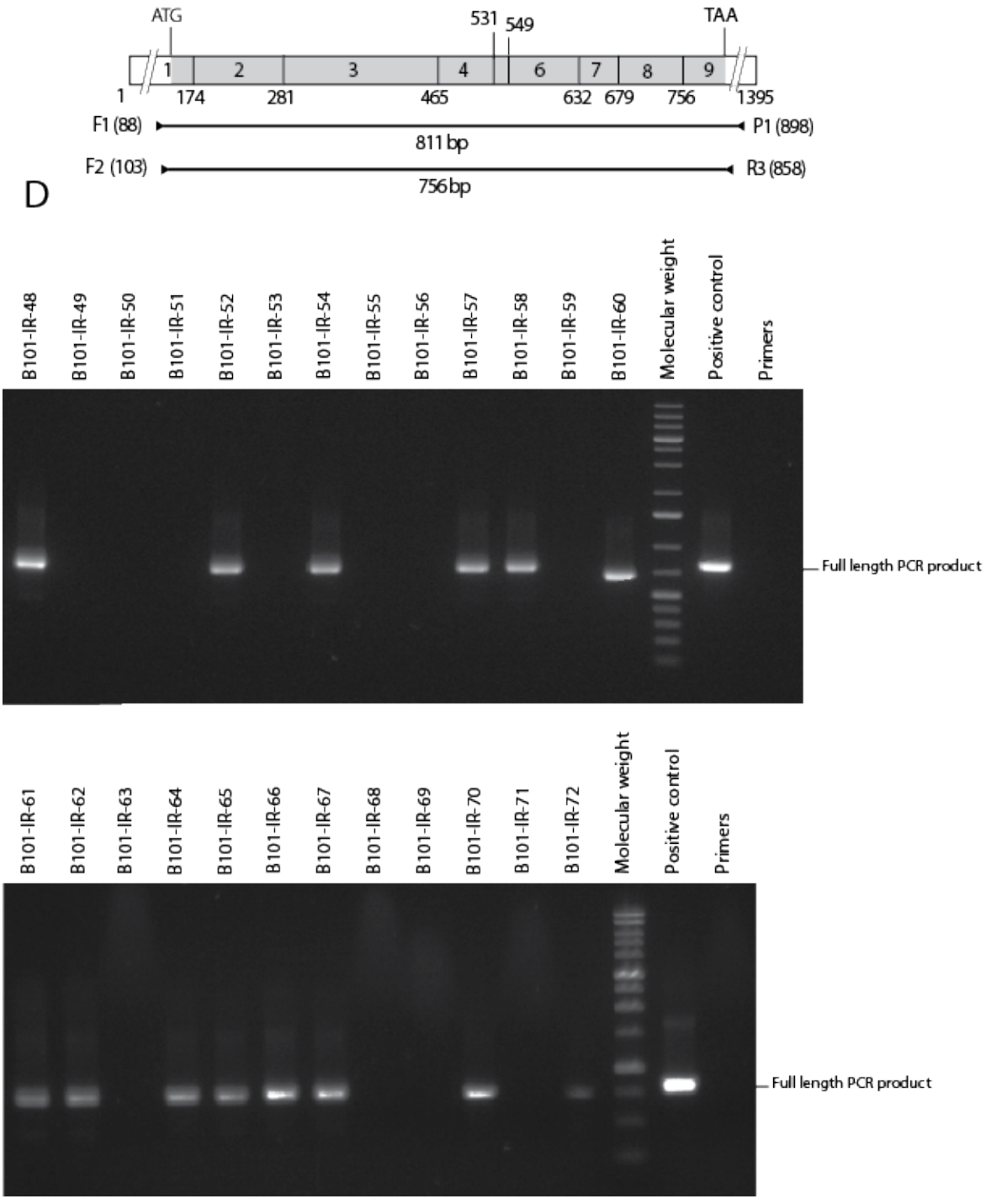

Figure 14: *HPRT* Reverse Transcriptase PCR Amplification Following Ionizing Radiation on 2020/10/01

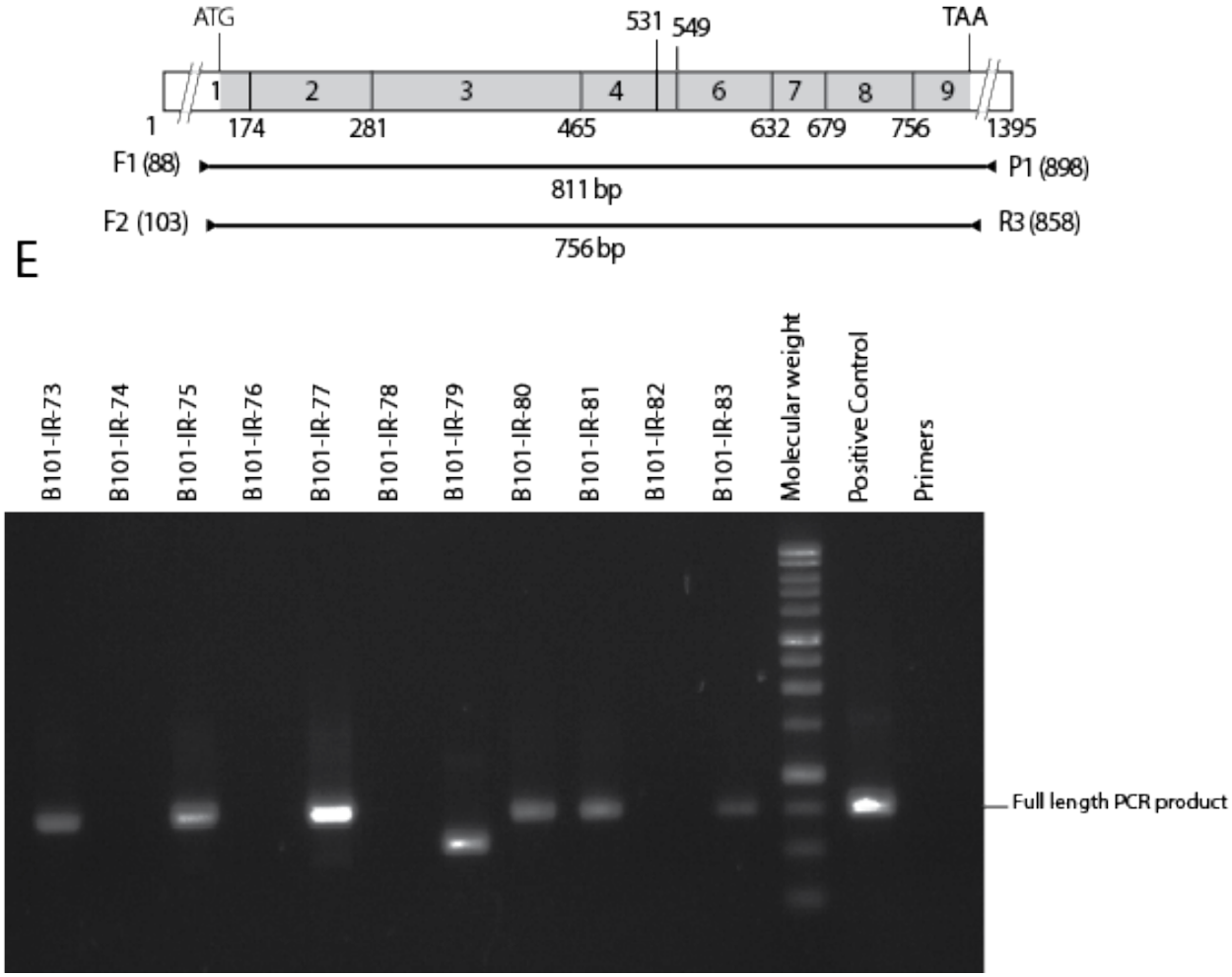

Figure 15: *HPRT* Reverse Transcriptase PCR Amplification Following Ionizing Radiation on 2021/04/06

The following images show electrophoresis results of *HPRT* RT-PCR amplification in *HPRT* mutants following radiation

Following RNA extraction of collected mutants and cDNA synthesis, *HPRT* RT-PCR amplification was performed through a nested PCR strategy, using F1 and P1 primers in the first round and F2 and R3 primers in the second round to amplify the coding part of the *HPRT* gene (all primers are indicated in the table 1). PCR amplification products were separated using 1% agarose gel by DNA electrophoresis.

Positive PCR amplification products, including those with full-length and shorter-length PCR amplification products, were sequenced. In addition, bands from multiple PCR amplification products were cut and sequenced individually.

Figure 15A show *HPRT* RT-PCR amplification results of TK6-parental-IR-41 to 62 from experiment 2021/04/06

Figure 15B shows *HPRT* RT-PCR amplification results of B101-IR-84 to 105 from experiment 2021/04/06

Figures 15C shows *HPRT* RT-PCR amplification results of B203-IR-24 to 44 from experiment 2021/04/06

Figure 15: *HPRT* Reverse Transcriptase PCR Amplification Following Ionizing Radiation on 2021/04/06

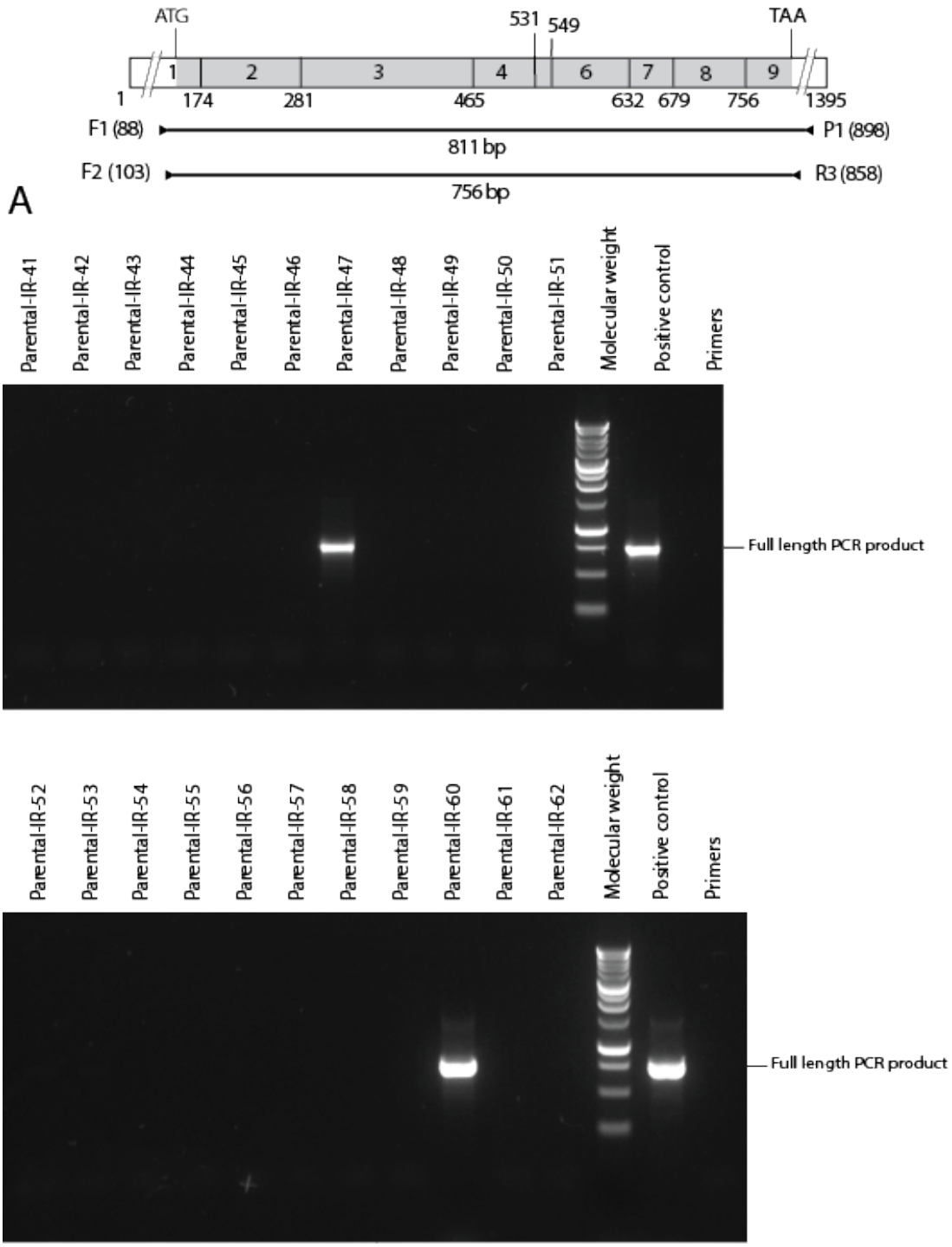

Figure 15: *HPRT* Reverse Transcriptase PCR Amplification Following Ionizing Radiation on 2021/04/06

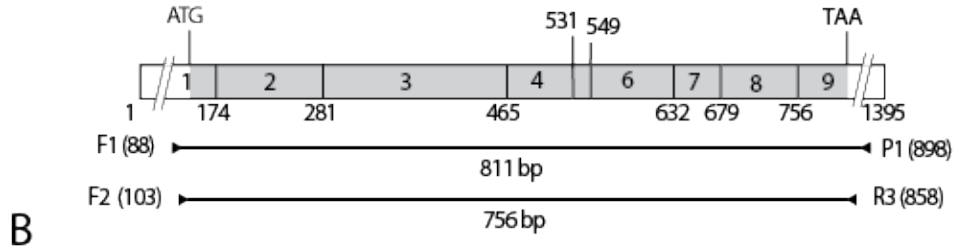

B

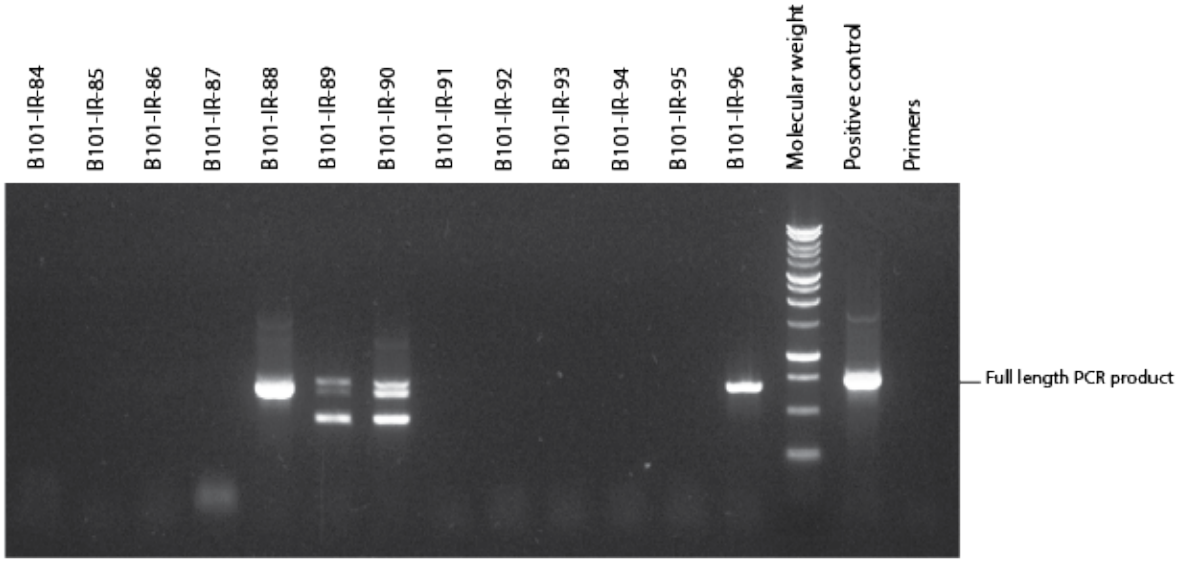

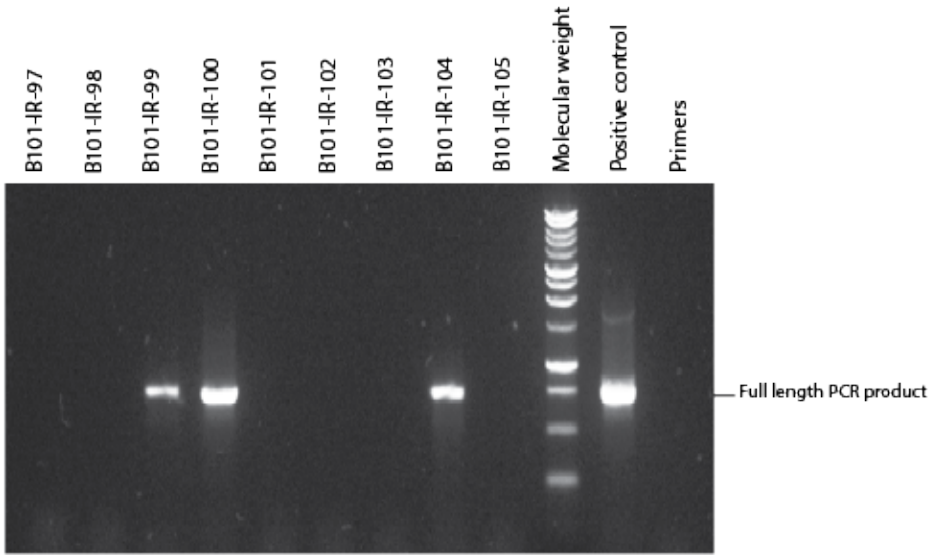

Figure 15: *HPRT* Reverse Transcriptase PCR Amplification Following Ionizing Radiation on 2021/04/06

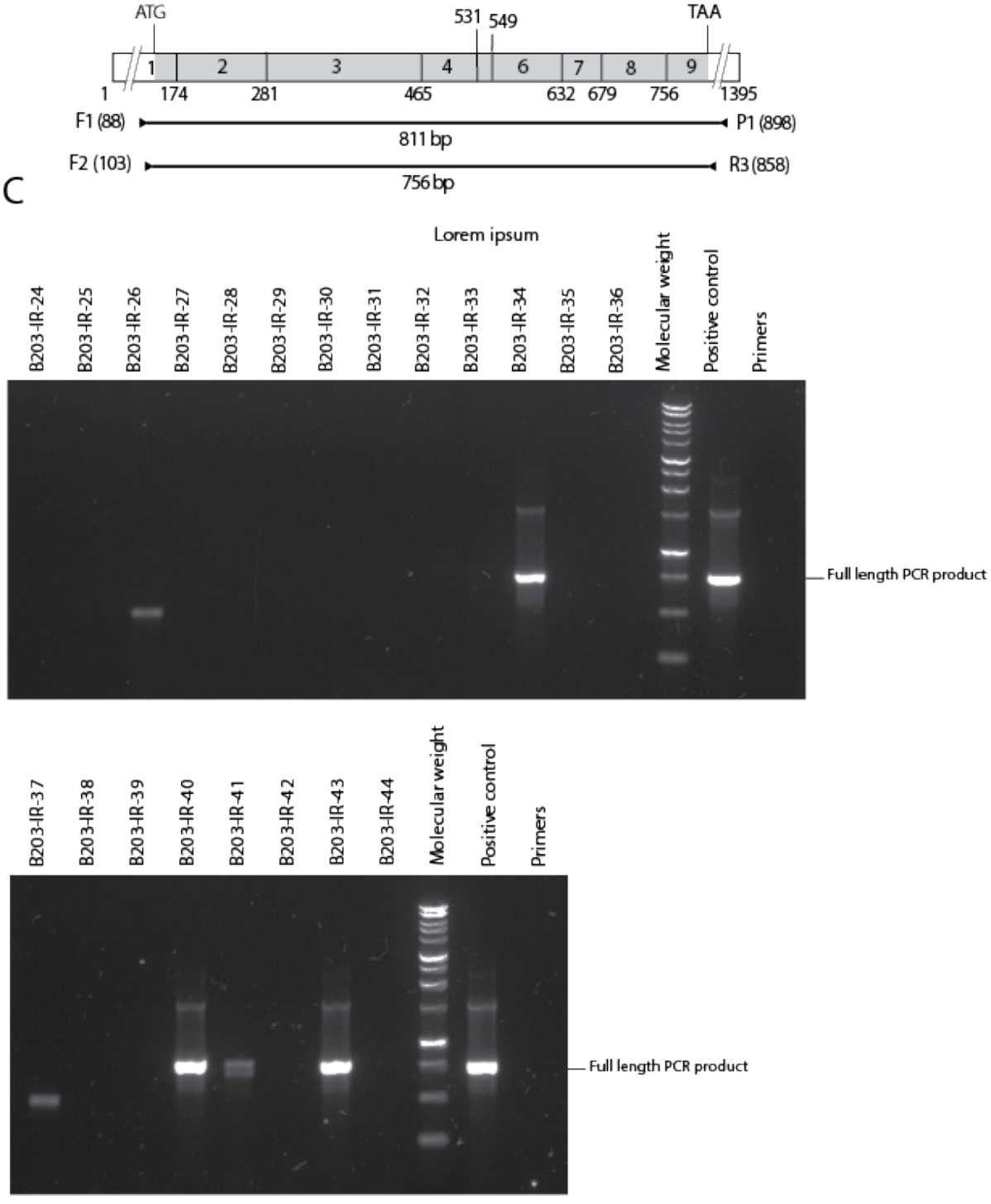

Figure 16: *GAPDH* Reverse Transcriptase PCR Results of Mutants with no *HPRT* RT-PCR Amplification Product Following Ionizing Radiation

Samples with no *HPRT* RT-PCR amplification product underwent *GAPDH* RT-PCR amplification to ensure that negative results with *HPRT* were not due to the bad quality of cDNAs or RNAs. *GAPDH* RT-PCR amplification was carried out using GAPDH RT-PCR primers mentioned in table 1. All samples showed the expected band size, 450 bp, which confirms the high quality of cDNAs and RNAs.

Figure 16: *GAPDH* Reverse Transcriptase PCR Results of Mutants with No *HPRT* RT-PCR Amplification Product Following Ionizing Radiation

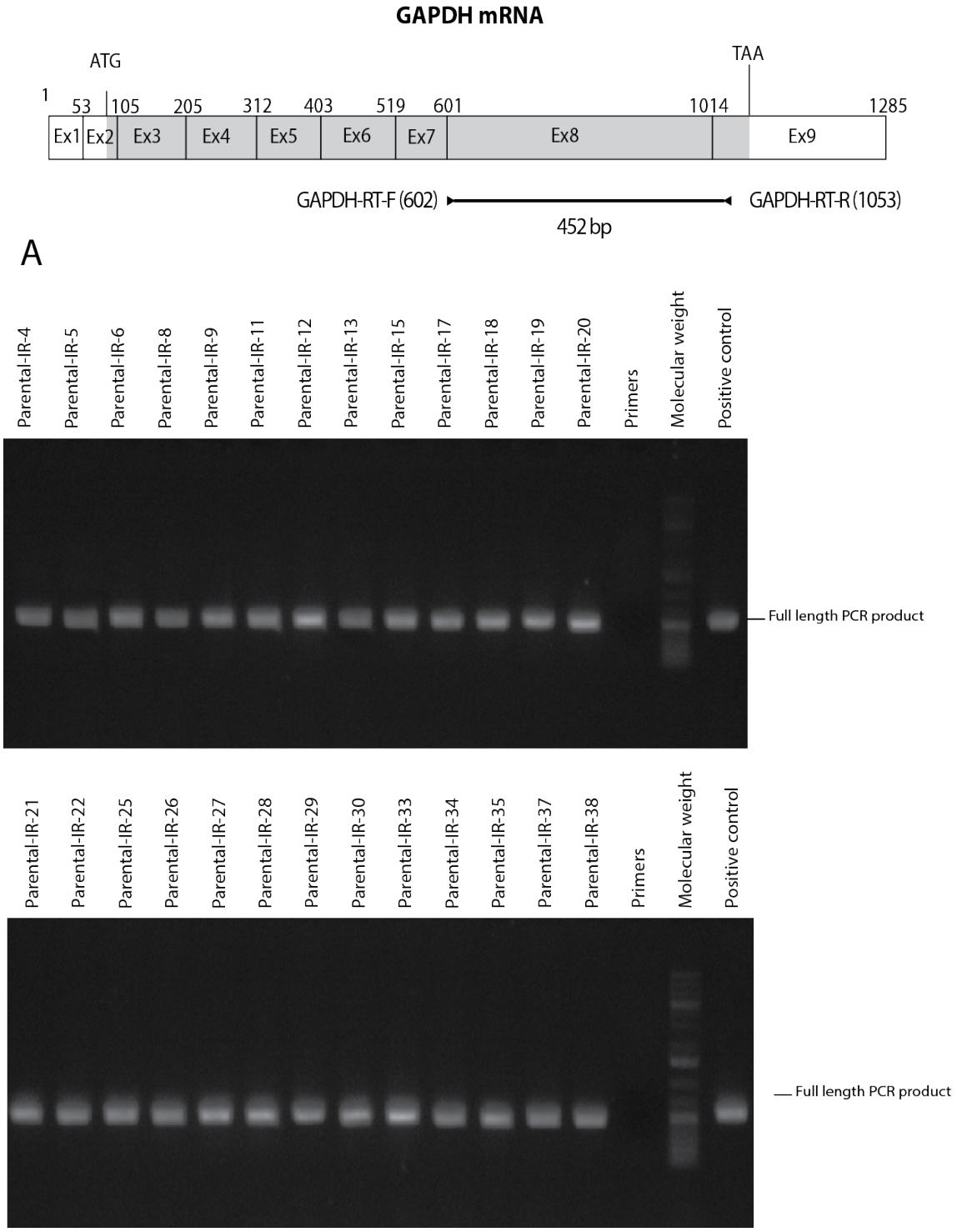

Figure 16: *GAPDH* Reverse Transcriptase PCR Results of Mutants with No *HPRT* RT-PCR Amplification Product Following Ionizing Radiation

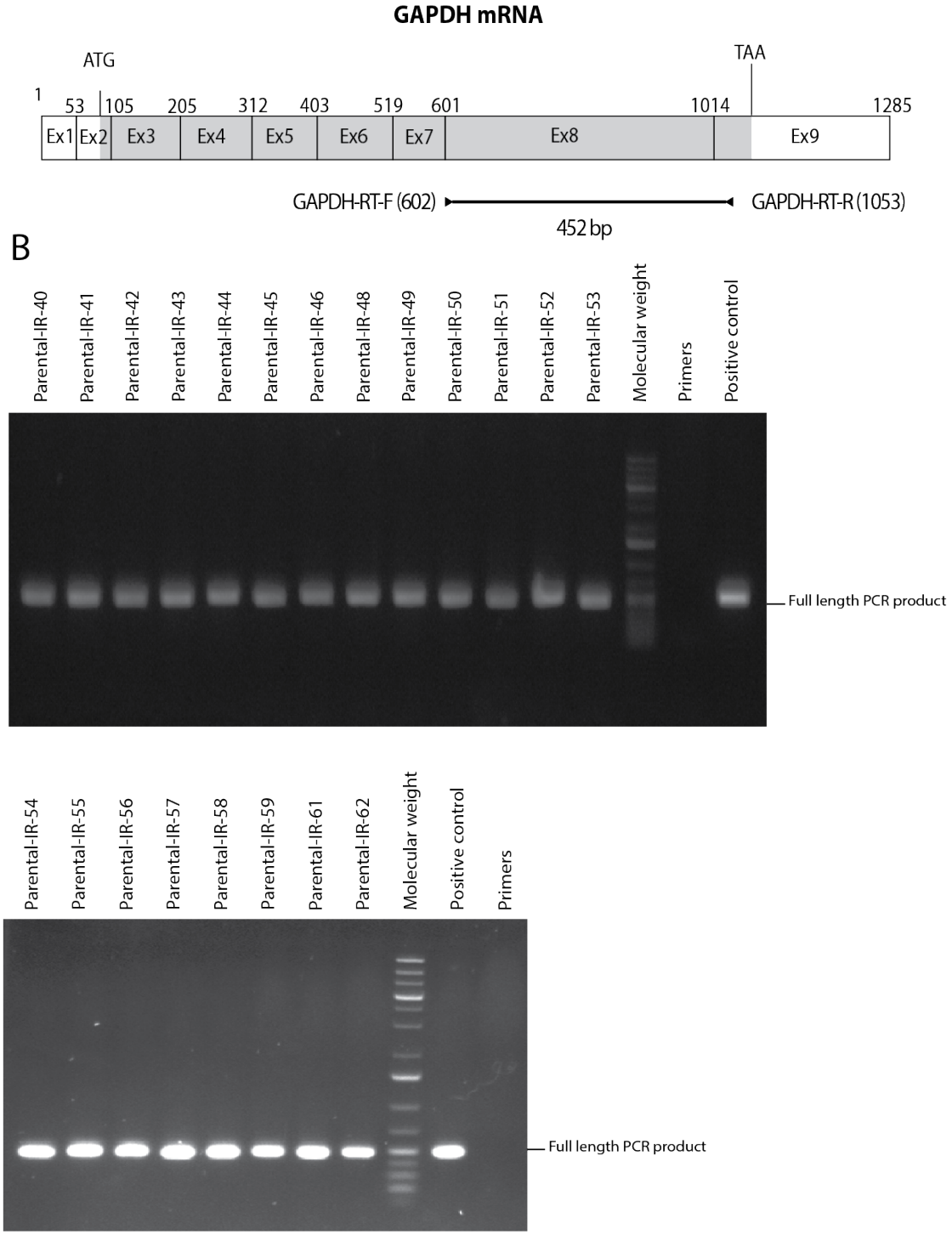

Figure 16: *GAPDH* Reverse Transcriptase PCR Results of Mutants with No *HPRT* RT-PCR Amplification Product Following Ionizing Radiation

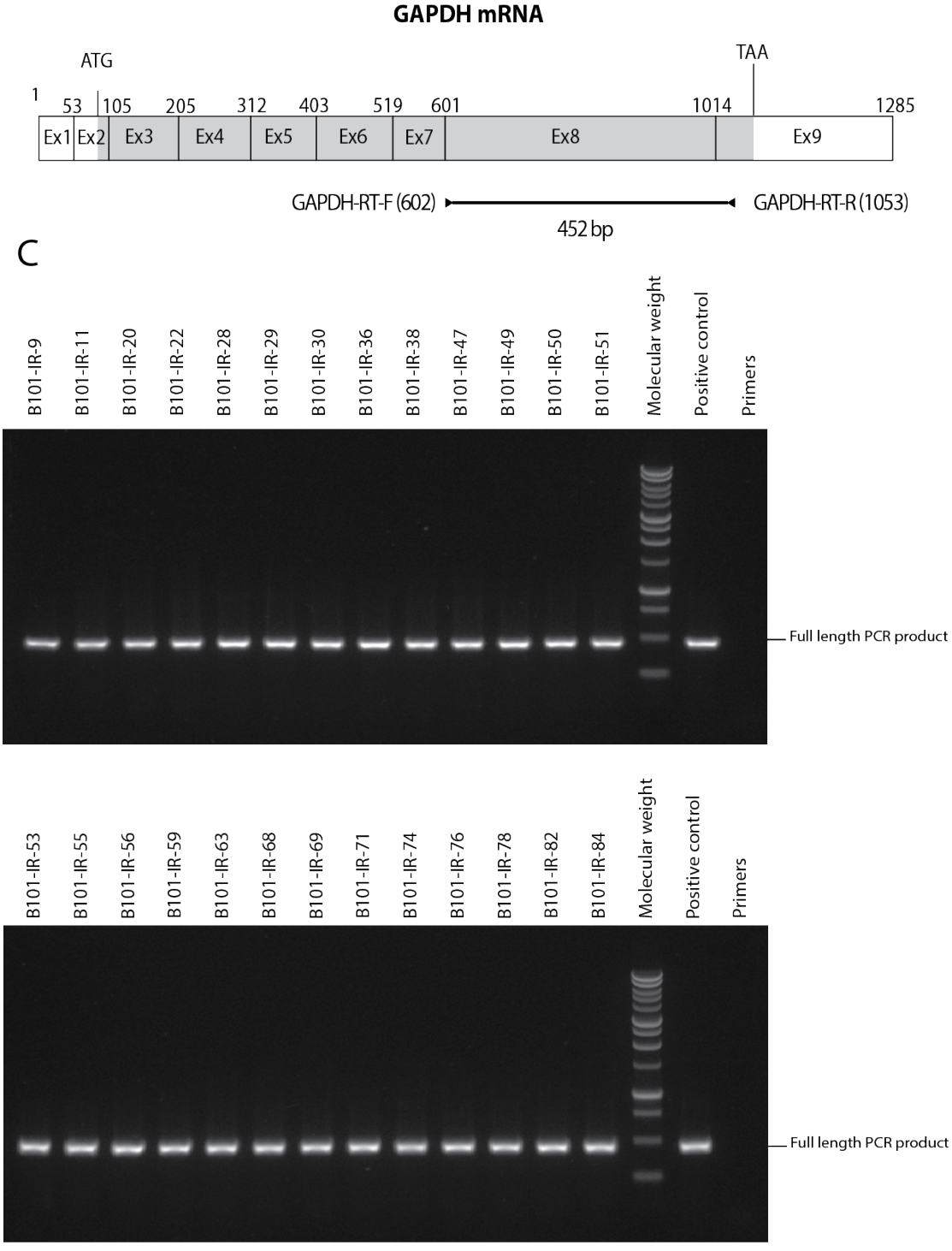

Figure 16: *GAPDH* Reverse Transcriptase PCR Results of Mutants with No *HPRT* RT-PCR Amplification Product Following Ionizing Radiation

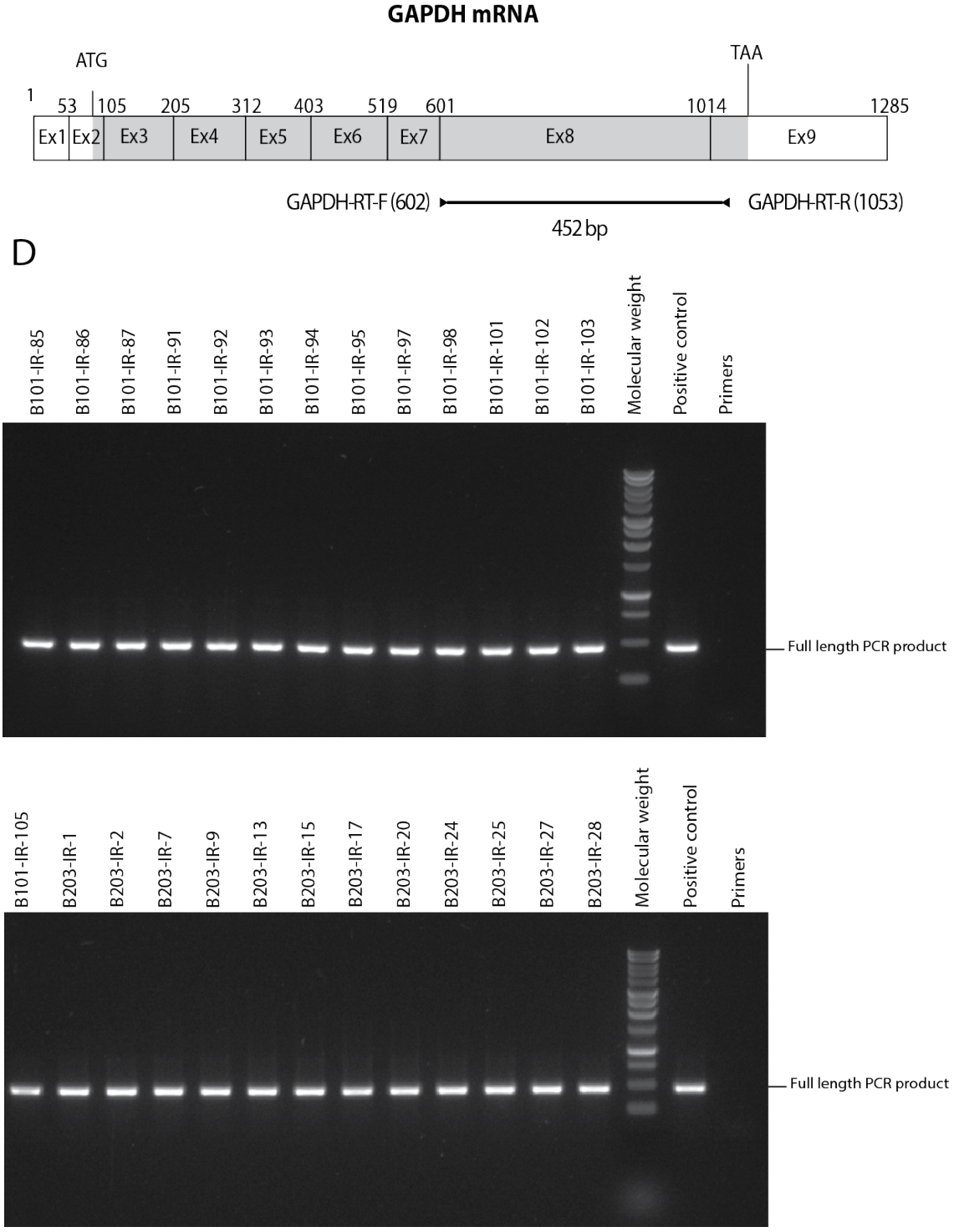

Figure 16: *GAPDH* Reverse Transcriptase PCR Results of Mutants with No *HPRT* RT-PCR Amplification Product Following Ionizing Radiation

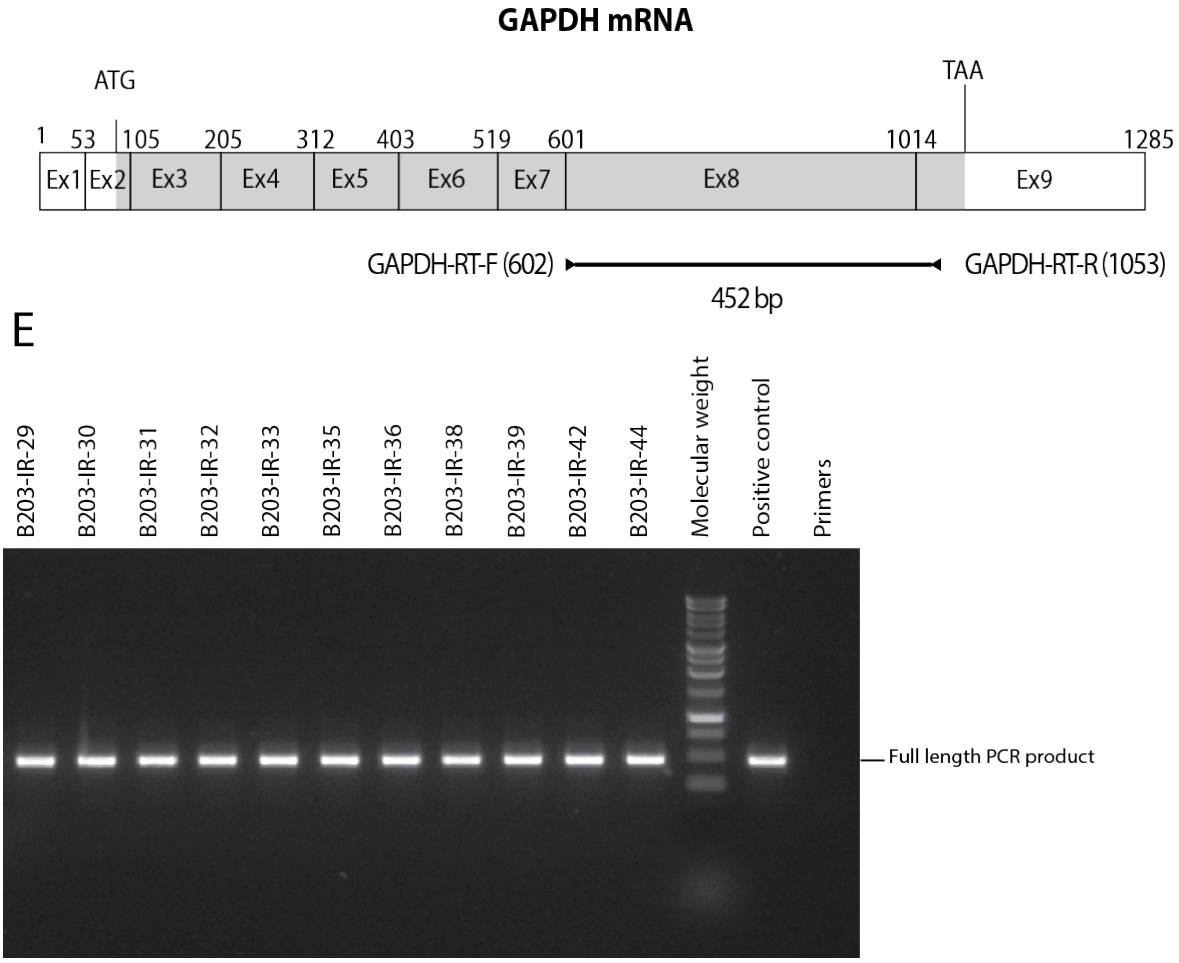

Figure 17: Genomic PCR Results Amplifying *HPRT* 5'- and 3'- Ends in Mutants from Irradiated Parental *BCL11B*$^{+/+}$ TK6 Cells

The images show the PCR amplification products of the *HPRT* gene 5'-end and 3'-end from *HPRT* mutants derived from BCL11B$^{+/+}$ T6 parental cells that did not show any *HPRT* RT-PCR amplification product following radiation. The *HPRT* gene 5'-end was amplified using HPRT-5gF and HPRT-5gR primers, whereas the *HPRT* gene 3'-end was amplified using HPRT-6F and HPRT-6R primers, as indicated in the figure and listed in table 1. The PCR amplification product for the gene 5'-end covers promoter sequences, the first exon and a portion of intron 1, whereas the 3'-end amplification product covers the end of the last exon and 3'-flanking sequences including the polyadenylation site. Samples were found to have both the 5'- and 3' ends, or miss both the 5'-end and 3'-end, or miss either the 5'-end or the 3-end. Overall, the genomic DNA of 46 *HPRT* mutants from the TK6 parental population were analyzed.

Figure 17: Genomic PCR Results Amplifying *HPRT* 5'- and 3'- Ends in Mutants from Irradiated Parental *BCL11B*$^{+/+}$ TK6 Cells

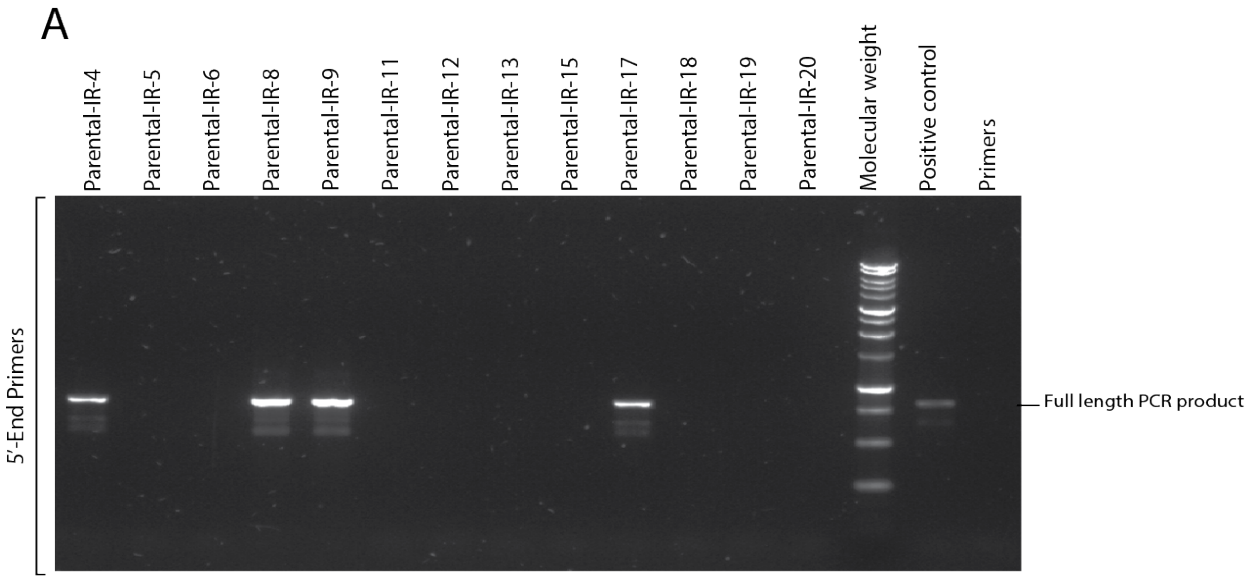

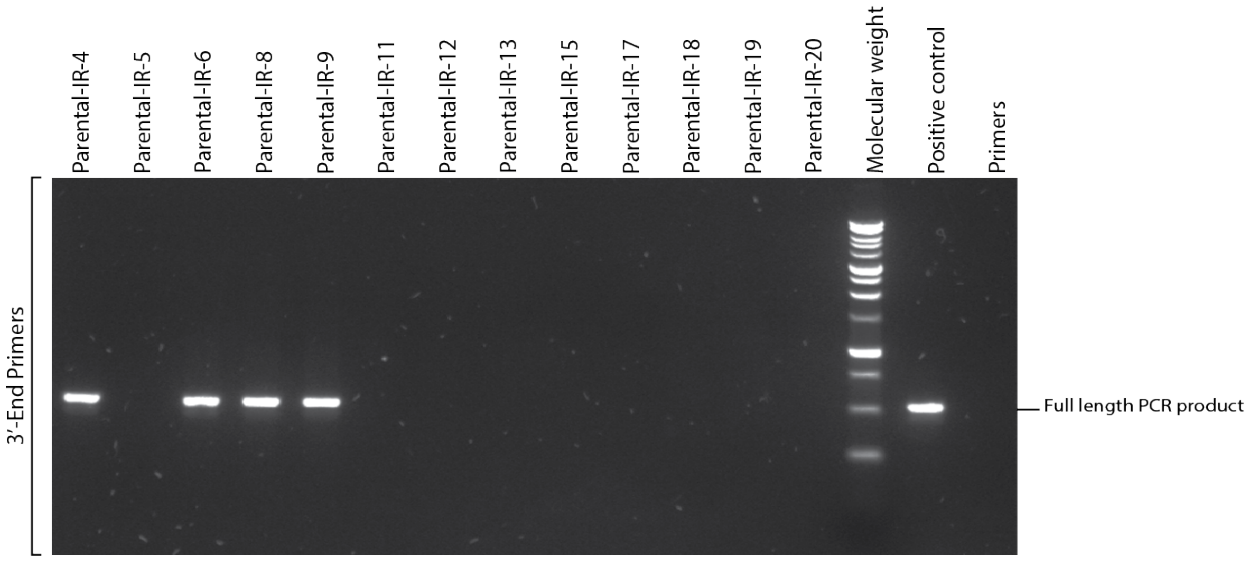

Figure 17: Genomic PCR Results Amplifying *HPRT* 5'- and 3'- Ends in Mutants from Irradiated Parental *BCL11B*$^{+/+}$ TK6 Cells

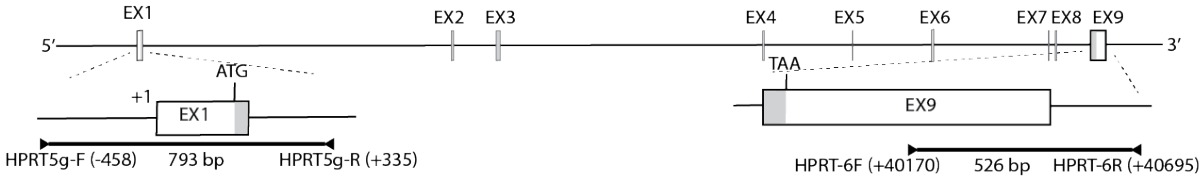

B

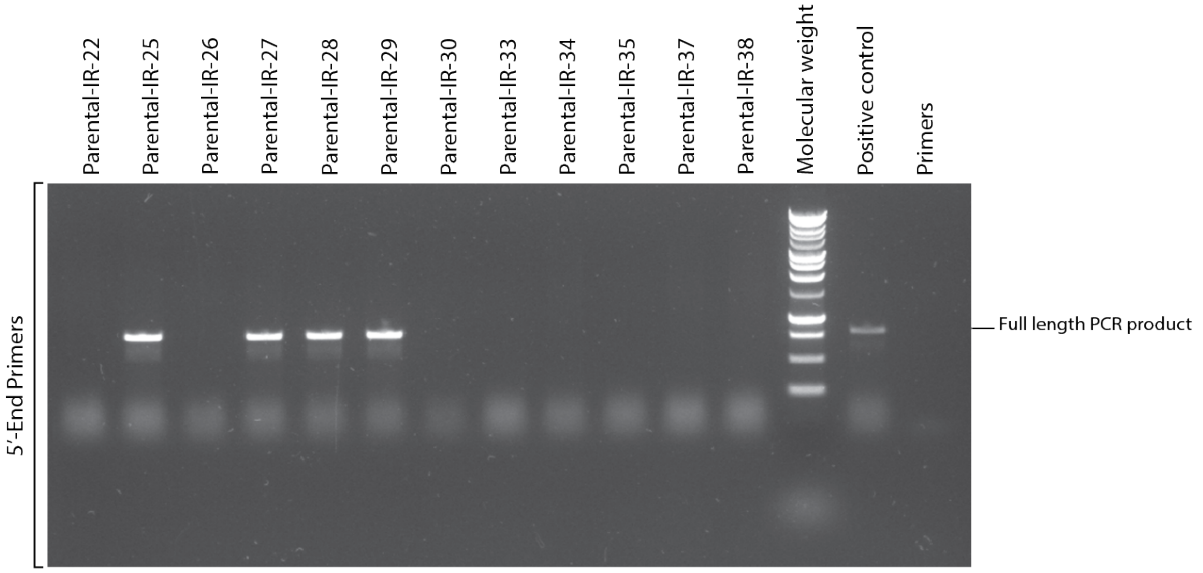

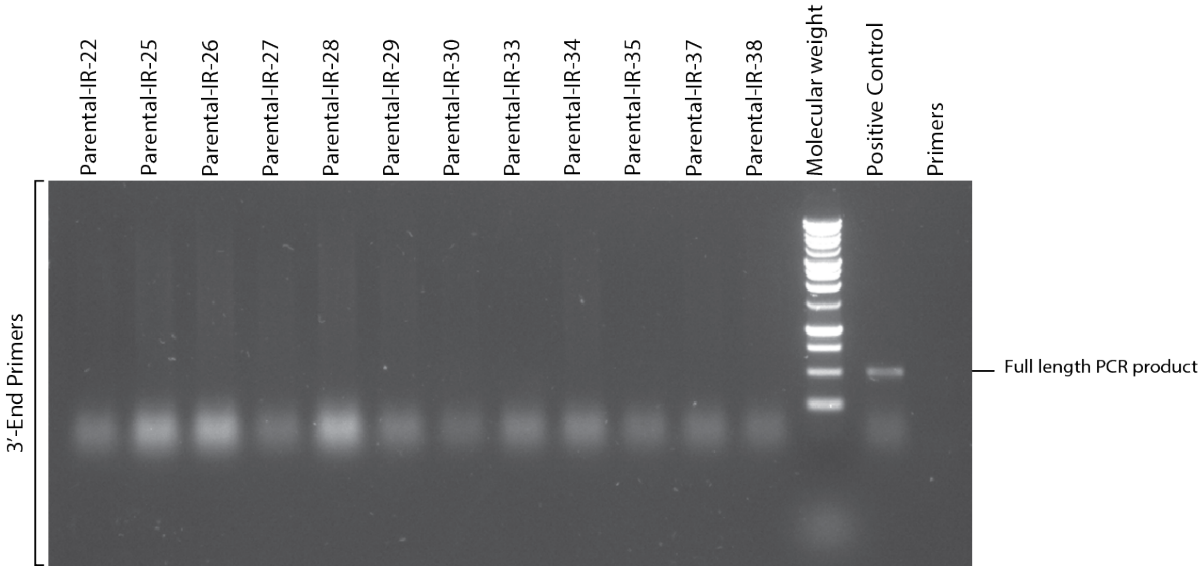

Figure 17: Genomic PCR Results Amplifying *HPRT* 5'- and 3'- Ends in Mutants from Irradiated Parental *BCL11B*$^{+/+}$ TK6 Cells

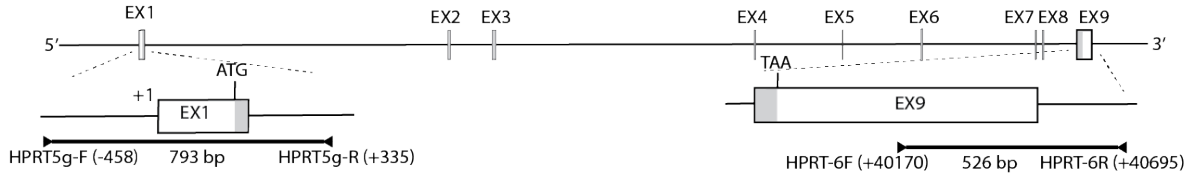

C

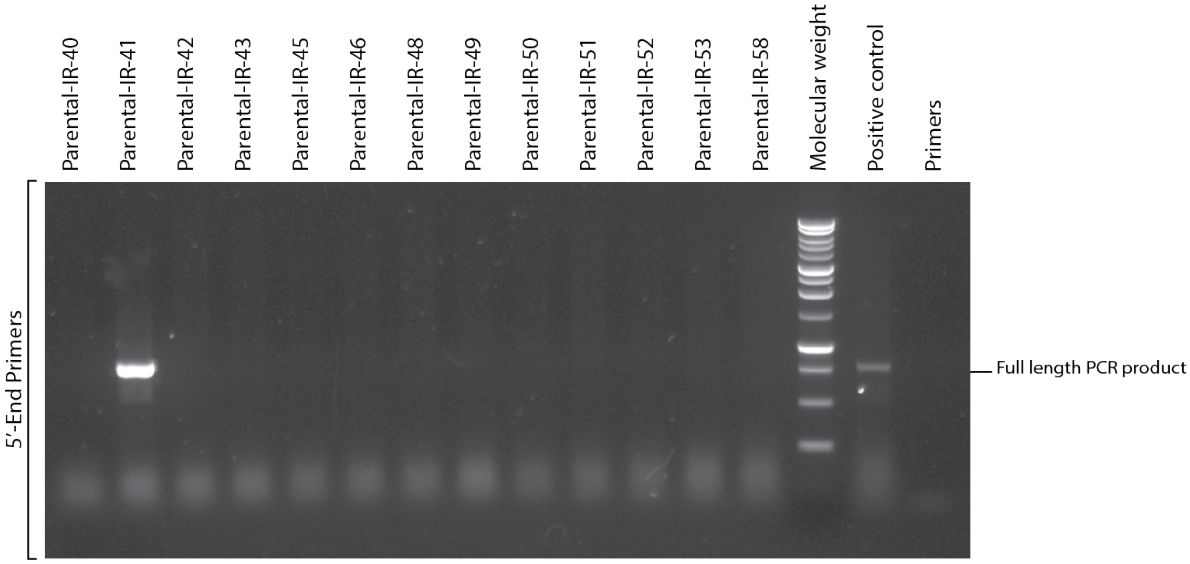

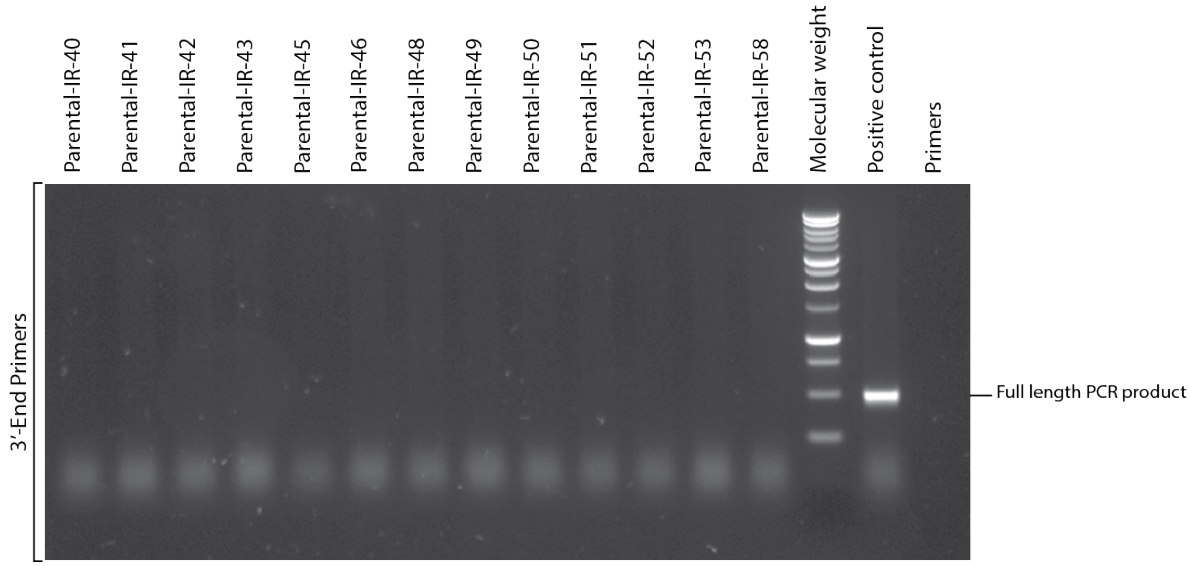

Figure 17: Genomic PCR Results Amplifying *HPRT* 5'- and 3'- Ends in Mutants from Irradiated Parental *BCL11B*$^{+/+}$ TK6 Cells

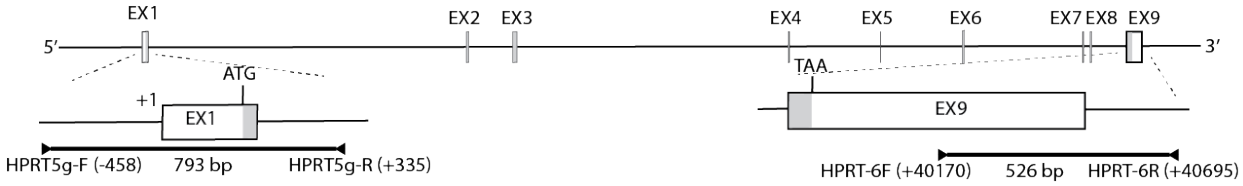

D

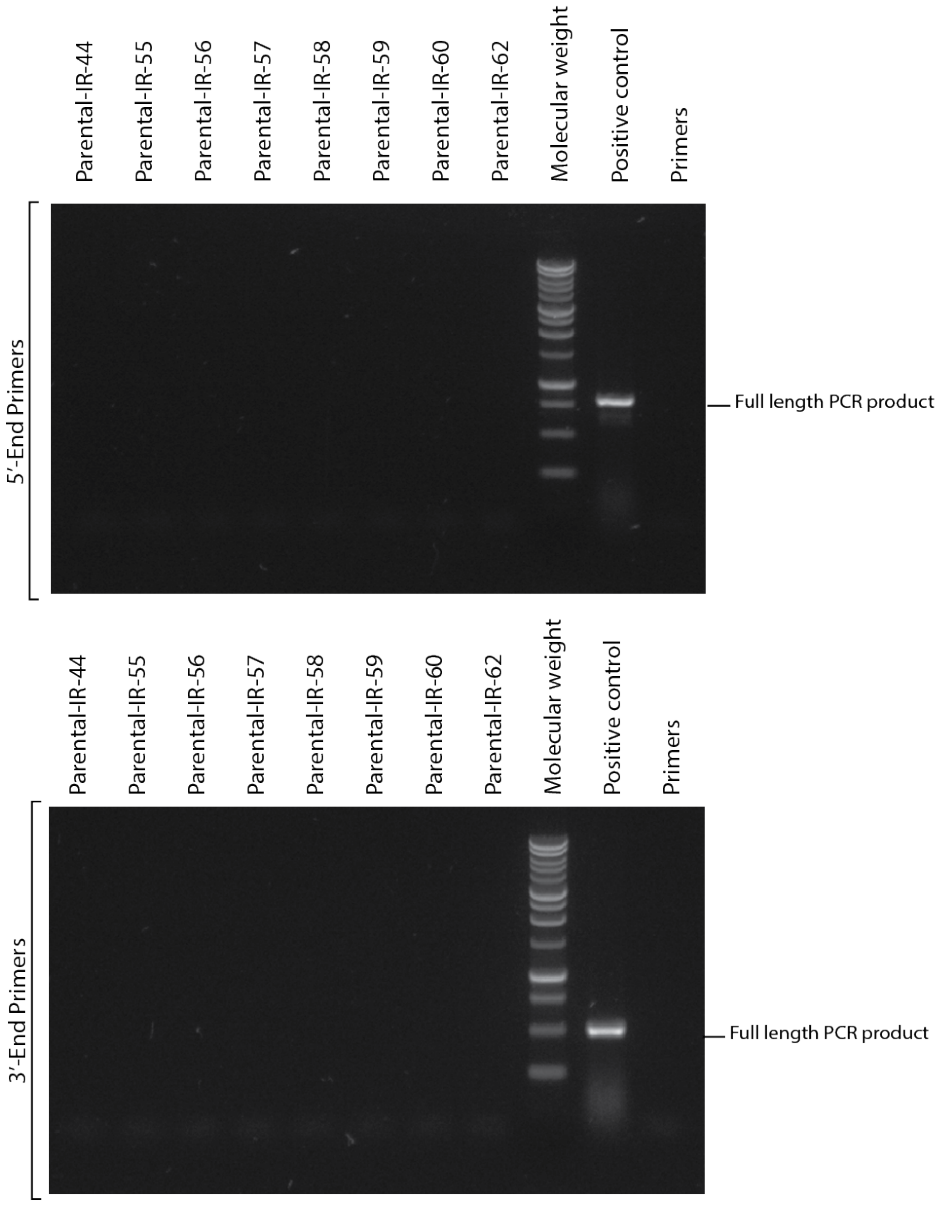

Figure 18: Genomic PCR Results Amplifying *HPRT* 5'- and 3'- Ends in Mutants from Irradiated *BCL11B*$^{+/-}$ B101 Cells

The images show the PCR amplification products of the *HPRT* gene 5'-end and 3'-end from *HPRT* mutants derived from BCL11B$^{+/+}$ TK6 parental cells that did not show any *HPRT* RT-PCR amplification product following radiation. The *HPRT* gene 5'-end was amplified using HPRT-5gF and HPRT-5gR primers, whereas the *HPRT* gene 3'-end was amplified using HPRT-6F and HPRT-6R primers, as indicated in the figure and listed in table 1. The PCR amplification product for the gene 5'-end covers promoter sequences, the first exon, and a portion of intron 1, whereas the 3'-end amplification product covers the end of the last exon and 3'-flanking sequences including the polyadenylation site. Samples were found to have both the 5'- and 3'- ends, or miss both the 5'-end and 3'-end, or miss either the 5'-end or the 3-end. Overall, the genomic DNA of 42 *HPRT* mutants from the B101 population were analyzed.

Figure 18: Genomic PCR Results Amplifying *HPRT* 5'- and 3'- Ends in Mutants from Irradiated *BCL11B*$^{+/-}$ B101 Cells

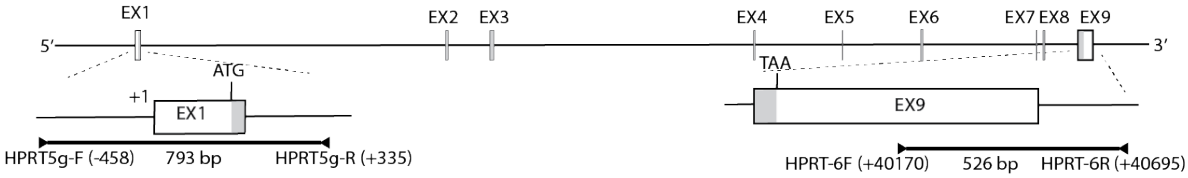

A

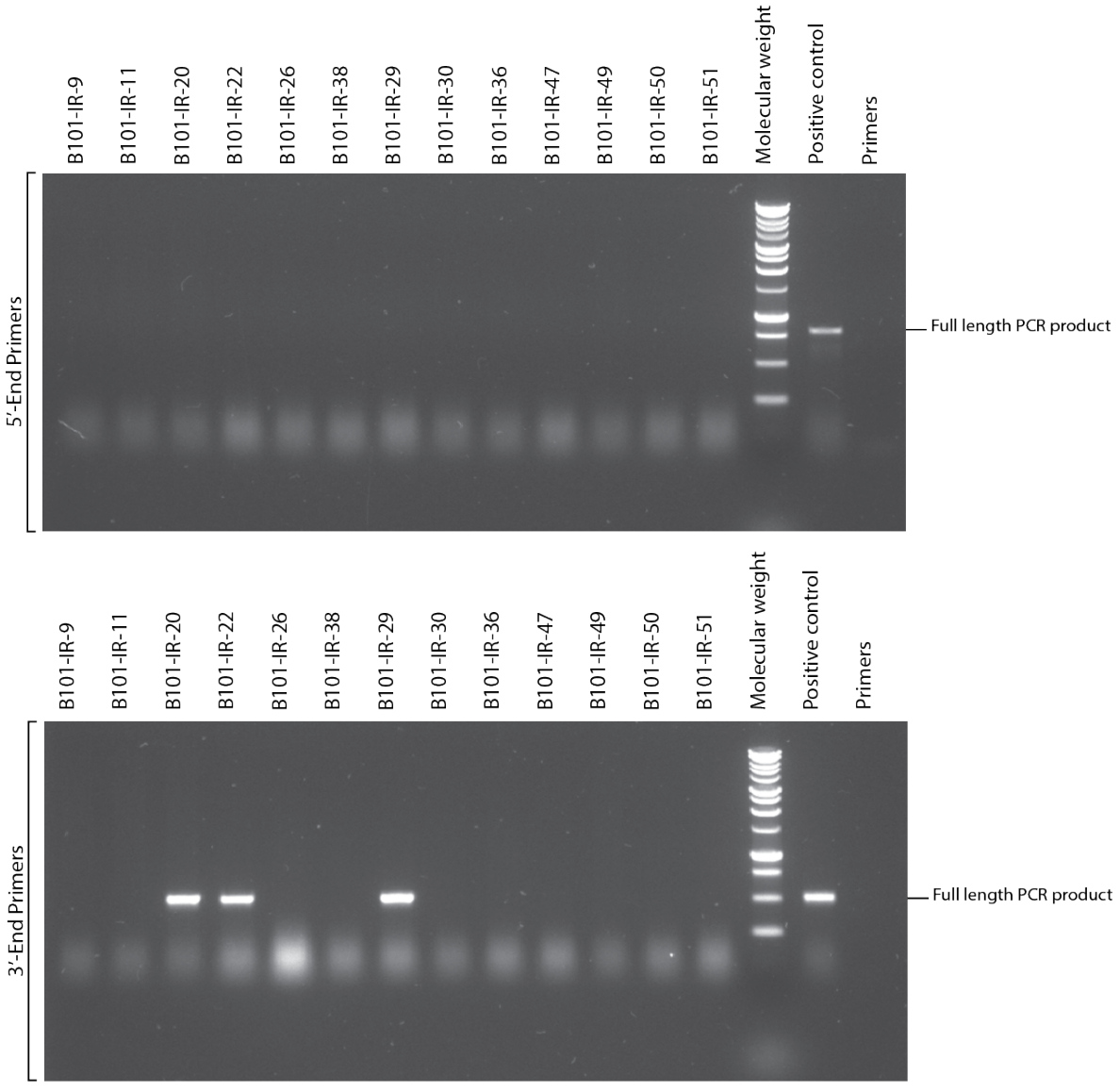

Figure 18: Genomic PCR Results Amplifying *HPRT* 5'- and 3'- Ends in Mutants from Irradiated *BCL11B*$^{+/-}$ B101 Cells

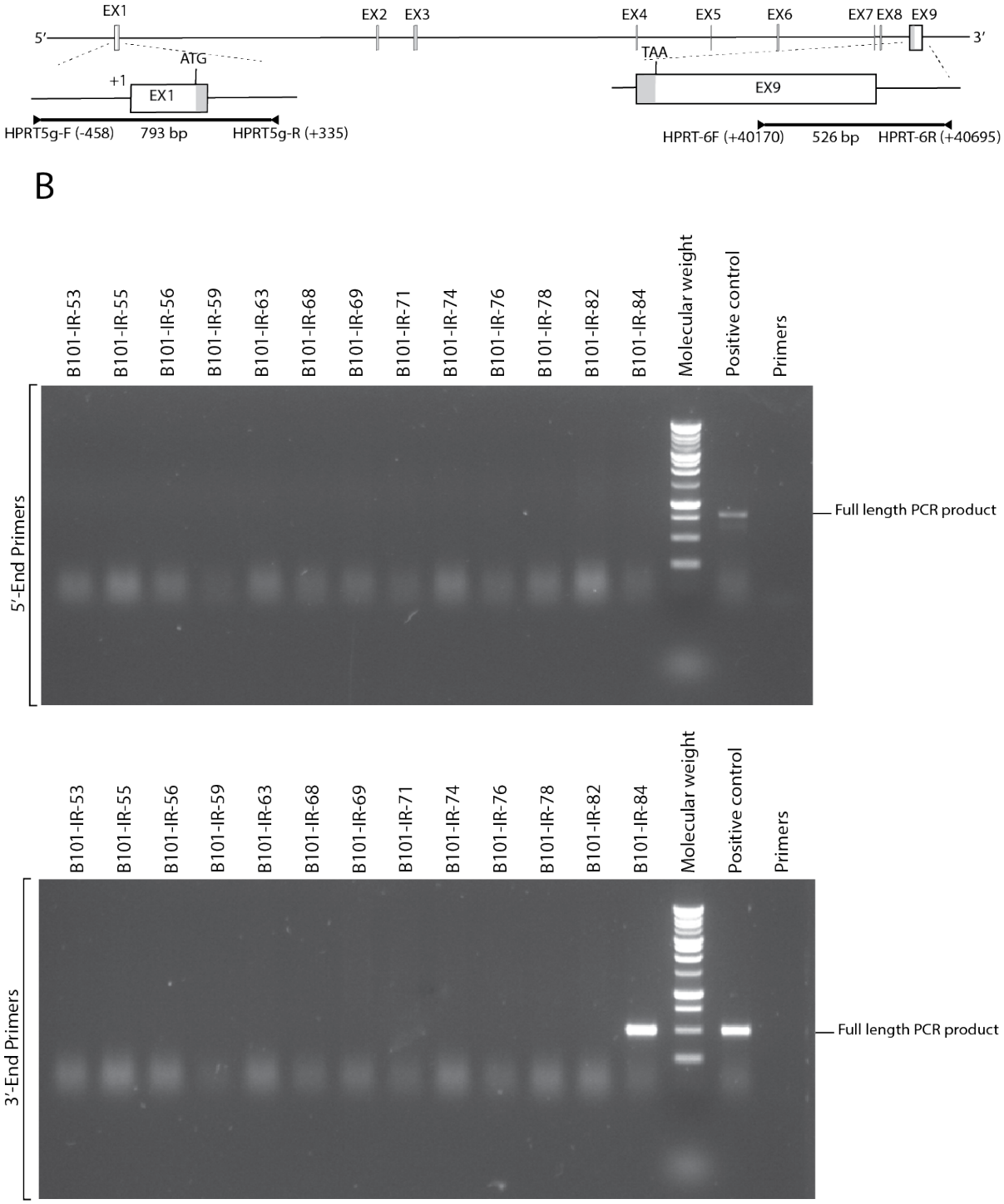

Figure 18: Genomic PCR Results Amplifying *HPRT* 5'- and 3'- Ends in Mutants from Irradiated *BCL11B*$^{+/-}$ B101 Cells

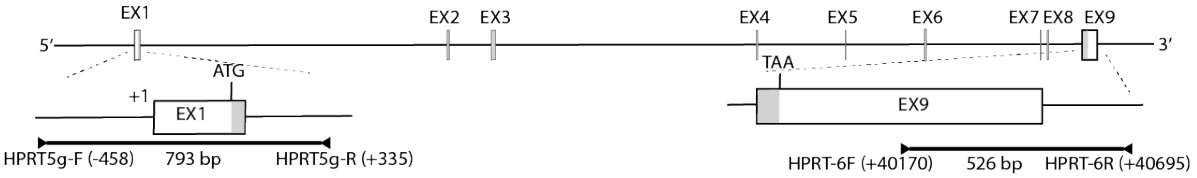

C

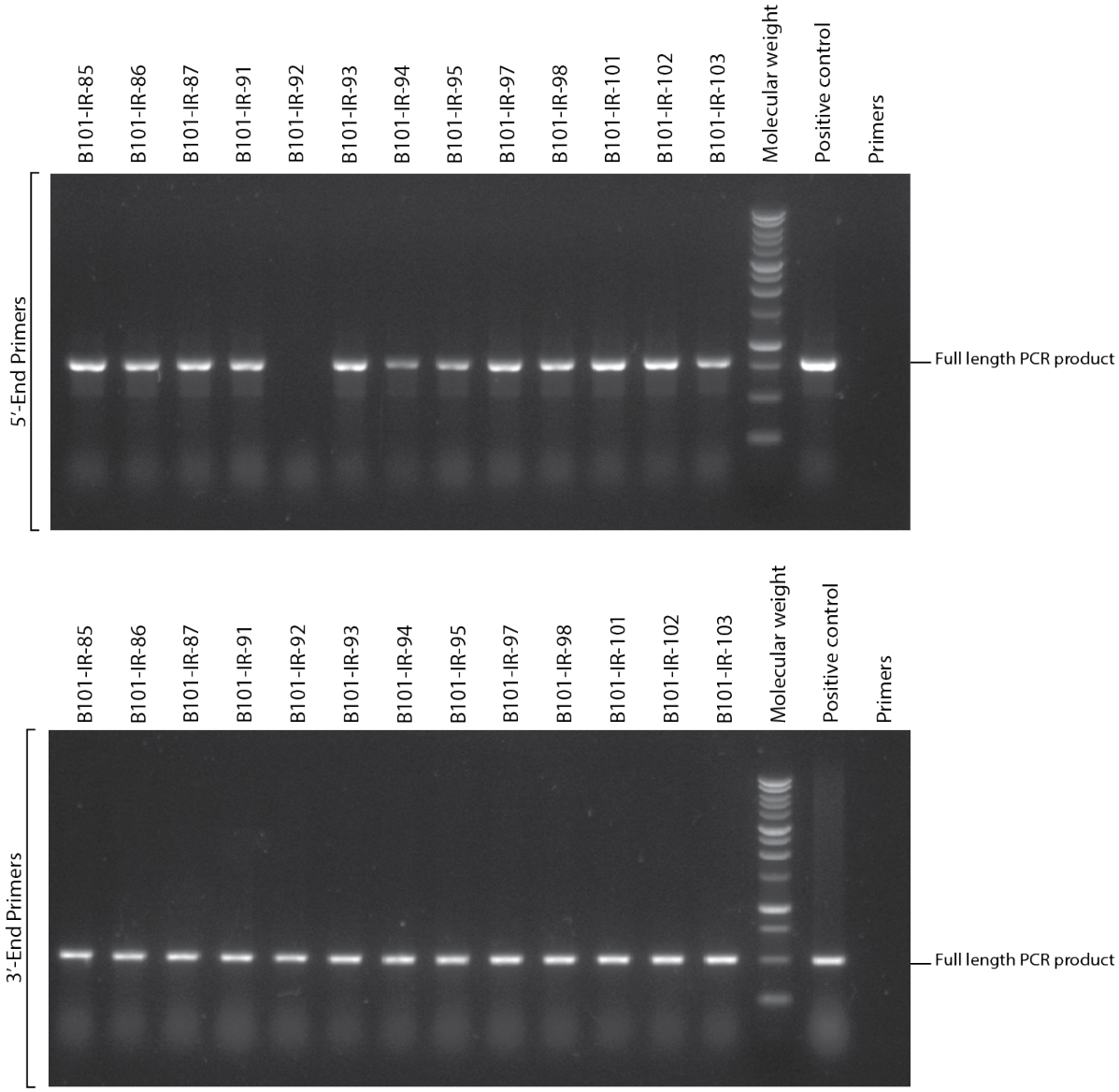

Figure 18: Genomic PCR Results Amplifying *HPRT* 5'- and 3'- Ends in Mutants from Irradiated *BCL11B*$^{+/-}$ B101 Cells

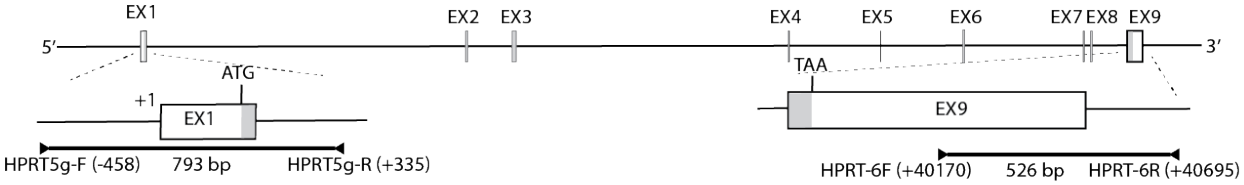

D

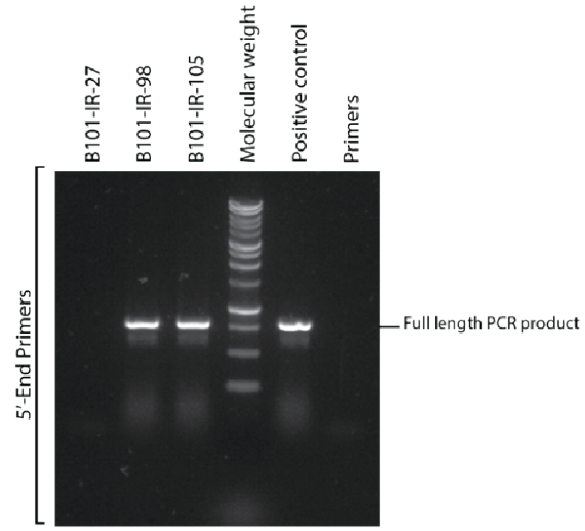

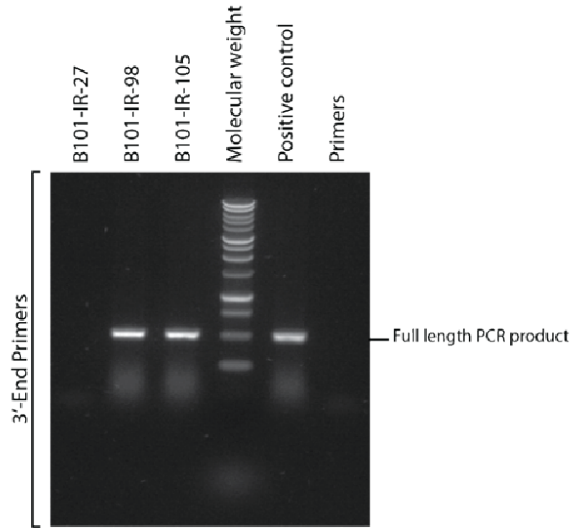

Figure 19: Genomic PCR Results Amplifying *HPRT* 5'- and 3'- Ends in Mutants from Irradiated *BCL11B*$^{+/-}$ B203 Cells

The images show the PCR amplification products of the *HPRT* gene 5'-end and 3'-end from *HPRT* mutants derived from BCL11B$^{+/+}$ TK6 parental cells that did not show any *HPRT* RT-PCR amplification product following radiation. The *HPRT* gene 5'-end was amplified using HPRT-5gF and HPRT-5gR primers, whereas the *HPRT* gene 3'-end was amplified using HPRT-6F and HPRT-6R primers, as indicated in the figure and listed in table 1. The PCR amplification product for the gene 5'-end covers promoter sequences, the first exon and a portion of intron 1, whereas the 3'-end amplification product covers the end of the last exon and 3'-flanking sequences including the polyadenylation site. Samples were found to have both the 5'- and 3' ends, or miss both the 5'-end and 3'-end, or miss either the 5'-end or the 3-end. Overall, the genomic DNA of 22 *HPRT* mutants from the B203 population were analyzed.

Figure 19: Genomic PCR Results Amplifying *HPRT* 5'- and 3'- Ends in Mutants from Irradiated *BCL11B*$^{+/-}$ B203 Cells

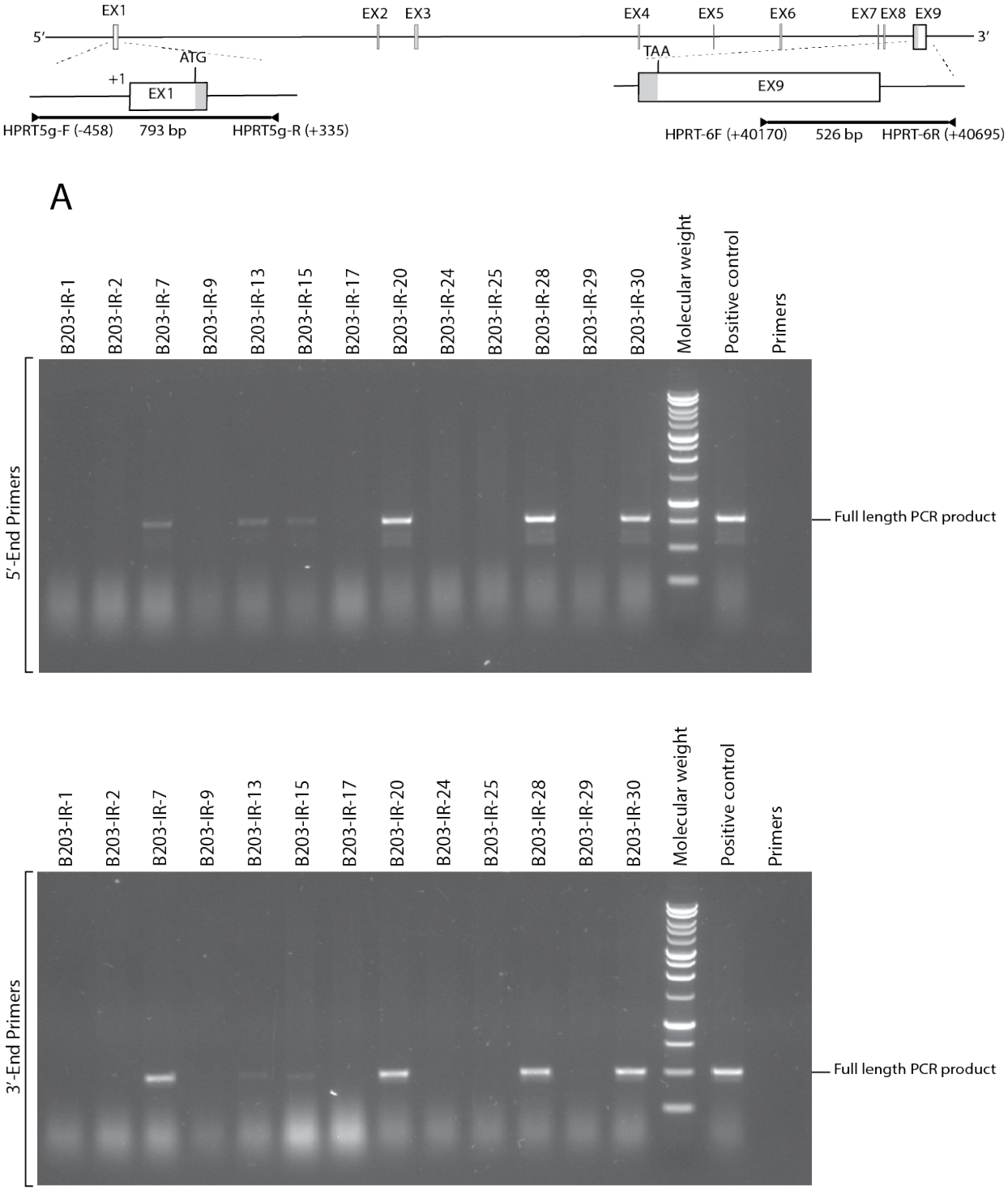

Figure 19: Genomic PCR Results Amplifying *HPRT* 5'- and 3'- Ends in Mutants from Irradiated *BCL11B*$^{+/-}$ B203 Cells

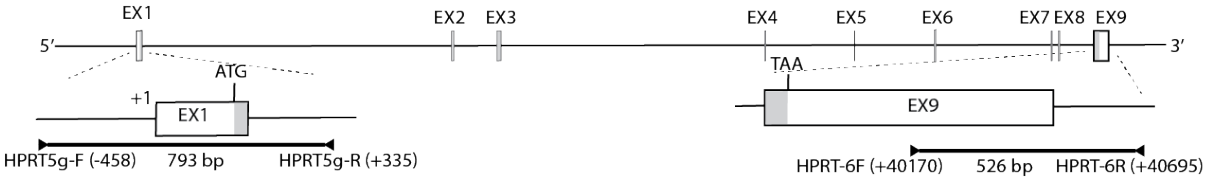

B

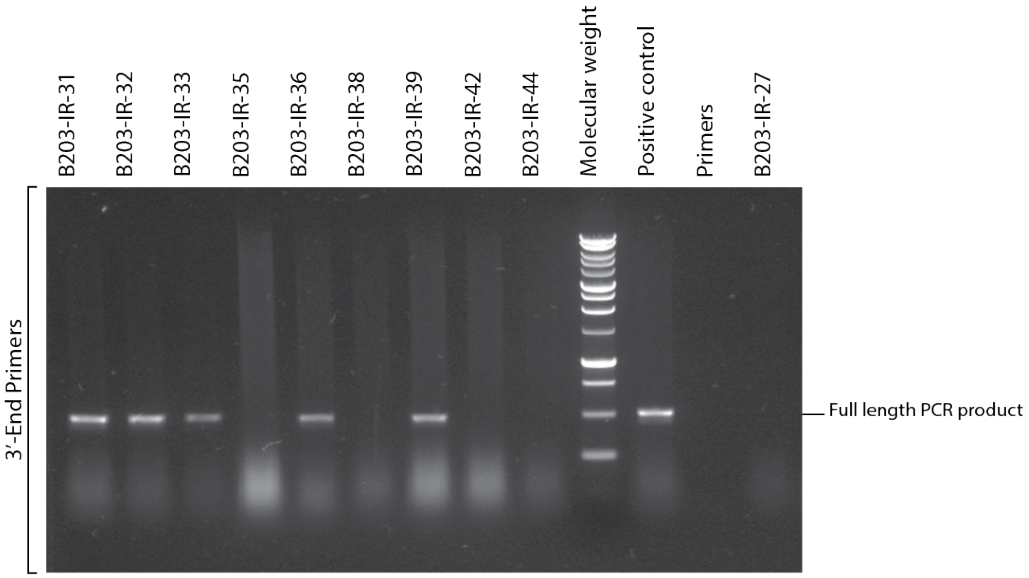

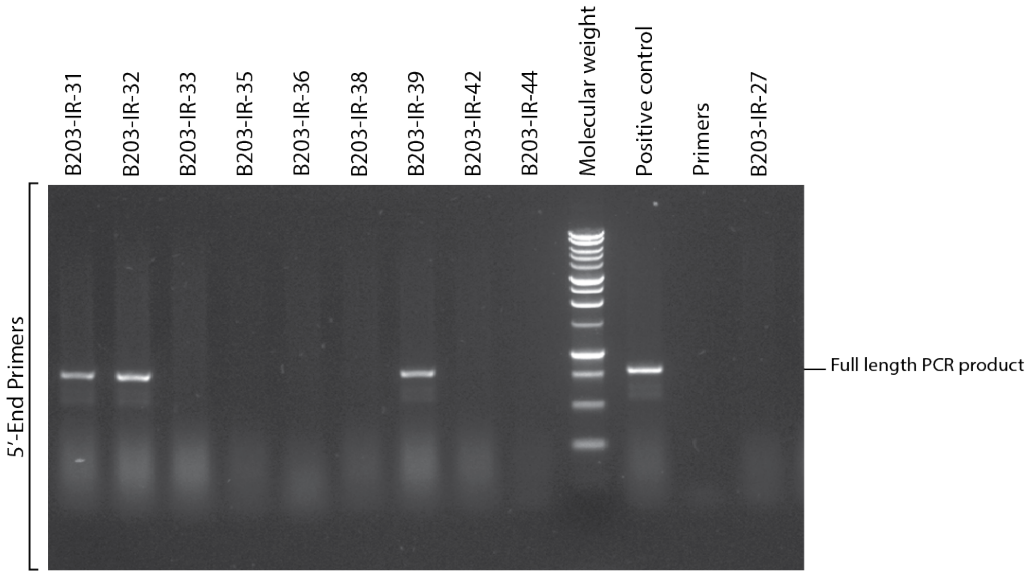

Figure 20: *GAPDH* Gene PCR Amplification Results of Mutants with No *HPRT* 5'- and 3'-Ends PCR Amplification Products Following Ionizing Radiation

The images show the PCR amplification products of the *GAPDH* gene from *HPRT* mutants following radiation. Using genomic DNA, *GAPDH* PCR amplification was performed on *HPRT* mutants that showed neither *HPRT* gene 3'-end nor 5'-end PCR amplification product to ensure the negative result is not due to DNA being of bad quality or not being abundant enough. *GAPDH* PCR amplification was performed using *GAPDH* genomic DNA primers, GAPDH-gDNA-F and GAPDH-gDNA-R, mentioned in table 1. Following the PCR amplification, samples were separated on 1% agarose gel by electrophoresis. All samples showed the expected *GAPDH* PCR amplification product, which confirms the high quality of genomic DNAs.

Figure 20: *GAPDH* Gene PCR Amplification Results of Mutants with No *HPRT* 5'- and 3'-Ends PCR Amplification Products Following Ionizing Radiation

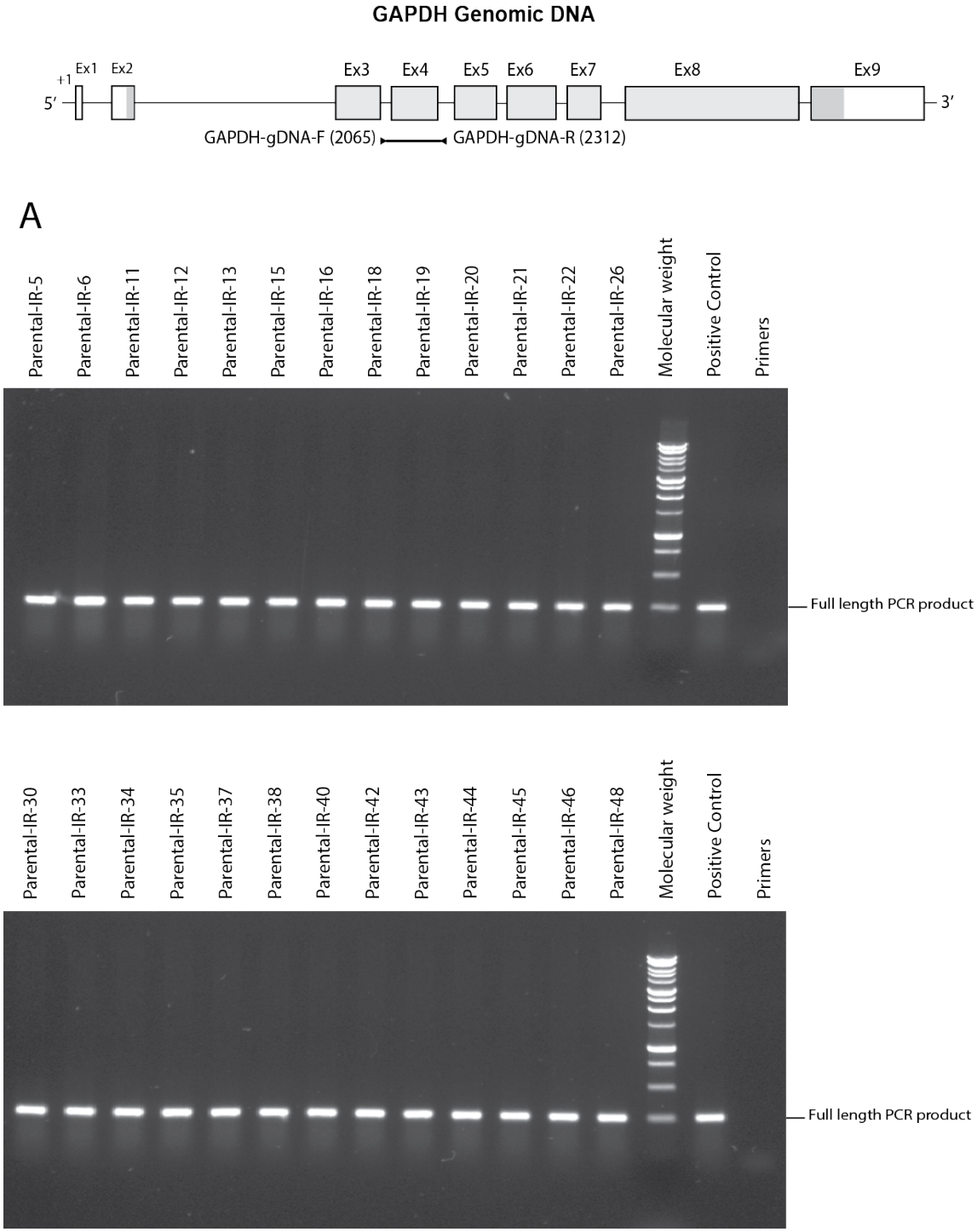

Figure 20: *GAPDH* Gene PCR Amplification Results of Mutants with No *HPRT* 5'- and 3'-Ends PCR Amplification Products Following Ionizing Radiation

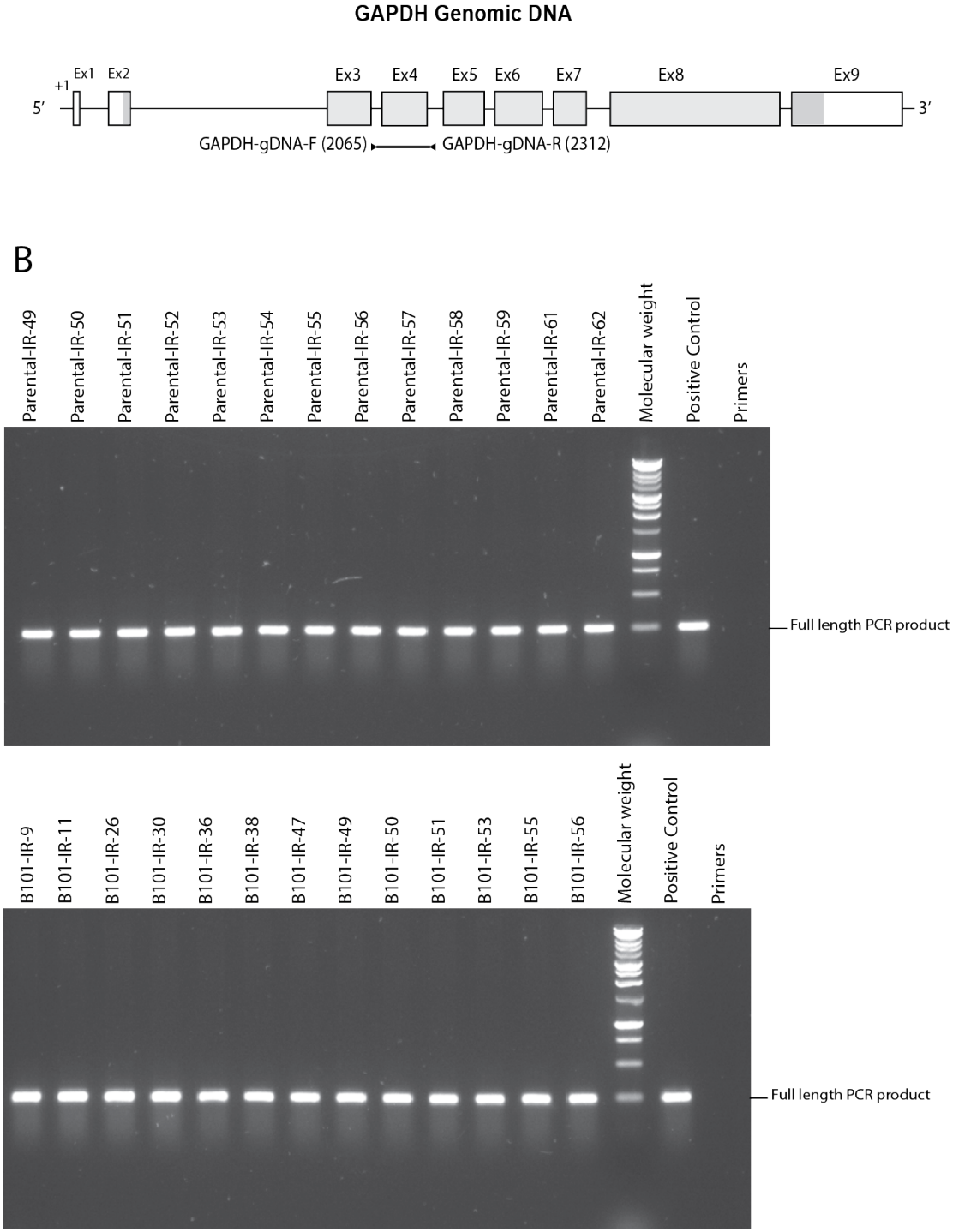

Figure 20: *GAPDH* Gene PCR Amplification Results of Mutants with No *HPRT* 5'- and 3'-Ends PCR Amplification Products Following Ionizing Radiation

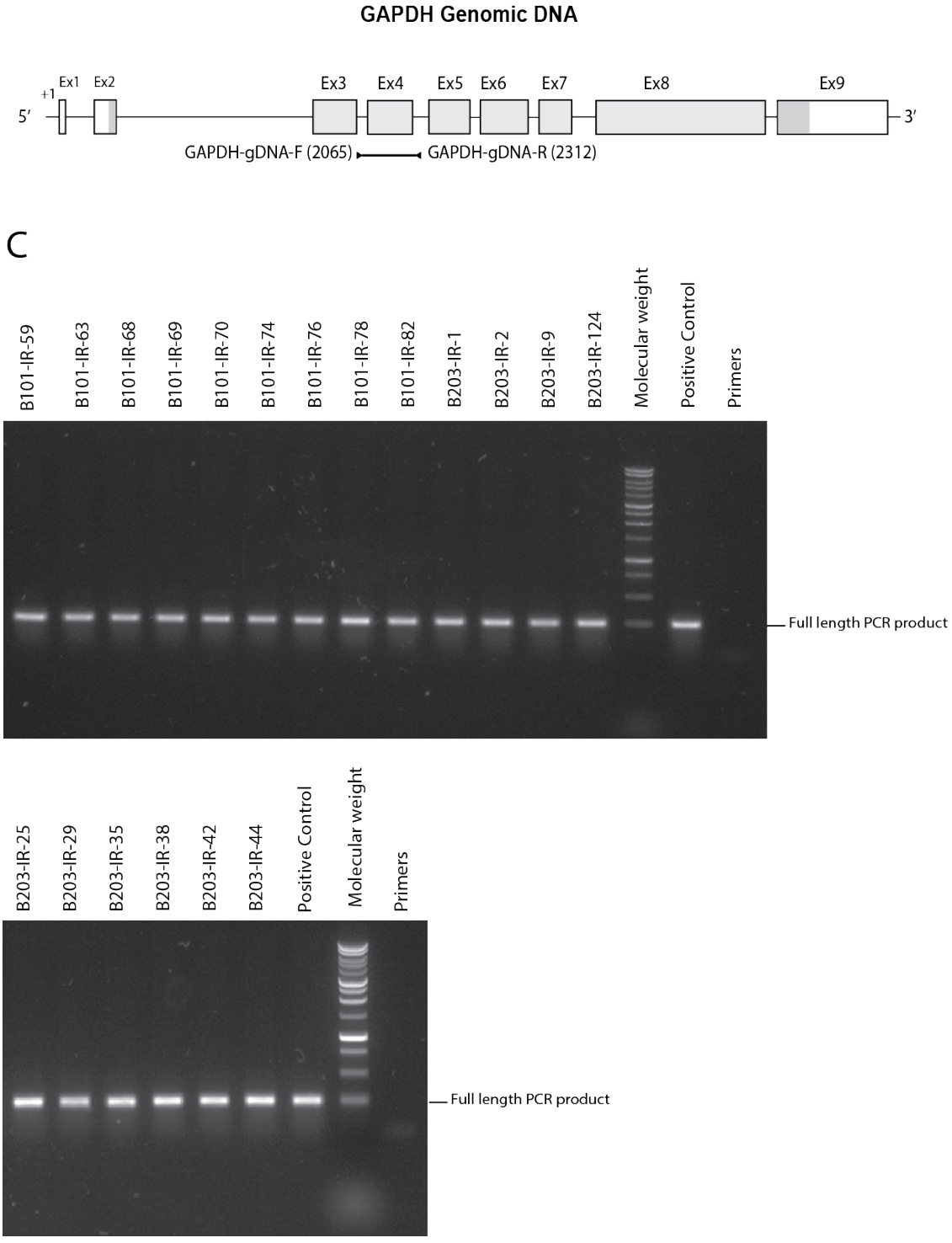

Figure 21: Positions of *HPRT* Mutations Following Ionizing Radiation

Diagrammatic representations of the *BCL11B* gene, mRNA and protein, and positions of mutations following radiation.

The *HPRT* gene has nine exons located on the X chromosome and extends for more than 40250 bp. Number 1 corresponds to the first base in exon 1. Below the gene map, the 5'-end and 3'-end of the gene are enlarged to show the positions of primers to amplify the 5'-end and 3'-end of the gene (all primer sequences are listed in table 1). The coding area is shown in light gray in the genomic DNA and mRNA map. The HPRT protein has two nucleotide-binding regions GMP (shown red) and two GMP binding sites (shown in blue), one of which is in the same position as the metal-binding site.

Positions and types of mutations are shown in the mRNA and protein map. A complex mutation, indicated with "C", is the occurrence of two non-adjacent mutations . Missense, nonsense, and silent mutation are shown with "M", "N" and "Si", respectively. Out-of-frame deletion "OFD" refers to a small deletion (less than one exon) leading to a frameshift and early stop codon. In-frame deletion "IFD" is the small deletion of bases that are devisable by three. Splicing mutation refers to the deletion of the entire length of one or more exons. "F-1" explains mutation with one base pair deletion leading to frameshift. Mutants with the same mutational event originating from the same experiment are written in the same line, with the type of mutation written at the end of the line. Excluded exons due to splicing mutation are shown with dash lines in the lower part of the mRNA and protein map.

Figure 21: Positions of *HPRT* Mutations Following Ionizing Radiation

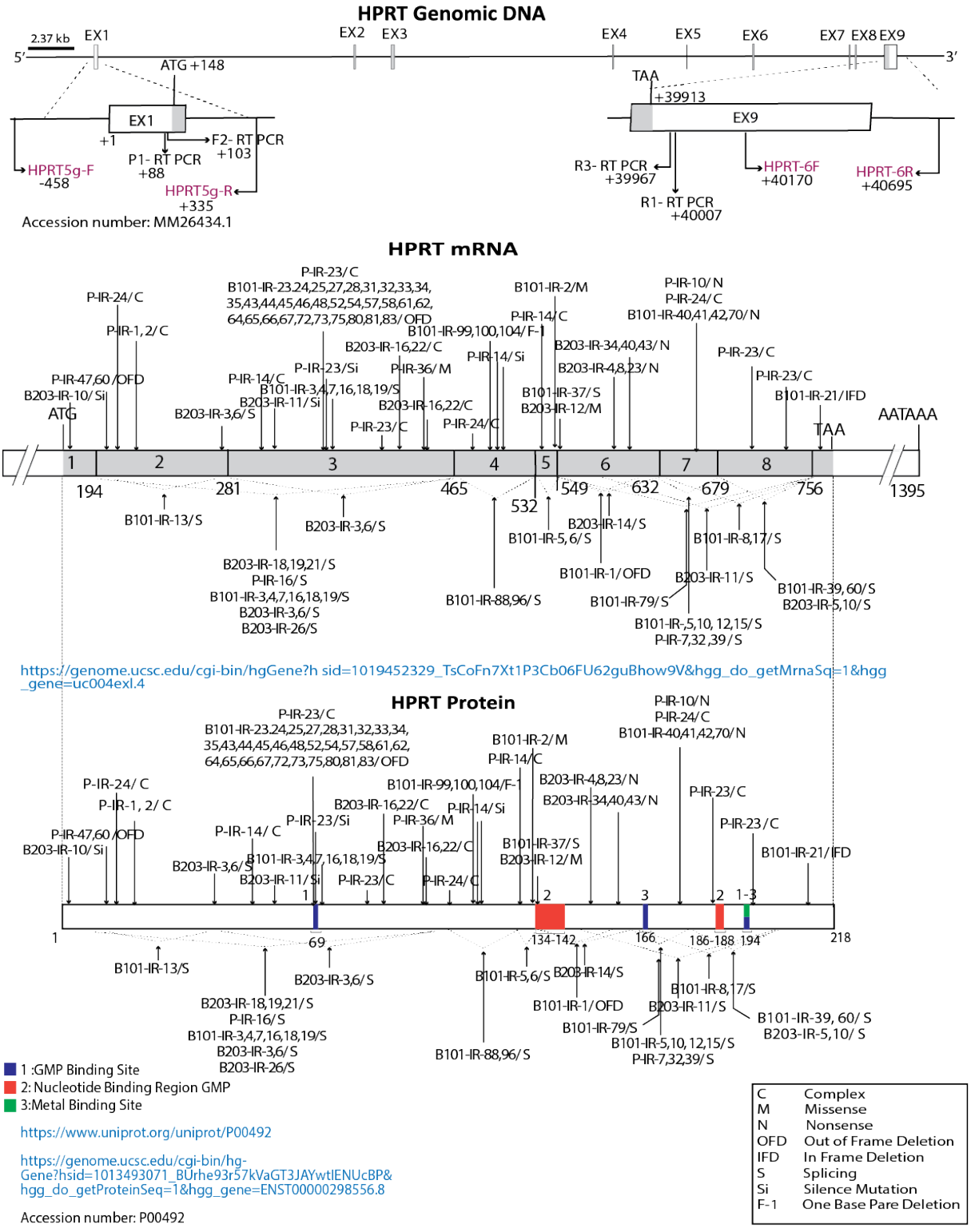

Figure 22: Clonogenic Efficiency in the Fluctuation Assay

The following plot illustrates the clonogenic efficiency results of the fluctuation assay. To perform the clonogenic efficiency assay in the fluctuation assay, 34, 26, and 25 wells of TK6 parental, B101, and B203 cells were plated with 100 cells and expanded for almost seven days until they reach 8×10^6. Each population was plated for clonogenic efficiency at low density (2 cells/well) and incubated for two weeks. Once the number of positive wells was counted, clonogenic efficiency for each population was calculated using the formula

$CE = 1/D_0 \times -\ln(X_0/N_0) \times 100$, where D_0 is the number of cells plated per well (2), X_0 is the number of wells without colonies and N_0 is the number of wells plated in total (192). While the Y-axis represents the clonogenic efficiency percentage, TK6 parental, B101, and B203 samples are specified with circles, squares, and triangles. The black lines indicate the mean, which later served in the calculation of mutation frequency.

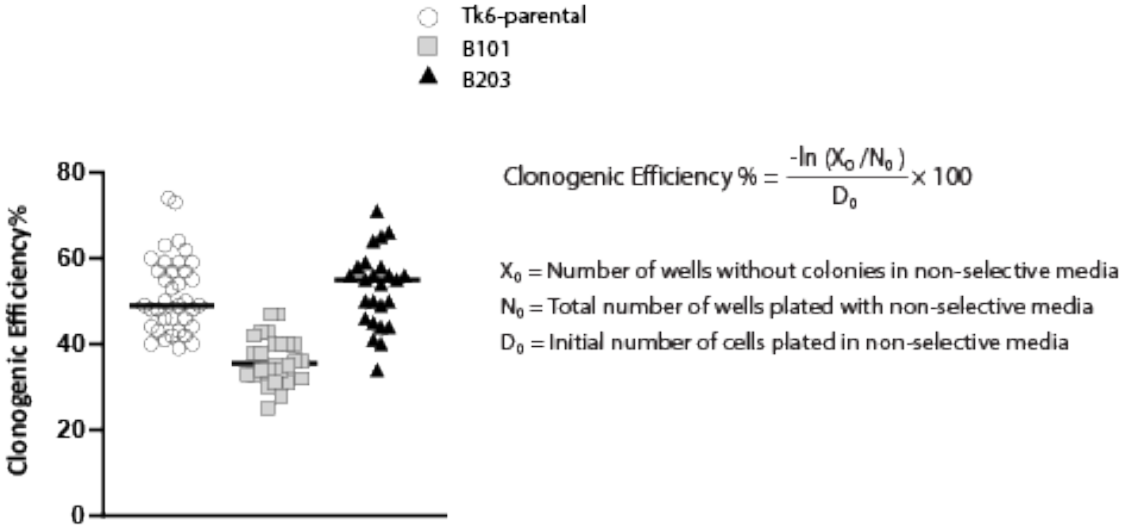

Figure 23: Mutation Rate in the Fluctuation Assay

This bar chart illustrates the spontaneous mutation rate as calculated by the fluctuation assay. Each cell population started with 100 cells and increased to more than 8 million cells during a period of eleven days for the parental cells and twelve days for the *BCL11B*$^{+/-}$ heterozygous cells. Cells were plated for mutation rate with 6-thioguanine at 40000 cells/well the same day as the plating for the clonogenic efficiency. Plates were maintained in culture for approximately 21 days before counting the number of wells with live cells. Mutation frequency was calculated using the equation $MF = -\frac{\ln(P_0/P)}{CE \times N_0}$, where P_0 is the number of populations without mutants, P is the total number of populations, N_0 is the total number of cells plated in selective medium (7680000), and CE is the mean of clonogenic efficiency. There is approximately a two-fold increase in the spontaneous mutation rate of BCL11B$^{+/-}$ TK6 cells compared to *BCL11B*$^{+/+}$ TK6 parental cells. Numbers are presented in table 7.

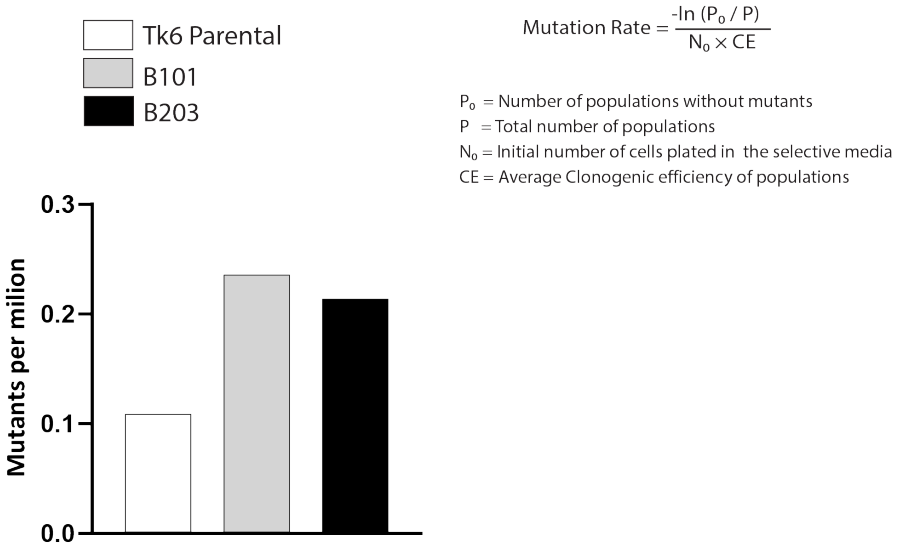

Figure 24: *HPRT* Reverse Transcriptase PCR Amplification in the Fluctuation Assay

The following images show electrophoresis results of *HPRT* RT-PCR amplification in spontaneous *HPRT* mutants from the fluctuation assay

Following RNA extraction of collected mutants and cDNA synthesis, *HPRT* RT-PCR amplification was performed through a nested PCR strategy, using F1 and P1 primers in the first round and F2 and R3 primers in the second round to amplify the coding part of the *HPRT* gene (all primers are indicated in the table 1). PCR amplification products were separated using 1% agarose gel by DNA electrophoresis.

Positive PCR amplification products, including those with full-length and shorter-length PCR amplification products, were sequenced. In addition, bands from multiple PCR amplification products were cut and sequenced individually.

Figures A shows *HPRT* RT-PCR amplification results of spontaneous mutants from the TK6-parental population

Figures B shows *HPRT* RT-PCR amplification results of spontaneous mutants from the B101 population

Figures C shows *HPRT* RT-PCR amplification results of spontaneous mutants from the B203 population

Figure 24: *HPRT* Reverse Transcriptase PCR Amplification in the Fluctuation Assay

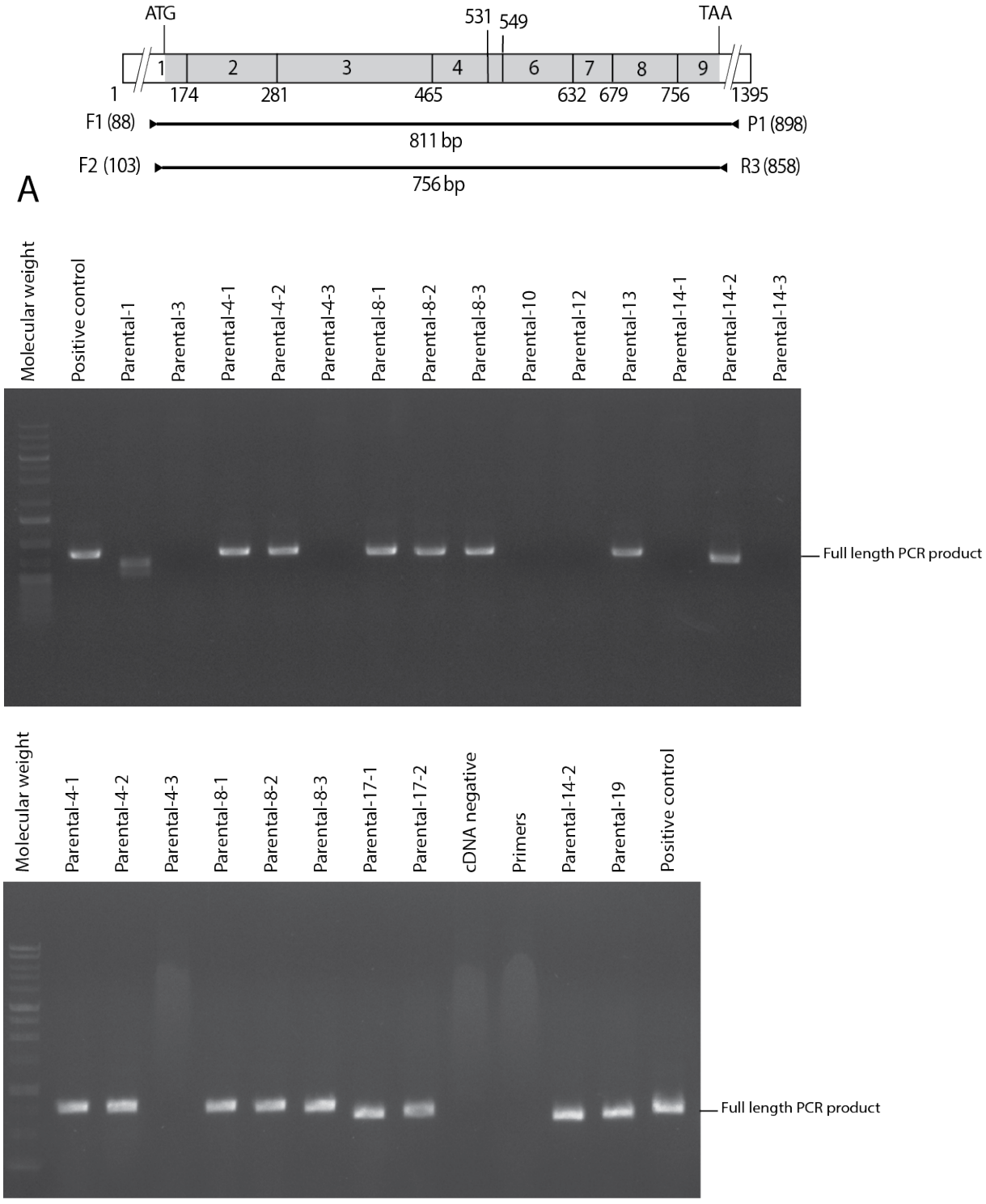

Figure 24: *HPRT* Reverse Transcriptase PCR Amplification in the Fluctuation Assay

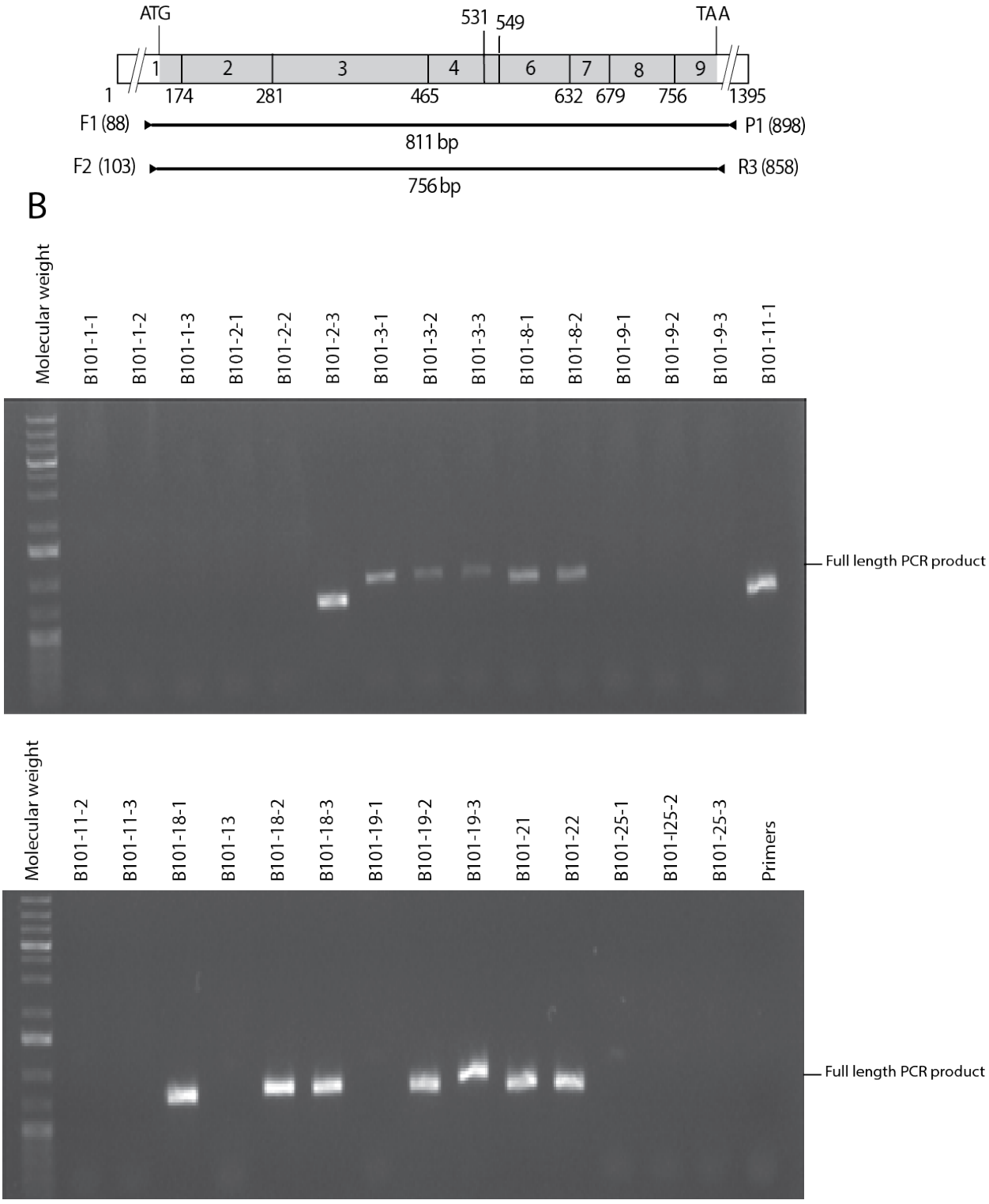

Figure 24: *HPRT* Reverse Transcriptase PCR Amplification in the Fluctuation Assay

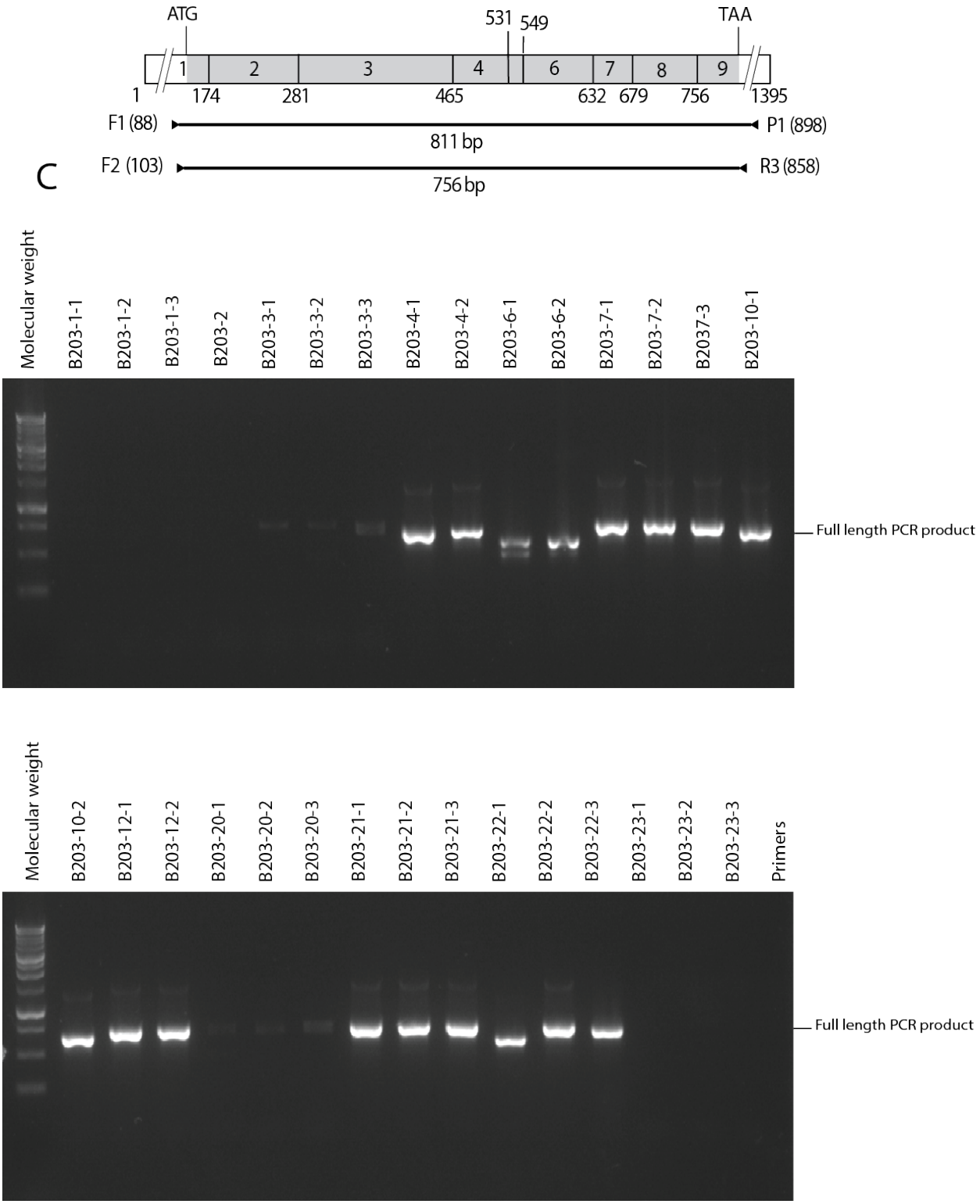

Figure 24: *HPRT* Reverse Transcriptase PCR Amplification in the Fluctuation Assay

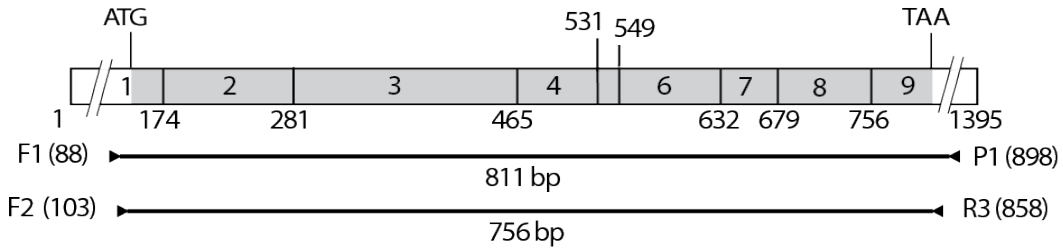

D

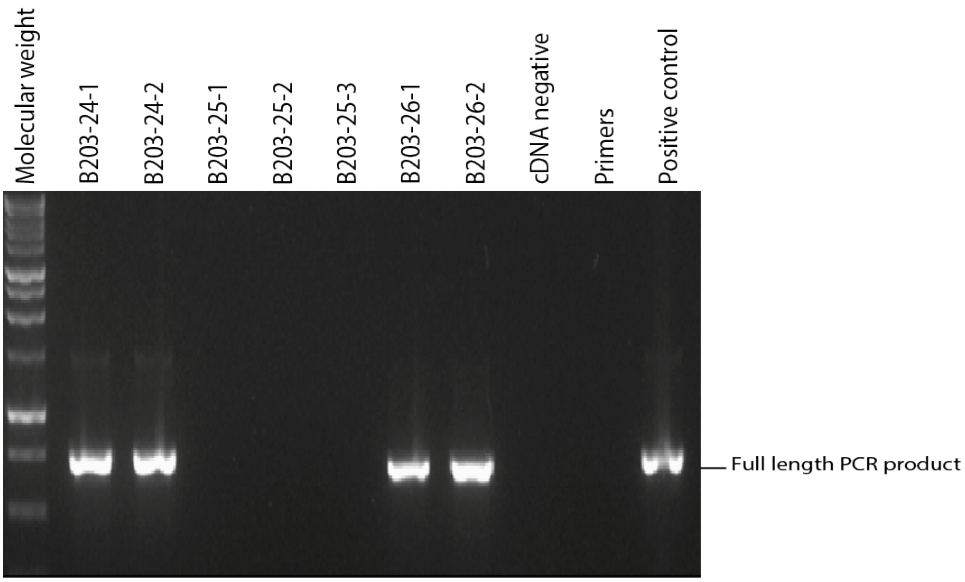

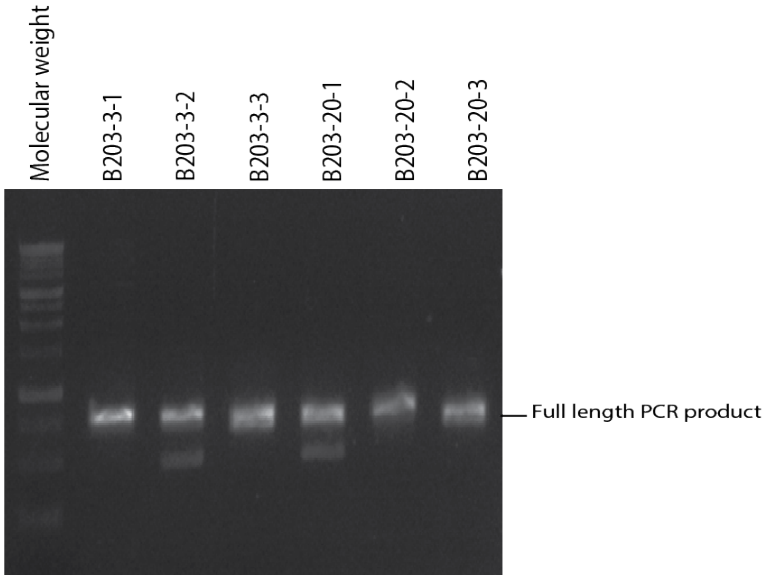

Figure 25: *GAPDH* Reverse Transcriptase PCR Results of Mutants with No *HPRT* RT-PCR Amplification Product in the Fluctuation Assay

Samples with no *HPRT*-RT PCR amplification product underwent *GAPDH* RT-PCR amplification to ensure that negative results with *HPRT* were not due to the bad quality of cDNAs or RNAs. *GAPDH* RT-PCR amplification was carried out using *GAPDH* RT-PCR primers mentioned in table 1. All samples showed the expected band size, 450 bp, which confirms the high quality of cDNAs and RNAs.

Figure 25: *GAPDH* Reverse Transcriptase PCR Results of Mutants with No *HPRT* RT-PCR Amplification Product in the Fluctuation Assay

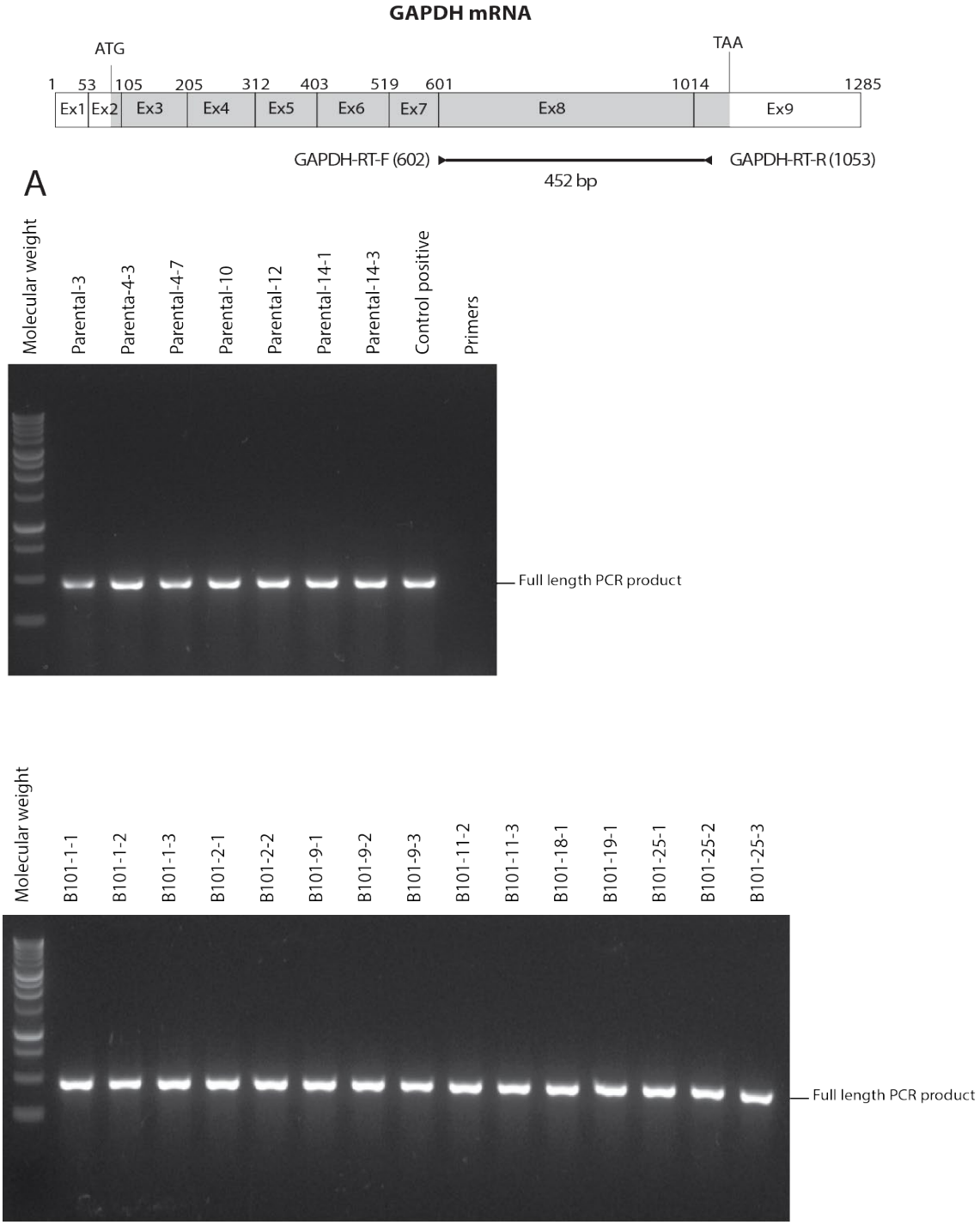

Figure 25: *GAPDH* Reverse Transcriptase PCR Results of Mutants with No *HPRT* RT-PCR Amplification Product in the Fluctuation Assay

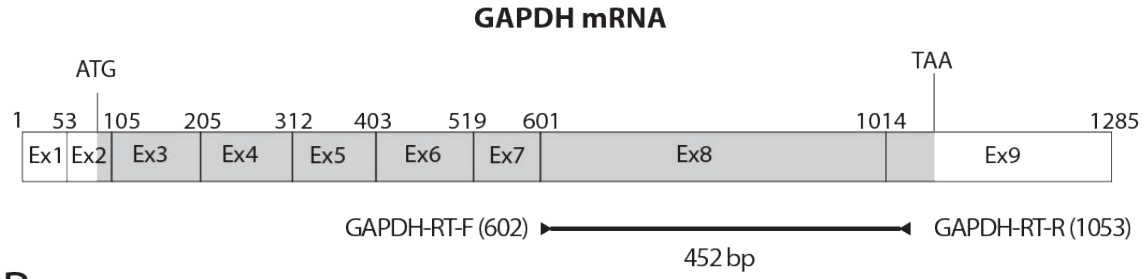

B

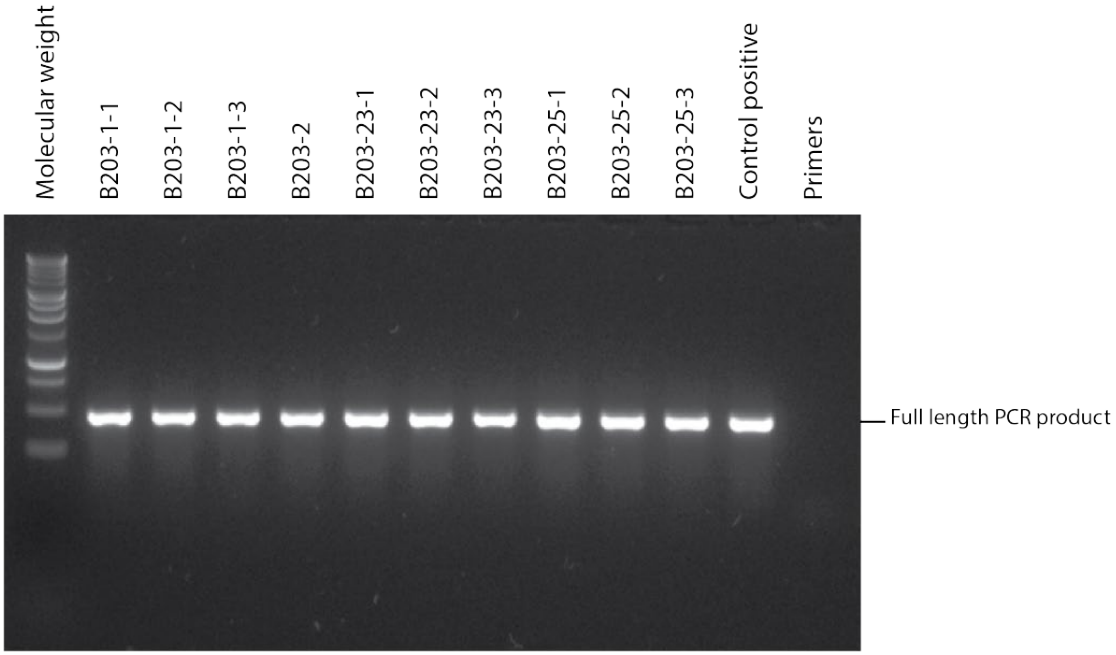

Figure 26: Genomic PCR Results Amplifying HPRT 5'- and 3'- Ends in the Fluctuation Assay

The images show the PCR amplification products of the *HPRT* gene 5'-end and 3'-end from *HPRT* mutants that did not show any *HPRT* RT-PCR amplification product in the fluctuation assay. The *HPRT* gene 5'-end was amplified using HPRT-5gF and HPRT-5gR primers, whereas the *HPRT* gene 3'-end was amplified using HPRT-6F and HPRT-6R primers, as indicated in the figure and listed in table 1. The PCR amplification product for the gene 5'-end covers promoter sequences, the first exon, and a portion of intron 1, whereas the 3'-end amplification product covers the end of the last exon and 3'-flanking sequences including the polyadenylation site. Samples were found to have both the 5'- and 3'-ends, or miss both the 5'-end and 3'-end, or miss either the 5'-end or the 3-end.

Figure 26: Genomic PCR Results Amplifying *HPRT* 5'- and 3'- Ends in the Fluctuation Assay

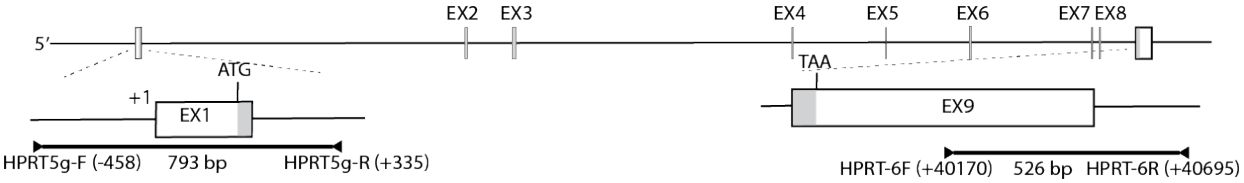

A

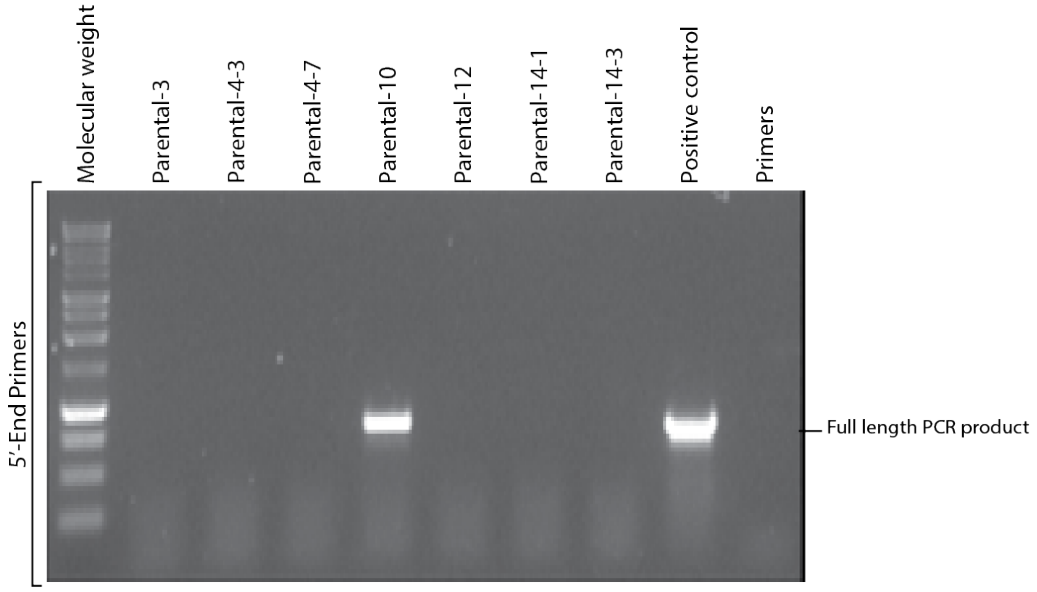

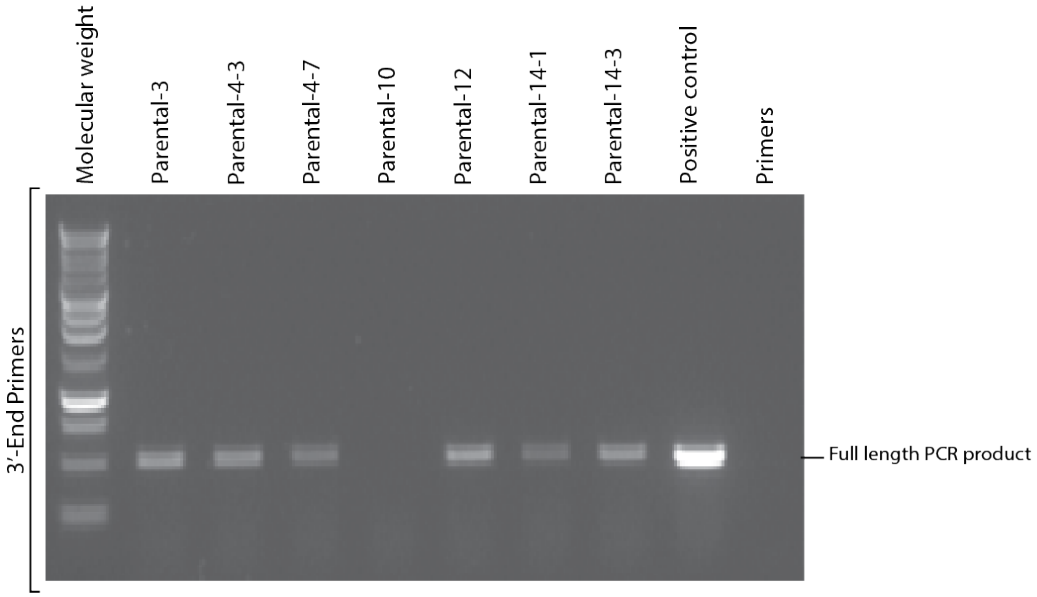

Figure 26: Genomic PCR Results Amplifying *HPRT* 5'- and 3'- Ends in the Fluctuation Assay

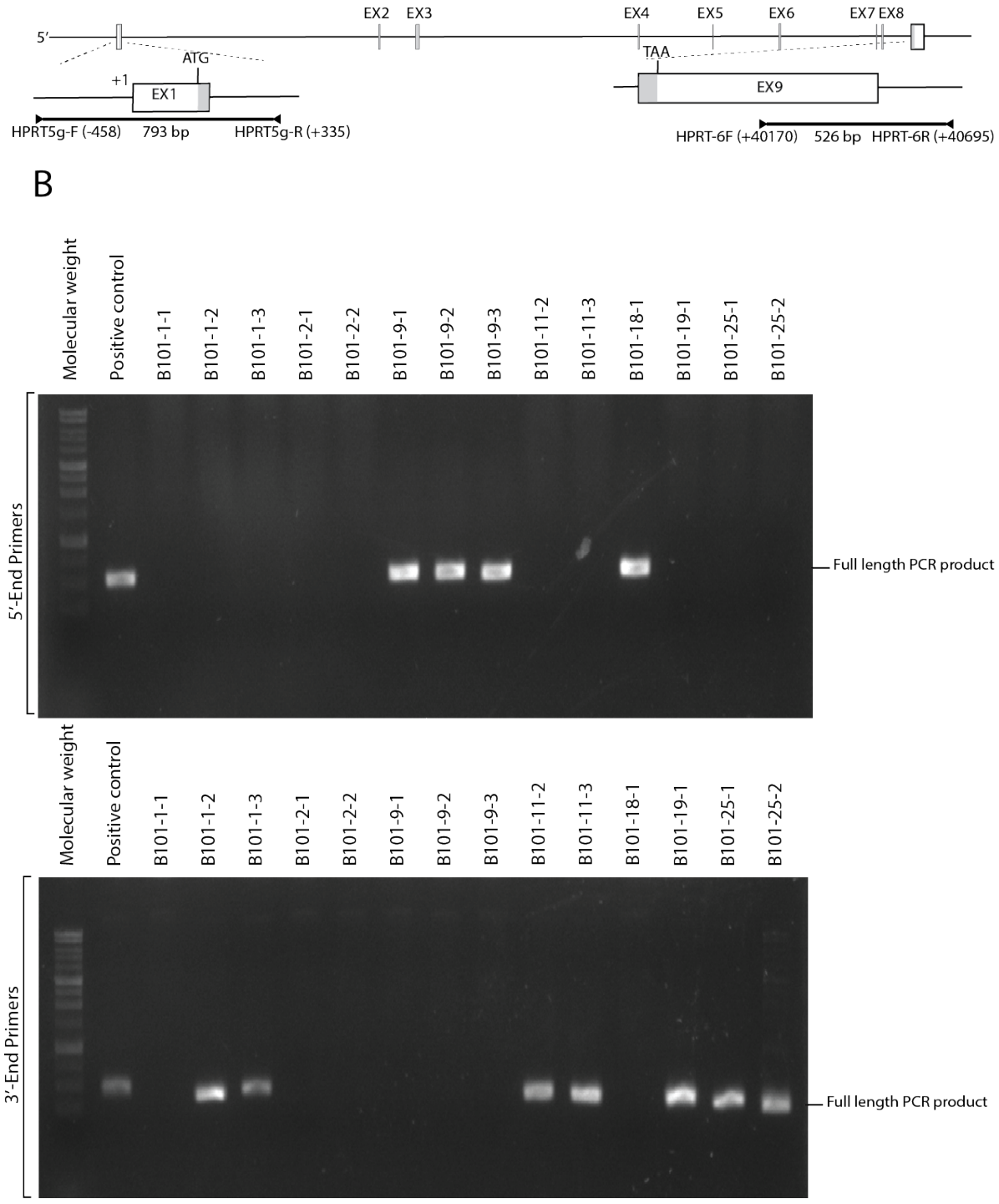

Figure 26: Genomic PCR Results Amplifying *HPRT* 5'- and 3'- Ends in the Fluctuation Assay

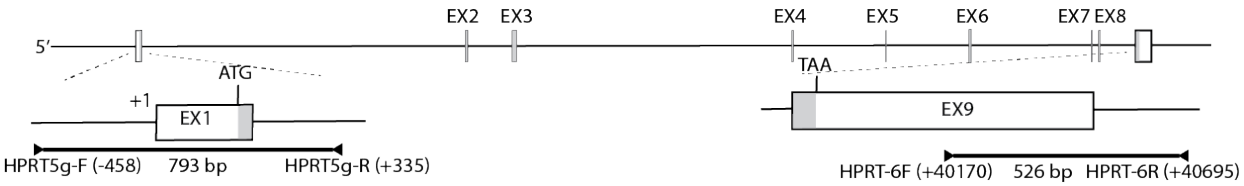

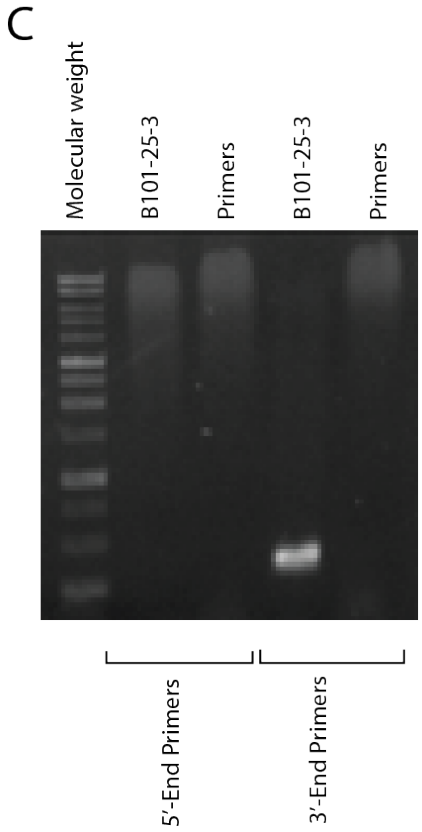

Figure 26: Genomic PCR Results Amplifying *HPRT* 5'- and 3'- Ends in the Fluctuation Assay

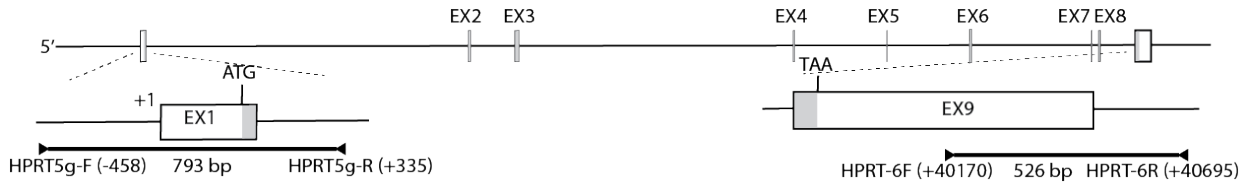

D

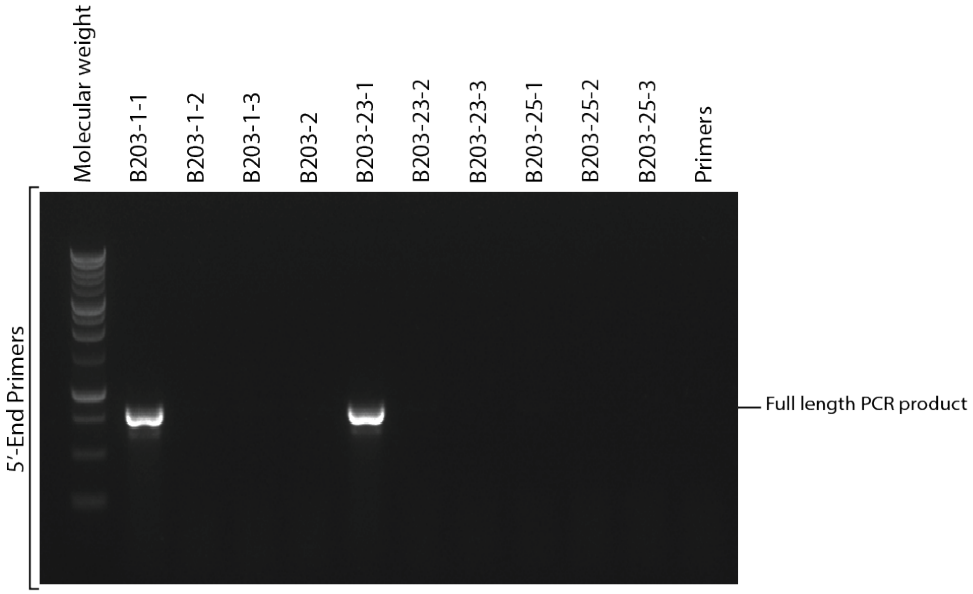

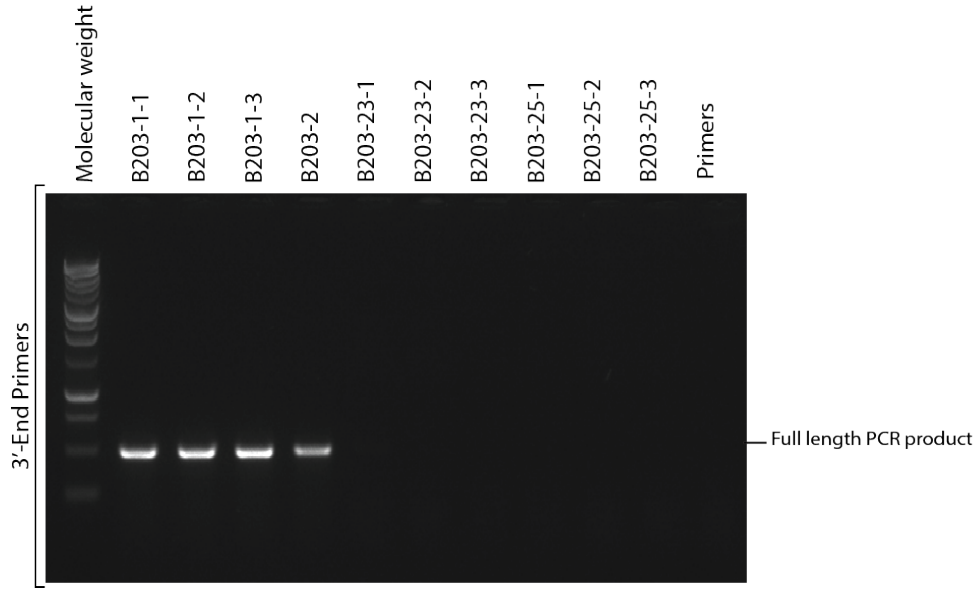

Figure 27: *GAPDH* Gene PCR Amplification Results of Mutants with No *HPRT* 5'- and 3'-Ends PCR Amplification Products in the Fluctuation Assay

The images show the PCR amplification products of the *GAPDH* gene from *HPRT* mutants in the fluctuation assay. Using genomic DNA, *GAPDH* PCR amplification was performed on *HPRT* mutants that showed no *HPRT* gene 3'-end and 5'-end PCR amplification products to ensure the negative result is not due to DNA being of bad quality or not being abundant enough. *GAPDH* PCR amplification was performed using *GAPDH* genomic DNA primers, GAPDH-gDNA-F and GAPDH-gDNA-R, mentioned in table 1. Following the PCR amplification, samples were separated on 1% agarose gel by electrophoresis. All samples showed the expected *GAPDH* PCR amplification product, which confirms the high quality of extracted DNAs

Figure 27: *GAPDH* Gene PCR Amplification Results of Mutants with No *HPRT* 5'- and 3'-Ends PCR Amplification Products in the Fluctuation Assay

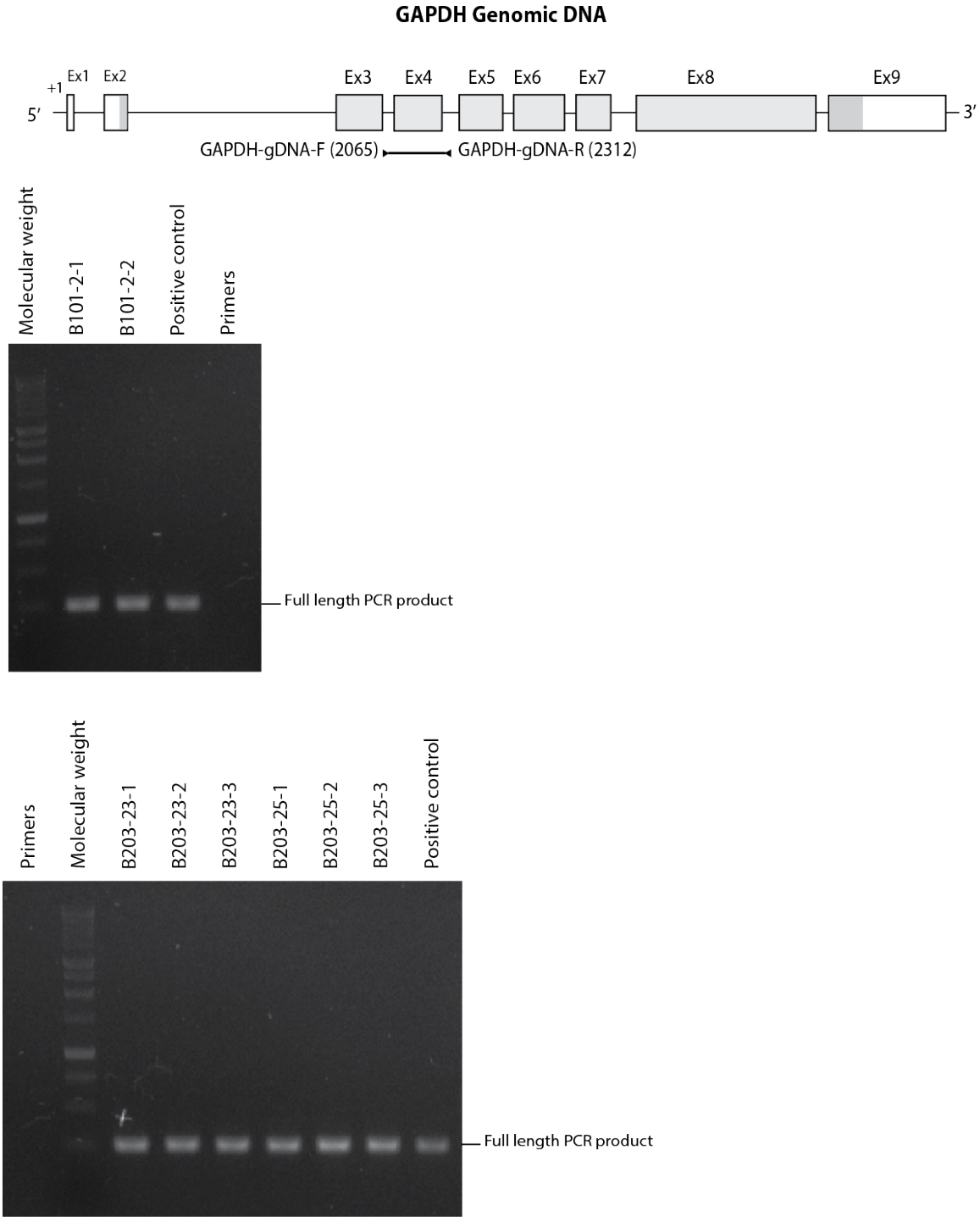

Figure 28: Positions of *HPRT* Mutations in the Fluctuation Assay

Diagrammatic representations of the *BCL11B* gene, mRNA and protein, and positions of mutations in the fluctuation assay.

HPRT gene has nine exons located on the X chromosome and extends for more than 40250 bp. Number 1 corresponds to the first base in exon 1. Below the gene map, the 5'-end and 3'-end of the gene are enlarged to show the positions of primers to amplify the 5’-end and 3'-end of the gene (all primer sequences are indicated in table 1). The coding area is shown in light gray in the genomic DNA and mRNA map. HPRT protein has two nucleotide-binding regions GMP (shown red) and two GMP binding sites (shown in blue), one of which is in the same position as the metal-binding site.

Positions and types of mutation are shown in the mRNA and protein map following *HPRT* RT-PCR amplification sequencing. A complex mutation, indicated with “C”, is the occurrence of two non-adjacent mutations. Missense and nonsense mutations are shown with “M” and “N. out-of-frame deletion “OFD” refers to a small deletion (less than one exon) leading to a frameshift and early stop codon. In-frame deletion “IFD” is the small deletion of bases that are devisable by three. Splicing mutation refers to the deletion of the entire length of one or more exons. “F-1” explains mutation with one base pair deletion leading to frameshift and introducing of an early stop codon. Mutants with the same mutational event originating from the same experiment are written in the same line, with the type of mutation written at the end of the line. Excluded exons due to splicing mutation are shown with dash lines at the lower part of the mRNA and protein map.

Figure 28: Positions of *HPRT* Mutations in the Fluctuation Assay

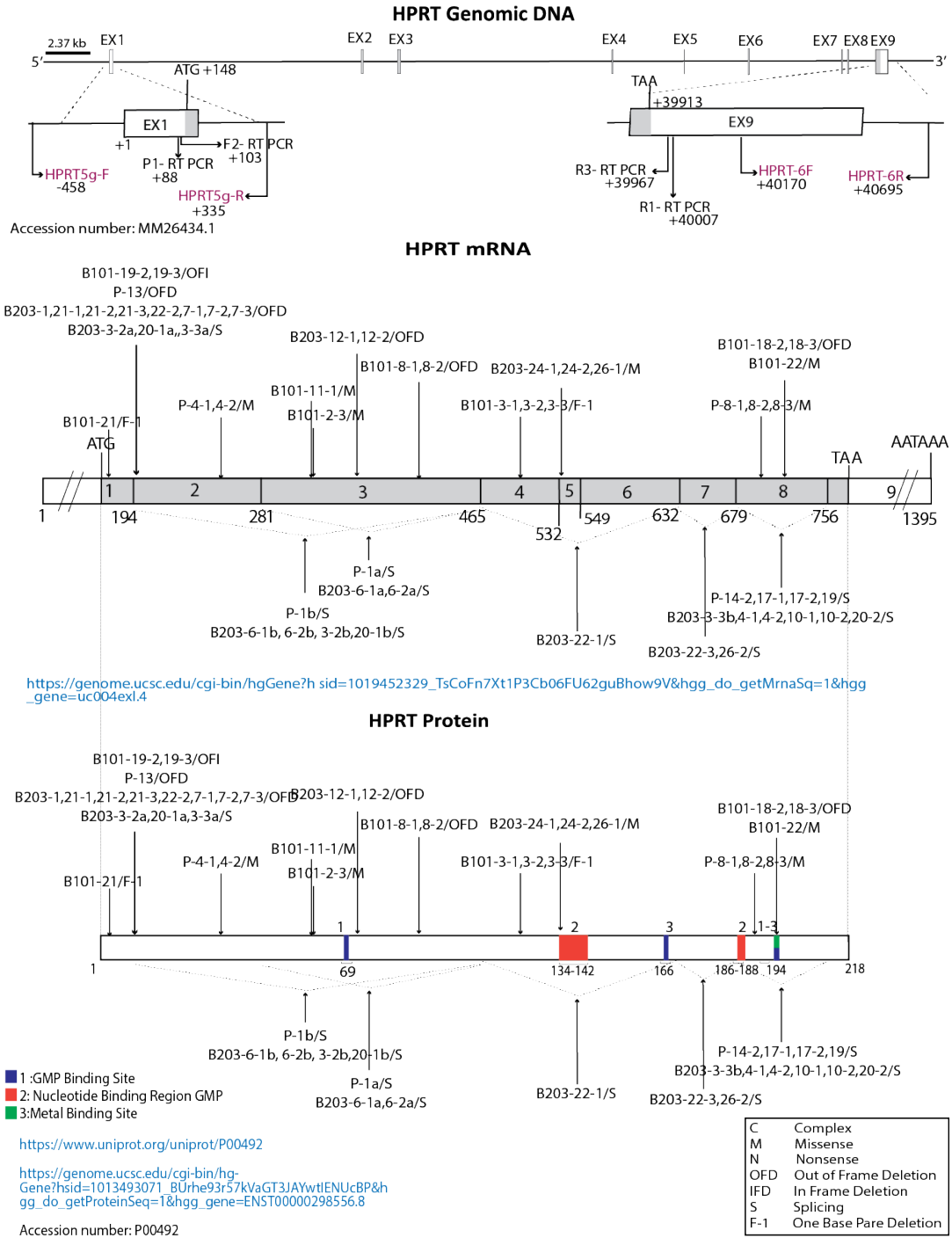

TABLES

Table 2: Indel Frequency of Three Guide RNAs Against *BCL11B*

The following table indicates the indel frequencies for three guide RNAs used in this study. Following nucleoporation, genomic DNA was purified from the cell population and a fragment of the *BCL11B* gene encompassing the targeted sequence was amplified using BCL11B long F1 and BCL11B long R primers (indicated in table 1). Next, PCR amplification products underwent denaturing and reannealing steps before incubation with the T7 endonuclease I enzyme. Cleaved fragments were quantified with ImageJ software following DNA electrophoresis on 7% agarose gel. Indel frequency was calculates using the formula $Indel\% = 100 \times (1\sqrt{1 - \frac{(b+c)}{(a+b+c)}})$ where "a" is the band intensity of the full-length PCR amplification product, and "b" and "c" are band intensities of the cleaved PCR amplification products.

Guide RNA Name	**Indel Frequency (%)**
***BCL11B* gRNA#1**	11.5
***BCL11B* gRNA#2**	19.0
***BCL11B* gRNA#3**	19.1

Table 3: Clonogenic Efficiency and Mutation Frequency of TK6 Parental, B101 and B203 Populations Following Ionizing Radiation

This table represents clonogenic efficiency and mutation frequency results following radiation from 0.5 to 2 Gy performed on different dates. In addition, the number of mutants in the two 96-well plates for the mutation frequency is indicated in the last column.

Date	Population	Clonogenic Efficiency %	Mutation Frequency ×10^-6	Number of Wells with Proliferating Cells in Selective Medium
2020/05/05	**TK6 Parental-nIR**	31%	4	9
	TK6 B101-nIR	22%	13	21
	TK6 B203-nIR	31%	0	1
	TK6 Parental-2Gy	4%	38	10 (10 out of 10 were collected)
	TK6 B101-2Gy	4%	76	21 (21 out of 21 were collected)
	TK6 B203-2Gy	2%	201	23 (23 out of 23 were collected)
2020/10/1	**TK6 Parental-nIR**	26%	4	7
	TK6 B101-nIR	20%	9	13
	TK6 B201-nIR	27%	2	4
	TK6 B203-nIR	29%	18	36
	TK6 Parental-2Gy	2%	237	31 (30 out of 31 were collected)
	TK6 B101-2 Gy	1%	1287	64 (62 out of 64 were collected)
	TK6 B201-2 Gy	2%	337	37
	TK6 B203-2 Gy	2%	315	40
2020/10/18	**TK6 Parental-nIR**	32%	4	10
	TK6 B101-nIR	12%	2	2
	TK6 B201-nIR	28%	3	7
	TK6 B203-nIR	19%	4	5
	TK6 Parental-2Gy	1%	433	32
	TK6 B101-2 Gy	1%	153	12
	TK6 B201-2 Gy	1%	498	19
	TK6 B203-2 Gy	1%	1936	64
2021/01/22	**TK6 Parental-nIR**	25%	2	3
	TK6 B101-nIR	23%	10	17
	TK6 B201-nIR	27%	9	17
	TK6 B203-nIR	19%	12	17
	TK6 Parental-1Gy	5%	34	13
	TK6 B101-1 Gy	5%	115	37
	TK6 B201-1 Gy	5%	47	17
	TK6 B203-1 Gy	5%	44	16

Table 3: Clonogenic Efficiency and Mutation Frequency of TK6 Parental, B101 and B203 Populations Following Ionizing Radiation (continued)

2021/01/24	**TK6 Parental-nIR**	21%	14	14
	TK6 B101-nIR	13%	7	7
	TK6 B201-nIR-d	19%	2	2
	TK6 B203-nIR-d	27%	2	2
	TK6 Parental-1Gy-d	4%	70	70
	TK6 B101-1 Gy	3%	153	153
	TK6 B201-1 Gy	4%	251	251
	TK6 B203-1 Gy	6%	32	32
	TK6 Parental-1.5Gy	3%	161	161
	TK6 B101-1.5 Gy	1%	114	114
	TK6 B201-1.5 Gy	3%	90	90
	TK6 B203-1.5 Gy	2%	204	204

Table 4: Detailed Information of Analyzed Mutants Through Sequencing of *HPRT* RT-PCR Amplification Products Following Ionizing Radiation

The following table details the type of mutations as defined from the sequencing analysis of *HPRT* RT-PCR amplification products following radiation. The column “Position” indicates the position of the mutation on mRNA, where 1 is the first base of the *HPRT* exon 1. The column "Mutations" indicate the type of mutation, either deletion or base substitution. The column “Nucleotide Change” shows the specific base substitution. The column “Kind” column indicates the type of mutation, either C, M, N. OFD, IFD, S orF-1. A complex mutation indicated with “C”, is the occurrence of two non-adjacent mutations. Missense, nonsense, and silent mutation are shown with “M”, “N”, and “Si”, respectively. Out-of-frame deletion, “OFD”, refers to a small deletion (less than one exon) leading to a frameshift and early stop codon. In-frame deletion, “IFD” is the small deletion of bases that are devisable by three. Splicing mutation refers to the deletion of the entire length of one or more exons. “F-1” indicates mutation with one base pair deletion leading to frameshift and introducing of an early stop codon. Lastly, U indicates samples that did not show any mutation in the *HPRT* RT-PCR amplification sequencing. The columns "aa#" and "Effect" show the effect of the mutation at the protein level.

Table 4: Detailed Information of Analyzed Mutants Through Sequencing of *HPRT* RT-PCR Amplification Products Following Ionizing Radiation

Mutant#	*Position	Mutation	Nucleotide Change	Kind	Codon Change	aa#	Effect
P-IR-1 P-IR-2	219-220 221 224 226	Deletion Base substitution Base substitution Base substitution	 C >T transition A >T transversion C >T transition	C			Frameshift
P-IR-3	No mutation was found			U			
P-IR-7	633-678	Deletion		S			Exon 7 exclusion leading to Frameshift
P-IR-10	655	Base substitution	C >T transition	N		170	Arg > stop codon
P-IR-14	307 504 538 633-679 (Ex7)	Base substitution Base substitution Base substitution Deletion	A>G transition A>G transition T>C transition	C Silent	ATG>GTG GGA>GGG TTG>CTG	54 119 131	Met>Val Gly>Gly Leu>ser Frameshift
P-IR-16	176-466	Deletion		S			Ex2. Ex3 exclusion

Table 4: Detailed Information of Analyzed Mutants Through Sequencing of *HPRT* RT-PCR Amplification Products Following Ionizing Radiation (continued)

Mutant#	*Position	Mutation	Nucleotide Change	Kind	Codon Change	aa#	Effect
P-IR-23	354-355	Deletion		C			Frameshift
	405	Base substitution	T>C transition	Silent	AAT>AAC	86	Asn>Asn
	708	Base substitution	T>G transversion		TTT>TTG	187	Phe> leo
	734	Base substitution	A>G transition		AAT>	196	Asn>Ser
P-IR-24	197	Base substitution	A>G transition	C	TAT>TGT	17	Tyr > Cys
	488	Base substitution	T>C transition		ATA> ACA	114	Ile > Thr
	655	Base substitution	C>T transition		CGA>TGA	170	Arg>stop codon
P-IR-32 P-IR-39	633-679	Deletion		S			Ex7 exclusion leading to Frameshift
P-IR-36	444	Base substitution	T>A transversion	M	TTT>TTA	99	Phe > leu
P-IR-47 P-IR-60	181-185	Deletion		OFD			Frameshift
B101-IR-1	550-616	Deletion		D			Frameshift
B101-IR-2	547	Base substitution	G>A transition	M	GAA>AAA	134	Glue > Lys
B101-IR-6 B101-IR-5	532-549	Deletion		S			Ex5 exclusion
B101-IR-3a B101-IR-4a B101-IR-7a B101-IR-14a B101-IR-16a B101-IR-18a B101-IR-19a	358	Deletion		F-1			Frameshift

f

Table 4: Detailed Information of Analyzed Mutants Through Sequencing of *HPRT* RT-PCR Amplification Products Following Ionizing Radiation (continued)

Mutant#	*Position	Mutation	Nucleotide Change	Kind	Codon Change	aa#	Effect
B101-IR-3b B101-IR-4b B101-IR-7b B101-IR-14a B101-IR-16b B101-IR-18b B101-IR-19b	Poor sequencing results						
B101-IR-3c B101-IR-4c B101-IR-7c B101-IR-14c B101-IR-16a B101-IR-18c B101-IR-19c	176-466	Deletion		S			Ex2-3 exclusion
B101-IR-8 B101-IR-17	634-757	Deletion		S			Ex7-8 exclusion
B101-IR-5 B101-IR-10 B101-IR-12 B101-IR-15	633-679	Deletion		S			Ex 7 exclusion
B101-IR-13	184-279	Deletion+46bp(from intron 2)		S			Frameshift
B101-IR-21	769-771	Deletion		IFD		208	Loss of Ile

Table 4: Detailed Information of Analyzed Mutants Through Sequencing of *HPRT* RT-PCR Amplification Products Following Ionizing Radiation (continued)

Mutant#	*Position	Mutation	Nucleotide Change	Kind	Codon Change	aa#	Effect
B101-IR23 B101-IR24 B101-IR25 B101-IR27 B101-IR28 B101-IR31 B101-IR32 B101-IR33 B101-IR34 B101-IR35 B101-IR43 B101-IR44 B101-IR45 B101-IR46 B101-IR48 B101-IR52 B101-IR54 B101-IR57 B101-IR58 B101-IR61 B101-IR62 B101-IR64 B101-IR65 B101-IR66 B101-IR67 B101-IR72 B101-IR73 B101-IR75 B101-IR80 B101-IR81 B101-IR83	354-355	Deletion		OFD			Frameshift
B101-IR-37	549	Insertion (67bp from intron 5)		S			Frameshift
B101-IR-39 B101-IR-60	680-756	Deletion		S			Ex8 exclusion
B101-IR-40 B101-IR-41 B101-IR-42 B101-IR-70	655	Base substitution	C>T transition	N	CGA>TGA	170	Arg > stop codon
B101-IR-79	550-756	Deletion		S			Ex6-7-8 exclusion leading to frameshift

Table 4: Detailed Information of Analyzed Mutants Through Sequencing of *HPRT* RT-PCR Amplification Products Following Ionizing Radiation (continued)

Mutant#	*Position	Mutation	Nucleotide Change	Kind	Codon Change	aa#	Effect
B101-IR-88 B101-IR-96	466-531	Deletion		S			Ex 4 exclusion
B101-IR-99 B101-IR-100 B101-IR-104	501	Deletion		F-1			Frameshift
B203-IR-3a B203-IR-6a	277 282-465	Base substitution Deletion	G>C transversion	C	GAC>TAC	44	Asp>Tyr Ex3 exclusion leading to frameshift
B203-IR-3b B203-IR-6b	176-466	Deletion		S			Ex2-3 exclusion
B203-IR-4 B203-IR-8 B203-IR-23	590-591	Base substitution	CC>AG transversion	N	TCC>TAG	148	Ser> stop codon
B203-IR-5	680-756	Deletion		S			Ex8 exclusion
B203-IR-10	680-756 165	Deletion Base substitution	 T>C transition	S silent	 CCT>CCC	 6	Ex8 exclusion
B203-IR-11	583-758 321	Deletion+ 2bp insertion Base substitution	 A>G transition	D silent	 GGA>GGG	 58	Partial Exclusion of Ex6 and complete exclusion of Ex7, 8
B203-IR-12	550	Base substitution	G>C transversion	M	GAT>CAT	135	Asp > His
B203-IR-14	550-632	Deletion		S			Exon 6 exclusion
B203-IR-16 B203-IR-22	412 448	Base substitution Base substitution	A>T transversion A>T transversion	C	AGT>TGT AGA>TGA	89 101	Ser >Cys Arg > stop codon
B203-IR-18 B203-IR-19 B203-IR-21	175-465	Deletion		S			EX2-3 exclusion

Table 4: Detailed Information of Analyzed Mutants Through Sequencing of *HPRT* RT-PCR Amplification Products Following Ionizing Radiation (continued)

B203-IR-26	175-465	Deletion		S			EX2-3 exclusion
B203-IR-34 B203-IR-40 B203-IR-43	613	Base substitution	A>T transversion	N	AAG>TAG	156	Lys>stop codon

Table 5: Analysis of Mutations and Types of Point Mutations Following Ionizing Radiation

Table A shows types of radiation-induced mutations according to the sequencing results of the *HPRT* RT-PCR amplification product and *HPRT* gene 3'-end and 5'-end PCR amplification product*s*. Replicates in mutants with full-length and shorter-length PCR amplification products are counted as a one-time mutational event in table A.

Full-length and shorter-length PCR amplification products display either point mutation or large genomic deletion according to the sequencing analysis. In addition, mutants with negative RT-PCR amplification product and 5'-end and/or 3'-end gene deletion represent large genomic deletion or rearrangement. However, some types of mutation could not be defined, such as mutants with multiple bands in RT-PCR amplification and mutants with no RT PCR amplification but positive 5'-end and 3'-end *HPRT* genes amplification. Finally, some collected mutants with positive RT-PCR amplification products could not be analyzed due to poor sequencing results.

Table B displays different types of point mutations indicated in the first row of table A.

Table 5: Analysis of Mutations and Types of Point Mutations Following Ionizing Radiation

A

Analysis	Type of Mutation	TK6	B101	B203
RT-PCR product (full length and shorter length due to splicing errors)	Point Mutation	11 (22%)	14 (24%)	8 (24.2 %)
RT-PCR product (shorter length)	Large Deletion	-	-	2 (6%)
RT-PCR product (Multiple bands)	Undefined (Multiple clones/ Point mutation)	-	2 (3.5 %)	2 (6%)
No RT-PCR product, 5'-end and/or 3'-end gene deletion	Large deletion or rearrangement	36 (65 %)	27 (47.3 %)	12 (36.3%)
No RT-PCR product, 5'-end and 3'-end gene present	Undefined	3 (5.45%)	14 (24.5 %)	9 (27.2%)
Full-length PCR product which could not be sequenced	Undefined	1	4	3

B

Type of mutation	TK6 Parental	B101	B203
Complex	4	-	1
Nonsense mutation	1	1	2
Missense Mutation	1	1	1
Out of frame deletion	1	2	-
In-frame deletion	-	1	-
1 bp deletion (F-1)	-	1	-
Splicing	3	8	6

Table 6: Clonogenic Efficiency and Number of Mutants Arising from Individual Populations in the Fluctuation Assay

The fluctuation assay was performed using 34, 26, and 25 populations of *BCL11B*$^{+/+}$ TK6 parental cells, *BCL11B*$^{+/-}$ B101 cells, and *BCL11B*$^{+/-}$ B203 cells. The table indicates the clonogenic efficiency percentage for each population and the number of positive wells in two 96-well plates of 6-tg selective medium. The clonogenic efficiency percentage was calculated using the equation $CE = 1/D_0 \times -\ln(X_0/N_0) \times 100$, where D_0 is the number of cells plated per well (2), X_0 is the number of wells without colonies and N_0 is the number of wells plated in total (192).

Table 6: Clonogenic Efficiency and Number of Mutants Arising from Individual Populations in the Fluctuation Assay

BCL11B$^{+/+}$ TK6 parental			BCL11B$^{+/-}$ B101 Clone			BCL11B$^{+/-}$ B203 Clone		
Population	Clonogenic Efficiency %	Positive Wells in the *HPRT*$^{-}$ Selective Media	Population	Clonogenic Efficiency %	Positive Wells in the *HPRT*$^{-}$ Selective Media	Population	Clonogenic Efficiency %	Positive Wells in the *HPRT*$^{-}$ Selective Media
1	43%	1	1	36%	10	1	55%	3
2	39%	0	2	40%	3	2	56%	1
3	54%	0	3	35%	8	3	59%	15
4	40%	0	4	36%	0	4	49%	2
5	41%	0	5	34%	0	5	50%	0
6	50%	0	6	33%	0	6	34%	2
7	42%	0	7	31%	0	7	41%	3
8	40%	2	8	43%	2	8	50%	0
9	43%	0	9	43%	7	9	58%	0
10	46%	5	10	33%	0	10	44%	2
11	53%	0	11	34%	9	11	46%	0
12	48%	0	12	30%	0	12	40%	2
13	57%	1	13	31%	1	13	56%	0
14	59%	0	14	47%	0	14	56%	0
15	50%	1	15	40%	0	15	58%	0
16	57%	7	16	38%	0	16	54%	0
17	62%	0	17	25%	0	17	66%	0
18	46%	0	18	40%	6	18	64%	0
19	42%	0	19	47%	8	19	44%	0
20	64%	36	20	28%	0	20	56%	4
21	55%	0	21	42%	1	21	71%	8
22	46%	1	22	32%	1	22	65%	5
23	48%	0	23	40%	0	23	45%	4
24	44%	1	24	35%	0	24	55%	2
25	48%	1	25	34%	13	25	50%	3
26	60%	3	26	38%	2			
27	59%	0						
28	49%	0						
29	57%	2						
30	49%	0						
31	74%	1						
32	49%	0						
33	55%	0						
34	44%	0						

Table 7: Mutation Rates of TK6 Parental, B101, and B203 Populations in the Fluctuation Assay

The table indicates the spontaneous mutation rate as calculated by the fluctuation assay. Each cell population started with 100 cells and increased to more than 8 million cells during a period of eleven days for the parental cells and twelve days for the *BCL11B*$^{+/-}$ heterozygous cells. Cells were plated for mutation rate with 6-thioguanine at 40000 cells/well the same day as the plating for the clonogenic efficiency. Plates were maintained in culture for approximately 21 days before counting the number of wells with live cells. The Mutation rate was calculated using the equation $MF = -\frac{\ln(P_0/P)}{CE \times N_0}$ where P_0 is the number of populations without mutants, P is the total number of populations, N_0 is the total number of cells plates for the mutation rate (7680000), and CE is the mean of clonogenic efficiency.

Population	Average Clonogenic Efficiency	Mutation Rate
TK6 Parental	0.52	0.1.09 E-07
B101	0.36	2.36 E-07
B203	0.52	2.14 E-07

Table 8: Detailed Information of Mutations from Sequencing of *HPRT* RT-PCR Amplification Products in the Fluctuation Assay

The following table details the type of mutations as defined from the sequencing analysis of *HPRT* RT-PCR amplification products following radiation. The column “Position” indicates the position of the mutation on mRNA, where 1 is the first base of the *HPRT* exon 1. The column "Mutations" indicate the type of mutation, either deletion or base substitution. The column “Nucleotide Change” shows the specific base substitution. The column “Kind” column indicates the type of mutation, either C, M, N. OFD, IFD, S orF-1. A complex mutation indicated with “C”, is the occurrence of two non-adjacent mutations. Missense, nonsense, and silent mutation are shown with “M”, “N”, and “Si”, respectively. Out-of-frame deletion, “OFD”, refers to a small deletion (less than one exon) leading to a frameshift and early stop codon. In-frame deletion, “IFD” is the small deletion of bases that are devisable by three. Splicing mutation refers to the deletion of the entire length of one or more exons. “F-1” indicates mutation with one base pair deletion leading to frameshift and introducing of an early stop codon. Lastly, U indicates samples that did not show any mutation in the *HPRT* RT-PCR amplification sequencing. The columns "aa#" and "Effect" show the effect of the mutation at the protein level.

Table 8: Detailed Information of Mutations from Sequencing of *HPRT* RT-PCR Amplification Products in the Fluctuation Assay

Mutant#	*Position	Mutation	Nucleotide Change	Kind	Effect	Codon Change	aa#
TK6p-1a	282-465	Deletion		S	Exon 3 exclusion		
TK6p-1b	176-465	Deletion		S	Exon 2 and 3 exclusions		
TK6P-4-1 TK6P-4-2	266	Base substitution	G>A Transition	M	Gly>Glu	GGA>GAA	40
TK6P-8-1 TK6P-8-2 TK6P-8-3	715	Base substitution	G>A Transition	M	Gly>Arg	GGA>AGA	190
TK6p-13	175-179	Deletion		OFD	Frameshift		
TK6p-14-2 TK6P-17-1 TK6P-17-2 TK6p-19	680-756	Deletion		S	Ex8 exclusion		
B101-2-3	343	Base substitution	T>A Transversion	M	Cys>Ser	TGT>AGT	66
B101-3-1 B101-3-2 B101-3-3	493	Deletion		F-1	Frameshift		
B101-8-1 B101-8-2	396-405	Deletion		OFD	Frameshift		
B101-11-1	341	Base substitution	T>C Transition	M	Leu>Pro	CTC>CCC	65
B101-18-2 B101-18-3	727-731	Deletion		OFD	Frameshift		
B101-19-2 B101-19-3	Insertion between 173-174	49 bp Insertion from the Intron 1		S	Frameshift		
B101-21	156	Deletion		F-1	Frameshift		
B101-22	729	Base substitution	C>A Transversion	M	Asp>Glu	GAC>GAA	194
B203-3-1 B203-21-1 B203-21-2 B203-21-3 B203-22-2	175-179	Deletion		OFD	Frameshift		
B203-3-2a B203-20-1a	175-179	Deletion		OFD	Frameshift		

Table 8: Detailed Information of Mutations from Sequencing of *HPRT* RT-PCR Amplification Products in the Fluctuation Assay (continued)

Mutant#	*Position	Mutation	Nucleotide Change	Kind	Effect	Codon Change	aa#
B203-3-2b B203-20-1b	175-565	Deletion		S	Exon 2 and 3 exclusions		
B203-3-3a	175-179	Deletion		OFD	Frameshift		
B203-3-3b	680-756	Deletion		S	Exon 8 exclusion		
B203-6-1a B203-6-2a	282-465	Deletion		S	Exon 3 exclusion		
B203-6-2b	176-465	Deletion		S	Exon2 and 3 exclusions		
B203-7-1 B203-7-2 B203-7-3	182-194	Deletion + 1 base substitution		OFD	Frameshift		
B203-10-1 B203-10-2 B203-20-2 B203-4-1 B203-4-2	680-756	Deletion		S	Exon 8 Exclusion		
B203-12-1 B203-12-2	358	Base substitution	G>T Transversion	M	Gly>Cyc	GGC>TGC	71
B203-22-1	466-632	Deletion		S	Exon 4, 5 and 6 Exclusion		
B203-22-3 B203-26-2	633-679	Deletion		S	Exon 7 Exclusion		
B203-24-1 B203-24-2 B203-26-1	544	Base substitution	G>T Transversion	M	Val>Leu	GTG>TTG	133

Table 9: Analysis of Mutations and Types of Point Mutation in the Fluctuation Assay

Table A shows types of spontaneous mutations according to the sequencing results of the *HPRT* RT-PCR amplification product and *HPRT* gene 3'-end and 5'-end PCR amplification product*s*. Replicates in mutants with full-length and shorter-length PCR amplification products are counted as a one-time mutational event in table A.

Full-length and shorter-length PCR amplification products display either point mutation or large deletion according to the sequencing analysis. In addition, mutants with negative RT-PCR amplification product and gene 5'-end and/or 3'-end deletion represent large genomic deletion or rearrangement. However, some types of mutation could not be defined, such as mutants with multiple bands in RT-PCR amplification and mutants with no RT-PCR amplification but positive *HPRT* gene 5'-end and 3'-end amplification. Finally, some collected mutants with positive RT-PCR amplification products could not be analyzed due to poor sequencing results.

Table B displays different types of point mutations indicated in the first row of table A.

Table 9: Analysis of Mutations and Types of Point Mutation in the Fluctuation Assay

A

Analysis	Type of Mutation	TK6	B101	B203
RT-PCR product (full length and shorter length due to splicing errors)	Point Mutation	6 (42.8%)	8 (34.7%)	13 (48%)
RT-PCR product (shorter length)	Large Deletion	-	-	-
RT-PCR product (Multiple bands)	Undefined	1 (7.1%)	-	4 (14.8%)
No RT-PCR product, 5'-end and/or 3'-end gene deletion	Large deletion or rearrangement	7 (50%)	15 (65.2%)	9 (33.3%)
No RT-PCR product, 5'-end and 3-end gene present	Undefined	-	-	1 (3.7%)

B

Type of mutation	TK6 Parental	B101	B203
Complex	-	-	-
Nonsense mutation	-	-	-
Missense Mutation	2	3	3
Out of frame deletion	1	2	4
In frame deletion	-	-	-
1 bp deletion (F-1)	-	2	-
Splicing	3	1	6

DISCUSSION

The role of *BCL11B* in cancer is complex. The *BCL11B* gene has been characterized genetically as a haplo-insufficient tumour suppressor gene (51,58-60), but *BCL11B* is overexpressed in many cancers, particularly in T-cell lymphomas and Ewing sarcomas (61-63). Moreover, *BCL11B* knockdown was shown to be synthetic lethal in T-cell lymphomas, while *BCL11B* overexpression was found to contribute to the resistance of cancer cells to genotoxic treatments (67-69). The BCL11B protein has been extensively characterized as a transcription factor that plays an important role in the development of several cell types and tissues (52-57). However, we have yet to identify transcriptional targets of BCL11B that could explain its roles as an oncogene and a tumour suppressor. Preliminary data in our lab suggested that BCL11B can function as a DNA repair accessory factor that stimulates the enzymatic activities of two enzymes of the base excision repair pathway. We therefore hypothesized that BCL11B's function in BER may explain its role as a haploinsufficient tumour suppressor gene. To test this hypothesis, we decided to look at the spontaneous mutation rate and radiation-induced mutation frequency in *BCL11B*$^{+/-}$ heterozygous cells. Results from the fluctuation assay indicated that the spontaneous mutation rate was increased approximately two-fold in two independent *BCL11B*$^{+/-}$ heterozygous TK6 clones. These results indicate that cells that exhibit loss-of-heterozygosity of *BCL11B* and express lower levels of the protein are more susceptible to accumulate mutations. As cancer is a genetic disease caused by the accumulation of mutations, some of which leading to oncogenes' activation while others causing the inactivation of tumour suppressor genes, *BCL11B* loss-of-heterozygosity would be expected to increase the probability that cancer cells emerge.

In the fluctuation assay, cells were not submitted to any genotoxic treatment and were allowed to proliferate normally. In this context, spontaneous mutations arise through three main processes: DNA replication errors, translesion synthesis and errors during the repair of DNA damage caused by endogenous metabolites. The error rate of replicative DNA polymerase is less than $1x10^{-7}$, while that of DNA pol β, the main polymerase involved in base excision repair is approximately $1x10^{-4}$ (91,92). As DNA replication involves the synthesis of $2x10^{9}$ bases, we can surmise that over 200 errors are made at each cell cycle. However, the mismatch repair pathway immediately corrects these replication errors. In bacteria, inactivation of the mismatch repair increases the mutation rate by ~1000-fold (93). Thus, there are very few mutations resulting from replication errors. Translesion synthesis, which enables the bypass of lesions that block the progression of replicative DNA polymerases and therefore enables the completion of DNA replication is believed to contribute to the spontaneous rate of mutations (94). In yeast cells, mutations that inactivate REV1 or REV3 reduce the rate of mutation by at least a hundred-fold (95-98), suggesting that most mutations are caused by translesion synthesis. In addition, it has been estimated that a normal human cell suffers ~30,000 base damage per day , and these base lesions are primarily repaired by the base excision repair (99). Considering the error rate of Pol β of 1 in 10,000, we can estimate that approximately 3 mutations are produced every day through this process. Our findings that $BCL11B^{+/-}$ heterozygous cells exhibit a two-fold increase in spontaneous mutation rate indicates that a lower level of this DNA repair accessory factor has an impact on the mutation rate. Perhaps the error rate of Pol β is higher in the absence of an accessory factor. Alternatively, we can envisage that as the speed and efficiency of Pol β is reduced in the absence of an accessory factor, many lesions will not be repaired fast enough

prior to the passage of replicative DNA polymerases. If some of these lesions cause the replicative DNA polymerase to stop and be replaced by a translesion synthesis polymerase, unavoidably some mutations will be produced.

Unfortunately, the experiments with ionizing radiation produced variable results that precludes us from reaching any conclusions. I discuss a number of issues that may explain the variations in these experiments:

1- One important variable is the moment at which a mutation occurs during the so-called "mutation expression time", the period between ionizing radiation treatment and *HPRT*$^-$ selection with 6-thioguanine. Mutants that occurred early in this period go through more divisions and produce a higher apparent number of mutants once the selection is applied. In 1999, Leonhardt et al. showed that most radiation-induced *HPRT* mutants are generated early following the treatment with ionizing radiation (100), and if it is the case, we should see several mutational events producing a high number of replicates and a few mutations with a few or no replicates. However, *HPRT* RT-PCR amplification analysis showed that *HPRT* mutants collected form the experiment 2020/10/01 (from B101-IR-22 to B101-IR-83), to have five mutational events, one of which (an OFD from nucleotide 354 to 355) was found in 32 out of 62 mutants (Table 4). Clearly, this mutation with 32 replicates happened early in culture as opposed to other HPRT mutations, such as a splicing mutation (exclusion of exon 8) in B101-IR 39 and B101-IR 60. One mutation event with several replicates and more mutational events with one or few replicates is more consistent with the idea that a significant ratio of *HPRT* mutation following radiation is of a delayed-type, due to radiation-induced genome instability (101). Therefore, final number of 6-tg selected mutants originating from an early mutation in culture could be

equal or more than that of a late mutation. Historically, this problem led to the development of the fluctuation assay by Salvador Luria and Max Delbruck in 1943 (78), who studied spontaneous mutations in *Escherichia coli* (E. coli) bacteria against T1 phage. They discovered that spontaneous mutations in independent bacterial cultures could not be explained by the poisson distribution, so they developed a new method named probability distribution (recognized as Luria and Delbruck distribution) in order to calculate the mutation rate (78,102). It is believed that spontaneous mutagenesis can be explained by mutation rate, whereas mutation frequency is a better indicator in case of induced mutagenesis (80). However, we suggest adjusting the fluctuation assay in a way that could be applicable to study induced mutagenesis. In this way, we can look at the number of mutational events induced by a treatment, regardless of the time of occurrence.

2-Recently, another member in our lab found that *BCL11B* downregulation in some cancer cells leads to an increase in the expression of BCL11A, which also functions as an accessory factor in BER by stimulating NTHL1. We suggest looking at the BCL11A expression in *BCL11B*$^{+/-}$ heterozygous TK6 cells, and in case of BCL11A upregulation, mutation assays can be performed in a *BCL11B*$^{+/-}$ model combined with *BCL11A* knockdown.

3- Since the *HPRT* gene is located on the human X chromosome, large genomic deletion in this locus could be lethal (74). Therefore, large genomic deletions covering the *HPRT* gene would not be included in the mutation frequency calculation. To address this issue, I suggest using the *TK* mutation assay instead of *HPRT* mutation assay, both of which follow the same methodology (82). Thymidine kinase gene (*TK*) is involved in the salvage pathway of DNA synthesis (103). Since it is an autosomal gene, even mutants with large genomic deletions in *TK* loci can survive

and be selected by Trifluorothymidine, a toxic analog of thymidine (82). This could explain why the spontaneous mutation rate of cells is higher in *TK* mutation assay than *HPRT* mutation assay (74).

According to the sequencing analysis of *HPRT* cDNAs, we identified a variety of mutations affecting the HPRT protein. One of the mutations founded in radiation-induced *HPRT* mutants and not in spontaneous *HPRT* mutants was a complex mutation. Nicklas et. al defined complex mutation as two nonadjacent mutations (77), whereas in this study we noticed some complex *HPRT* mutants with three or even four nonadjacent mutations. These complex mutations represent clustered DNA lesions, a hallmark of exposure to ionizing radiation, which was found to have a poor repair ability (104).

Sequencing analysis of shorter length *HPRT RT*-PCR amplification revealed some *HPRT* mutants with exclusion of one or more exons. Moreover, there were some *HPRT* mutants with inclusion of an intronic sequence with or without an exon exclusion (such as B101-IR-13, B101-IR-37, B101-19-2 and B101-19-3). These two categories were interpreted to harbour splicing mutations, which is due to a point mutation in a splice donor or acceptor sequences (85). However, to recognize the specific point mutations in this category, we would need to analyze genomic sequences of *HPRT* mutants. In the study conducted by Nicklas et al., all reported *HPRT* mutants with splicing errors were found to harbour base substitution in the consensus splice site (77).

In addition, in some *HPRT* mutants, multiple *HPRT* RT-PCR amplification products were found to be present (such as B101-IR-3, B203-IR-3, and etc.). Some groups stated that it could be because two or more *HPRT* mutants fell into the same well when plated with 6-tg (77,88).

However, others reported that this condition might happen due to a mutation in a splicing sequence or a nonsense mutation, making a full-length and two to three shorter-length RT-PCR amplification products (89,90). In addition, *cDNA* analysis of T-lymphocytes *HPRT* mutants from a family with Lesch-Nyhan syndrome showed that a single base deletion in the splice site sequence of exon 5 could lead to multiple RT-PCR amplification products (105,106). In our study, there were seven *HPRT* mutants (B101-IR-3,4,7,14,16,18, and 19) with three RT-PCR amplification products (Figure 13B), including a full-length and two shorter-length RT-PCR amplification products. We were able to analyze the sequencing information from the first (full-length amplification) and the third one. While the full-length PCR amplification product showed one base pair deletion, the third PCR amplification product showed exon 2 and 3 exclusion, which is consistent with previous works reporting the correlation between a nonsense mutation and alternative splicing (89,90). Furthermore, the probability of growing the same three *HPRT* mutants in seven wells must be very low. On the other hand, Tk6p-1 mutant in the fluctuation assay displayed shorter 2 bands (Figure 24A), one of which showed exon 3 exclusion, whereas the shorter one missed exon2 and 3. This mutant is more consistent with the idea of two mutants growing in the same well. Ultimately, we interpreted *HPRT* mutants with multiple *HPRT* RT-PCR amplifications as “undefined” because explaining the underlying mutational event in this category would have required sequencing analysis of genomic DNAs.

No *HPRT* RT-PCR amplification products were obtained for some *HPRT* mutants. We therefore purified the genomic DNA and performed PCR amplification to investigate the integrity of the HPRT gene at its 5'- and 3'- ends. *HPRT* mutants with one or both deleted extremities were considered to have large genomic deletions. However, we could not define the type of

mutation in mutants whose intact *HPRT* gene 5'- and 3'- ends were analyzed by DNA sequencing and did not include any mutation (such as B101-IR-85, 86 and etc. in figure18C). There are some possibilities and approaches to verify the type of mutation in this category:

1- These *HPRT* mutants were selected due to an alteration in promoter or distant regulatory sequences, leading to low levels or absence of *HPRT* mRNAs (107). Therefore, one suggestion is to amplify and analyze the promoter or distant regulatory sequences to detect a potential mutation.

2-Although it seems unlikely, but we cannot exclude the possibility that RT-PCR assay failed to amplify a product due to a point mutation in primer binding sites (107). Therefore, the RT-PCR assay can be repeated with one or two different pairs of primers to confirm the absence of *HPRT* mRNA.

3- Although PCR amplification is a highly sensitives assay, there is a small chance that *HPRT* RT-PCR amplification is not able to amplify *HPRT* cDNA due to nonsense-mediated RNA decay mechanism, which is a surveillance mechanism identifying and degrading mRNAs with a premature translation-termination codon (PTC) (108). Nonsense-mediated RNA decay mechanism can be suppressed by some chemicals, such as cycloheximide, that inhibit translation (109). Our hypothesis regarding RNA degradation due to nonsense-mediated RNA decay could be verified by treating cells with cycloheximide for a few hours prior to RNA extraction, which prevent mRNA degradation.

Finally, to test whether the inactivation of one *BCL11B* allele in non-transformed cells could increase the radiation-induced mutation rate, I propose an alternative to the *HPRT* mutation assay to calculate the mutation rate instead of mutation frequency following irradiation. I

suggest performing the *PIG-A* mutation assay to measure the radiation-induced mutation rate in *BCL11B*$^{+/-}$ mutants. The *PIG-A* mutation assay has been introduced as a novel high throughput mutation assay which is designed based on the *PIG-A* gene mutation that disrupts glycosylphosphatidylinositol (GPI) biosynthesis (110). GPI is a complex that tether several proteins to the surface of cells (111). There are at least 22 different genes associated with GPI biosynthesis among which only the *PIG-A* gene is located on X chromosome (112). Having one active allele of *PIG-A*, like the *HPRT* gene, cells originating from a male gender can acquire the GPI mutation phenotype with one hit. In 2015, Krüger et al. established the *PIG-A* mutation assay, using flow cytometry analysis of TK6 cells with antibodies against the GPI-anchored proteins CD55 and CD59 (113). Interestingly, bacterial toxin proaerolysin can selectively kills GPI^{+} cells too, and background GPI^{-} cells can be removed by fluorescence-activated cell sorting or using antibody-coated cell culture dishes to increase the sensitivity of the assay (114,115). *PIG-A* mutation assay is a fast and less labor-intensive mutation assay compared to the *HPRT* mutation assay, because there is no need to analyze the plating efficiency (113). In addition, GPI mutants can be analyzed through flow cytometry once the mutation phenotype is expressed following the mutation expression time (113).

In addition, next generation sequencing (NGS)-based assays can be used to determine the mutation frequency as well as the spectrum of mutations (116). However, some mutations can be recognized by the NGS-based assays which do not occur due to the mutagenic treatment. These unwanted mutations may be the results of the library preparation procedure or sequencing errors which can be filtered out through some strategies such as single cell approach, PCR copy consensus assay and circle sequencing (117). Recently, Zou et al. in 2018

took advantage of high-depth whole genome sequencing to analyze the mutational signature of cells with CRISPR Cas9-mediated knockouts of genes associated with different DNA repair pathways (118).

CONCLUSION

The results of our *HPRT* assays do not confirm or infirm the hypothesis that the function of BCL11B in DNA repair explains its role as a haploinsufficient tumour suppressor gene in cells that have been submitted to radiation. Although we were able to define the mutational events in a large proportion of *HPRT* mutants, some mutations remained as "undefined". Finding the underlying mutation in this category by genomic DNA analysis would help us to understand the effect of *BCL11B* heterozygosity on mutational events.

REFERENCES

1. Haites N. Oncogenes. In: Brenner S, Miller JH, editors. Encyclopedia of Genetics. New York: Academic Press; 2001. p 1370-2.
2. Bergonzini V, Salata C, Calistri A, Parolin C, Palù G. View and review on viral oncology research. Infectious Agents and Cancer **2010**;5:11
3. Neumann J, Zeindl-Eberhart E, Kirchner T, Jung A. Frequency and type of KRAS mutations in routine diagnostic analysis of metastatic colorectal cancer. Pathology - Research and Practice **2009**;205:858-62
4. Haluska FG, Tsujimoto Y, Croce CM. The t(8;14) chromosome translocation of the Burkitt lymphoma cell line Daudi occurred during immunoglobulin gene rearrangement and involved the heavy chain diversity region. **1987**;84:6835-9
5. Ren R. Mechanisms of BCR–ABL in the pathogenesis of chronic myelogenous leukaemia. Nature Reviews Cancer **2005**;5:172-83
6. Albertson DG. Gene amplification in cancer. Trends in Genetics **2006**;22:447-55
7. Watt PM, Kumar R, Kees UR. Promoter demethylation accompanies reactivation of the HOX11 proto-oncogene in leukemia. Genes, chromosomes & cancer **2000**;29:371-7
8. Hanada M, Delia D, Aiello A, Stadtmauer E, Reed JC. bcl-2 Gene Hypomethylation and High-Level Expression in B-Cell Chronic Lymphocytic Leukemia. Blood **1993**;82:1820-8

9. Nishigaki M, Aoyagi K, Danjoh I, Fukaya M, Yanagihara K, Sakamoto H*, et al.* Discovery of aberrant expression of R-RAS by cancer-linked DNA hypomethylation in gastric cancer using microarrays. Cancer Res **2005**;65:2115-24
10. Vogelstein B, Kinzler KW. Cancer genes and the pathways they control. Nature Medicine **2004**;10:789-99
11. Vogelstein B, Papadopoulos N, Velculescu VE, Zhou S, Diaz LA, Kinzler KW. Cancer Genome Landscapes. **2013**;339:1546-58
12. Tamborero D, Gonzalez-Perez A, Perez-Llamas C, Deu-Pons J, Kandoth C, Reimand J*, et al.* Comprehensive identification of mutational cancer driver genes across 12 tumor types. Scientific Reports **2013**;3:2650
13. Qiu B, Simon MC. Oncogenes strike a balance between cellular growth and homeostasis. Seminars in Cell & Developmental Biology **2015**;43:3-10
14. Wang LH, Wu CF, Rajasekaran N, Shin YK. Loss of Tumor Suppressor Gene Function in Human Cancer: An Overview. Cellular Physiology and Biochemistry **2018**;51:2647-93
15. Knudson AG, Jr. Mutation and cancer: statistical study of retinoblastoma. Proc Natl Acad Sci U S A **1971**;68:820-3
16. Inoue K, Fry EA. Haploinsufficient tumor suppressor genes. Adv Med Biol **2017**;118:83-122
17. Fero ML, Randel E, Gurley KE, Roberts JM, Kemp CJ. The murine gene p27Kip1 is haplo-insufficient for tumour suppression. Nature **1998**;396:177-80
18. Weinstein IB. Disorders in cell circuitry during multistage carcinogenesis: the role of homeostasis. Carcinogenesis **2000**;21:857-64
19. Nowell PC, Hungerford DAJJotNCI. Chromosome studies on normal and leukemic human leukocytes. **1960**;25:85-109
20. Torti D, Trusolino L. Oncogene addiction as a foundational rationale for targeted anti-cancer therapy: promises and perils. EMBO Mol Med **2011**;3:623-36
21. Nagel R, Semenova EA, Berns A. Drugging the addict: non-oncogene addiction as a target for cancer therapy. EMBO Rep **2016**;17:1516-31
22. Hartwell LH, Szankasi P, Roberts CJ, Murray AW, Friend SH. Integrating Genetic Approaches into the Discovery of Anticancer Drugs. Science **1997**;278:1064
23. Solimini NL, Luo J, Elledge SJ. Non-Oncogene Addiction and the Stress Phenotype of Cancer Cells. Cell **2007**;130:986-8
24. Freije J, Fraile J, Lopez-Otin C. Protease Addiction and Synthetic Lethality in Cancer. **2011**;1
25. Friedberg EC, Walker GC, Siede W, Wood RD. DNA repair and mutagenesis. American Society for Microbiology Press; 2005.
26. Dianov GL, Hübscher U. Mammalian base excision repair: the forgotten archangel. Nucleic Acids Res **2013**;41:3483-90
27. Hegde ML, Hazra TK, Mitra S. Early steps in the DNA base excision/single-strand interruption repair pathway in mammalian cells. Cell Res **2008**;18:27-47
28. Jeppesen DK, Bohr VA, Stevnsner T. DNA repair deficiency in neurodegeneration. Prog Neurobiol **2011**;94:166-200
29. Allinson SL, Dianova II, Dianov GL. DNA polymerase beta is the major dRP lyase involved in repair of oxidative base lesions in DNA by mammalian cell extracts. EMBO J **2001**;20:6919-26
30. Horton JK, Prasad R, Hou E, Wilson SH. Protection against Methylation-induced Cytotoxicity by DNA Polymerase β-Dependent Long Patch Base Excision Repair*. Journal of Biological Chemistry **2000**;275:2211-8
31. Ramdzan ZM, Vadnais C, Pal R, Vandal G, Cadieux C, Leduy L*, et al.* RAS Transformation Requires CUX1-Dependent Repair of Oxidative DNA Damage. PLOS Biology **2014**;12:e1001807

32. Ramdzan ZM, Pal R, Kaur S, Leduy L, Bérubé G, Davoudi S*, et al.* The function of CUX1 in oxidative DNA damage repair is needed to prevent premature senescence of mouse embryo fibroblasts. Oncotarget **2015**;6:3613-26
33. Pal R, Ramdzan ZM, Kaur S, Duquette PM, Marcotte R, Leduy L*, et al.* CUX2 Protein Functions as an Accessory Factor in the Repair of Oxidative DNA Damage *. Journal of Biological Chemistry **2015**;290:22520-31
34. Kaur S, Coulombe Y, Ramdzan ZM, Leduy L, Masson J-Y, Nepveu A. Special AT-rich Sequence-binding Protein 1 (SATB1) Functions as an Accessory Factor in Base Excision Repair *. Journal of Biological Chemistry **2016**;291:22769-80
35. Kaur S, Ramdzan ZM, Guiot M-C, Li L, Leduy L, Ramotar D*, et al.* CUX1 stimulates APE1 enzymatic activity and increases the resistance of glioblastoma cells to the mono-alkylating agent temozolomide. Neuro-Oncology **2017**;20:484-93
36. Ramdzan ZM, Vickridge E, Li L, Faraco CCF, Djerir B, Leduy L*, et al.* CUT Domains Stimulate Pol β Enzymatic Activities to Accelerate Completion of Base Excision Repair. Journal of Molecular Biology **2021**;433:166806
37. Ramdzan ZM, Vickridge E, Faraco CCF, Nepveu A. CUT Domain Proteins in DNA Repair and Cancer. Cancers **2021**;13
38. Schoenmakers EFPM, Bunt J, Hermers L, Schepens M, Merkx G, Janssen B*, et al.* Identification of CUX1 as the recurrent chromosomal band 7q22 target gene in human uterine leiomyoma. **2013**;52:11-23
39. Jerez A, Sugimoto Y, Makishima H, Verma A, Jankowska AM, Przychodzen B*, et al.* Loss of heterozygosity in 7q myeloid disorders: clinical associations and genomic pathogenesis. Blood **2012**;119:6109-17
40. McNerney ME, Brown CD, Wang X, Bartom ET, Karmakar S, Bandlamudi C*, et al.* CUX1 is a haploinsufficient tumor suppressor gene on chromosome 7 frequently inactivated in acute myeloid leukemia. Blood **2013**;121:975-83
41. Hindersin S, Niemeyer CM, Germing U, Göbel U, Kratz CP. Mutation analysis of CUTL1 in childhood myeloid neoplasias with monosomy 7. Leukemia research **2007**;31:1323-4
42. Patrikis MI, Bryan EJ, Thomas NA, Rice GE, Quinn MA, Baker MS*, et al.* Mutation analysis of CDP, TP53, and KRAS in uterine leiomyomas. **2003**;37:61-4
43. Michl P, Ramjaun AR, Pardo OE, Warne PH, Wagner M, Poulsom R*, et al.* CUTL1 is a target of TGF(beta) signaling that enhances cancer cell motility and invasiveness. Cancer cell **2005**;7:521-32
44. Muzny DM, Bainbridge MN, Chang K, Dinh HH, Drummond JA, Fowler G*, et al.* Comprehensive molecular characterization of human colon and rectal cancer. Nature **2012**;487:330-7
45. Ramdzan ZM, Nepveu A. CUX1, a haploinsufficient tumour suppressor gene overexpressed in advanced cancers. Nature Reviews Cancer **2014**;14:673-82
46. Serrano M, Lin AW, McCurrach ME, Beach D, Lowe SWJC. Oncogenic ras provokes premature cell senescence associated with accumulation of p53 and p16INK4a. **1997**;88:593-602
47. Weyemi U, Lagente-Chevallier O, Boufraqech M, Prenois F, Courtin F, Caillou B*, et al.* ROS-generating NADPH oxidase NOX4 is a critical mediator in oncogenic H-Ras-induced DNA damage and subsequent senescence. **2012**;31:1117-29
48. Ramdzan ZM, Ginjala V, Pinder JB, Chung D, Donovan CM, Kaur S*, et al.* The DNA repair function of CUX1 contributes to radioresistance. Oncotarget **2017**;8:19021-38
49. Zhang L-j, Vogel WK, Liu X, Topark-Ngarm A, Arbogast BL, Maier CS*, et al.* Coordinated regulation of transcription factor Bcl11b activity in thymocytes by the mitogen-activated protein kinase (MAPK) pathways and protein sumoylation. The Journal of biological chemistry **2012**;287:26971-88

50. Avram D, Fields A, Pretty On Top K, Nevrivy DJ, Ishmael JE, Leid M. Isolation of a novel family of C(2)H(2) zinc finger proteins implicated in transcriptional repression mediated by chicken ovalbumin upstream promoter transcription factor (COUP-TF) orphan nuclear receptors. The Journal of biological chemistry **2000**;275:10315-22
51. Wakabayashi Y, Inoue J, Takahashi Y, Matsuki A, Kosugi-Okano H, Shinbo T*, et al.* Homozygous deletions and point mutations of the Rit1/Bcl11b gene in gamma-ray induced mouse thymic lymphomas. Biochemical and biophysical research communications **2003**;301:598-603
52. Arlotta P, Molyneaux BJ, Jabaudon D, Yoshida Y, Macklis JD. Ctip2 controls the differentiation of medium spiny neurons and the establishment of the cellular architecture of the striatum. The Journal of neuroscience : the official journal of the Society for Neuroscience **2008**;28:622-32
53. Enomoto T, Ohmoto M, Iwata T, Uno A, Saitou M, Yamaguchi T*, et al.* Bcl11b/Ctip2 controls the differentiation of vomeronasal sensory neurons in mice. The Journal of neuroscience : the official journal of the Society for Neuroscience **2011**;31:10159-73
54. Golonzhka O, Liang X, Messaddeq N, Bornert JM, Campbell AL, Metzger D*, et al.* Dual role of COUP-TF-interacting protein 2 in epidermal homeostasis and permeability barrier formation. The Journal of investigative dermatology **2009**;129:1459-70
55. Golonzhka O, Metzger D, Bornert JM, Bay BK, Gross MK, Kioussi C*, et al.* Ctip2/Bcl11b controls ameloblast formation during mammalian odontogenesis. Proc Natl Acad Sci U S A **2009**;106:4278-83
56. Kastner P, Chan S, Vogel WK, Zhang LJ, Topark-Ngarm A, Golonzhka O*, et al.* Bcl11b represses a mature T-cell gene expression program in immature CD4+ CD8+ thymocytes. **2010**;40:2143-54
57. Li L, Leid M, Rothenberg EV. An early T cell lineage commitment checkpoint dependent on the transcription factor Bcl11b. Science **2010**;329:89-93
58. De Keersmaecker K, Real PJ, Gatta GD, Palomero T, Sulis ML, Tosello V*, et al.* The TLX1 oncogene drives aneuploidy in T cell transformation. Nature medicine **2010**;16:1321-7
59. Gutierrez A, Kentsis A, Sanda T, Holmfeldt L, Chen S-C, Zhang J*, et al.* The BCL11B tumor suppressor is mutated across the major molecular subtypes of T-cell acute lymphoblastic leukemia. Blood **2011**;118:4169-73
60. Kamimura K, Ohi H, Kubota T, Okazuka K, Yoshikai Y, Wakabayashi Y-i*, et al.* Haploinsufficiency of Bcl11b for suppression of lymphomagenesis and thymocyte development. Biochemical and biophysical research communications **2007**;355:538-42
61. Wiles ET, Lui-Sargent B, Bell R, Lessnick SL. BCL11B is up-regulated by EWS/FLI and contributes to the transformed phenotype in Ewing sarcoma. PLoS One **2013**;8:e59369
62. Gu X, Wang Y, Zhang G, Li W, Tu P. Aberrant expression of BCL11B in mycosis fungoides and its potential role in interferon-induced apoptosis. The Journal of dermatology **2013**;40:596-605
63. Oshiro A, Tagawa H, Ohshima K, Karube K, Uike N, Tashiro Y*, et al.* Identification of subtype-specific genomic alterations in aggressive adult T-cell leukemia/lymphoma. Blood **2006**;107:4500-7
64. Ganguli-Indra G, Wasylyk C, Liang X, Millon R, Leid M, Wasylyk B*, et al.* CTIP2 Expression in Human Head and Neck Squamous Cell Carcinoma Is Linked to Poorly Differentiated Tumor Status. PLoS One **2009**;4:e5367
65. Liao CK, Fang KM, Chai K, Wu CH, Ho CH, Yang CS*, et al.* Depletion of B cell CLL/Lymphoma 11B Gene Expression Represses Glioma Cell Growth. Molecular neurobiology **2016**;53:3528-39
66. Zweier-Renn LA, Riz I, Hawley TS, Hawley RG. The DN2 Myeloid-T (DN2mt) Progenitor is a Target Cell for Leukemic Transformation by the TLX1 Oncogene. J Bone Marrow Res **2013**;1
67. Grabarczyk P, Nähse V, Delin M, Przybylski G, Depke M, Hildebrandt P*, et al.* Increased expression of bcl11b leads to chemoresistance accompanied by G1 accumulation. PLoS One **2010**;5:e12532

68. Huang X, Chen S, Shen Q, Chen S, Yang L, Grabarczyk P*, et al.* Down regulation of BCL11B expression inhibits proliferation and induces apoptosis in malignant T cells by BCL11B-935-siRNA. Hematology (Amsterdam, Netherlands) **2011**;16:236-42
69. Grabarczyk P, Przybylski GK, Depke M, Völker U, Bahr J, Assmus K*, et al.* Inhibition of BCL11B expression leads to apoptosis of malignant but not normal mature T cells. Oncogene **2007**;26:3797-810
70. Chu EH, Malling HV. Mammalian cell genetics. II. Chemical induction of specific locus mutations in Chinese hamster cells in vitro. Proc Natl Acad Sci U S A **1968**;61:1306-12
71. Albertini RJ, Nicklas JA, O'Neill JP, Robison SH. IN VIVO SOMATIC MUTATIONS IN HUMANS: MEASUREMENT AND ANALYSIS. **1990**;24:305-26
72. Agrahari AK, Krishna Priya M, Praveen Kumar M, Tayubi IA, Siva R, Prabhu Christopher B*, et al.* Understanding the structure-function relationship of HPRT1 missense mutations in association with Lesch–Nyhan disease and HPRT1-related gout by in silico mutational analysis. Computers in Biology and Medicine **2019**;107:161-71
73. Finette BA, Kendall H, Vacek PM. Mutational spectral analysis at the HPRT locus in healthy children. Mutation Research/Fundamental and Molecular Mechanisms of Mutagenesis **2002**;505:27-41
74. Johnson GE. Mammalian cell HPRT gene mutation assay: test methods. Methods in molecular biology (Clifton, NJ) **2012**;817:55-67
75. Keohavong P, Xi L, Grant SG. Molecular analysis of mutations in the human HPRT gene. Methods in molecular biology (Clifton, NJ) **2014**;1105:291-301
76. Maiti AK, Boldogh I, Spratt H, Mitra S, Hazra TK. Mutator phenotype of mammalian cells due to deficiency of NEIL1 DNA glycosylase, an oxidized base-specific repair enzyme. DNA Repair **2008**;7:1213-20
77. Nicklas JA, Albertini RJ, Vacek PM, Ardell SK, Carter EW, McDiarmid MA*, et al.* Mutagenicity monitoring following battlefield exposures: Molecular analysis of HPRT mutations in Gulf War I veterans exposed to depleted uranium. Environmental and molecular mutagenesis **2015**;56:594-608
78. Luria SE, Delbrück M. Mutations of Bacteria from Virus Sensitivity to Virus Resistance. Genetics **1943**;28:491-511
79. Lea DE, Coulson CA. The distribution of the numbers of mutants in bacterial populations. Journal of Genetics **1949**;49:264
80. Foster PL. Methods for determining spontaneous mutation rates. Methods Enzymol **2006**;409:195-213
81. Lang GI. Measuring Mutation Rates Using the Luria-Delbrück Fluctuation Assay. Methods in molecular biology (Clifton, NJ) **2018**;1672:21-31
82. Liber HL, Thilly WG. Mutation assay at the thymidine kinase locus in diploid human lymphoblasts. Mutation Research/Fundamental and Molecular Mechanisms of Mutagenesis **1982**;94:467-85
83. Furth EE, Thilly WG, Penman BW, Liber HL, Rand WM. Quantitative assay for mutation in diploid human lymphoblasts using microtiter plates. Analytical biochemistry **1981**;110:1-8
84. Lang GI. Measuring Mutation Rates Using the Luria-Delbrück Fluctuation Assay. In: Muzi-Falconi M, Brown GW, editors. Genome Instability: Methods and Protocols. New York, NY: Springer New York; 2018. p 21-31.
85. Anna A, Monika G. Splicing mutations in human genetic disorders: examples, detection, and confirmation. J Appl Genet **2018**;59:253-68

86. Reid LH, Gregg RG, Smithies O, Koller BH. Regulatory elements in the introns of the human HPRT gene are necessary for its expression in embryonic stem cells. Proc Natl Acad Sci U S A **1990**;87:4299-303
87. Kim SH, Moores JC, David D, Respess JG, Jolly DJ, Friedmann TJNar. The organization of the human HPRT gene. **1986**;14:3103-18
88. Rossi AM, Tates AD, van Zeeland AA, Vrieling H. Molecular analysis of mutations affecting hprt mRNA splicing in human T-lymphocytes in vivo. Environmental and molecular mutagenesis **1992**;19:7-13
89. Manjanatha MG, Lindsey LA, Mittelstaedt RA, Heflich RH. Low hprt mRNA levels and multiple hprt mRNA species in 6-thioguanine-resistant Chinese hamster cell mutants possessing nonsense mutations. Mutation research **1994**;308:65-75
90. Pluth JM, O'Neill JP, Nicklas JA, Albertini RJ. Molecular bases of hprt mutations in malathion-treated human T-lymphocytes. Mutation research **1998**;397:137-48
91. Kunkel TA. Considering the cancer consequences of altered DNA polymerase function. Cancer cell **2003**;3:105-10
92. Loeb LA. Mutator Phenotype May Be Required for Multistage Carcinogenesis. **1991**;51:3075-9
93. Schaaper RM. Base selection, proofreading, and mismatch repair during DNA replication in Escherichia coli. The Journal of biological chemistry **1993**;268:23762-5
94. Sale JE. Translesion DNA synthesis and mutagenesis in eukaryotes. Cold Spring Harb Perspect Biol **2013**;5:a012708-a
95. Gibbs PEM, Wang X-D, Li Z, McManus TP, McGregor WG, Lawrence CW*, et al.* The function of the human homolog of Saccharomyces cerevisiae REV1 is required for mutagenesis induced by UV light. **2000**;97:4186-91
96. Lawrence CW, Christensen R. UV mutagenesis in radiation-sensitive strains of yeast. Genetics **1976**;82:207-32
97. Lemontt JF. Mutants of yeast defective in mutation induced by ultraviolet light. Genetics **1971**;68:21-33
98. Lawrence CW. Cellular roles of DNA polymerase zeta and Rev1 protein. DNA Repair (Amst) **2002**;1:425-35
99. Marsden CG, Dragon JA, Wallace SS, Sweasy JB. Base Excision Repair Variants in Cancer. Methods Enzymol **2017**;591:119-57
100. Leonhardt EA, Trinh M, Chu K, Dewey WC. Evidence that most radiation-induced HPRT mutants are generated directly by the initial radiation exposure. Mutation research **1999**;426:23-30
101. Loucas BD, Cornforth MN. Postirradiation growth in HAT medium fails to eliminate the delayed appearance of 6-thioguanine-resistant clones in EJ30 human epithelial cells. Radiation research **1998**;149:171-8
102. Qi Z. The Luria-Delbrück distribution. CHANCE **2010**;23:15-8
103. Awan FT, Byrd JC. Chapter 77 - Chronic Lymphocytic Leukemia. In: Hoffman R, Benz EJ, Silberstein LE, Heslop HE, Weitz JI, Anastasi J*, et al.*, editors. Hematology (Seventh Edition): Elsevier; 2018. p 1244-64.
104. Sage E, Shikazono N. Radiation-induced clustered DNA lesions: Repair and mutagenesis. Free Radical Biology and Medicine **2017**;107:125-35
105. Hunter TC, Melancon SB, Dallaire L, Taft S, Skopek TR, Albertini RJ*, et al.* Germinal HPRT splice donor site mutation results in multiple RNA splicing products in T-lymphocyte cultures. Somatic cell and molecular genetics **1996**;22:145-50
106. Andersson B, Hou SM, Lambert B. Mutations causing defective splicing in the human hprt gene. Environmental and molecular mutagenesis **1992**;20:89-95

107. Lichtenauer-Kaligis EGR, Thijssen JCP, Dulk Hd, van de Putte P, Giphart-Gassler M, Jong JGT-d. Spontaneous mutation spectrum in the hprt gene in human lymphoblastoid TK6 cells. Mutagenesis **1995**;10:137-43
108. da Costa PJ, Menezes J, Romão L. The role of alternative splicing coupled to nonsense-mediated mRNA decay in human disease. The International Journal of Biochemistry & Cell Biology **2017**;91:168-75
109. Nickless A, Bailis JM, You Z. Control of gene expression through the nonsense-mediated RNA decay pathway. Cell & Bioscience **2017**;7:26
110. Peruzzi B, Araten DJ, Notaro R, Luzzatto L. The use of PIG-A as a sentinel gene for the study of the somatic mutation rate and of mutagenic agents in vivo. Mutation research **2010**;705:3-10
111. Kinoshita T, Murakami Y, Morita YS. 4.21 - Diseases Associated with GPI Anchors. In: Kamerling H, editor. Comprehensive Glycoscience. Oxford: Elsevier; 2007. p 393-419.
112. Krüger CT, Fischer BM, Armant O, Morath V, Strähle U, Hartwig A. The in vitro PIG-A gene mutation assay: glycosylphosphatidylinositol (GPI)-related genotype-to-phenotype relationship in TK6 cells. Archives of toxicology **2016**;90:1729-36
113. Krüger CT, Hofmann M, Hartwig A. The in vitro PIG-A gene mutation assay: mutagenicity testing via flow cytometry based on the glycosylphosphatidylinositol (GPI) status of TK6 cells. Archives of toxicology **2015**;89:2429-43
114. Araten DJ, Martinez-Climent JA, Perle MA, Holm E, Zamechek L, DiTata K*, et al.* A quantitative analysis of genomic instability in lymphoid and plasma cell neoplasms based on the PIG-A gene. Mutation research **2010**;686:1-8
115. Krüger CT, Hofmann M, Hartwig A. The in vitro PIG-A gene mutation assay: mutagenicity testing via flow cytometry based on the glycosylphosphatidylinositol (GPI) status of TK6 cells. Archives of toxicology **2015**;89:2429-43
116. Du H, Pan B, Chen T. Evaluation of chemical mutagenicity using next generation sequencing: A review. Journal of Environmental Science and Health, Part C **2017**;35:140-58
117. Maslov AY, Quispe-Tintaya W, Gorbacheva T, White RR, Vijg J. High-throughput sequencing in mutation detection: A new generation of genotoxicity tests? Mutation research **2015**;776:136-43
118. Zou X, Owusu M, Harris R, Jackson SP, Loizou JI, Nik-Zainal S. Validating the concept of mutational signatures with isogenic cell models. Nature Communications **2018**;9:1744